
Article:

Shi, C., Qu, B. and Provis, J.L. (2019) Recent progress in low-carbon binders. Cement and Concrete Research, 122. pp. 227-250. ISSN: 0008-8846

https://doi.org/10.1016/j.cemconres.2019.05.009

Recent Progress in Low-Carbon Binders

Caijun Shi[1*], Bo Qu[1], John L. Provis[2]

[1] College of Civil Engineering, Hunan University, Changsha 410082, China

[2] Department of Materials Science & Engineering, University of Sheffield, Sheffield S1 3JD, UK

Abstract:

The development of low-carbon binders has been recognized as a means of reducing the carbon footprint of the Portland cement industry, in response to growing global concerns over CO_2 emissions from the construction sector. This paper reviews recent progress in the three most attractive low-carbon binders: alkali-activated, carbonate, and belite-ye'elimite-based binders. Alkali-activated binders/materials were reviewed at the past two ICCC congresses, so this paper focuses on some key developments of alkali-activated binders/materials since the last keynote paper was published in 2015. Recent progress on carbonate and belite-ye'elimite-based binders are also reviewed and discussed, as they are attracting more and more attention as essential alternative low-carbon cementitious materials. These classes of binders have a clear role to play in providing a sustainable future for global construction, as part of the available toolkit of cements.

Keywords: low-carbon cementitious binders; alkali-activated material; carbonated binders; belite-ye'elimite binders; sustainability

*corresponding author: C. Shi (cshi@hnu.edu.cn)

1. Introduction

Growing concerns over the greenhouse emissions profile of the Portland cement and concrete industry have led to a very high level of recent interest in the development of low-carbon binders as alternatives to Portland-based cements. This paper reviews recent progress in the three most prominent classes of low-carbon binders: alkali-activated or geopolymer, carbonate, and belite-ye'elimite-based binders. Alkali-activated binders/materials were reviewed at the past two (13th and 14th) International Congresses on the Chemistry of Cement (ICCC) [1, 2], and in discussing these materials, this paper focuses on some of their key developments since the last keynote paper was published in 2015 [2]. These include rheological properties, setting behavior, structural characterization, dimensional stability, durability, and their applications. However, this paper does not aim to provide a detailed overview with respect to all existing insights into these materials, which can be obtained in other references including [3-5], but rather focuses on the most important new information that has been obtained in the past 4 years. Recent progress on carbonate and belite-ye'elimite-based binders will also be reviewed and discussed in detail, as these are attracting more and more attention as essential parts of the 'toolkit' of alternative low-carbon cementitious materials.

2. Alkali-Activated Binders

2.1. Raw materials

2.1.1 Activators

As numerous workers have promoted alkali-activated binders as a potentially low-carbon cementing system during the past decades (see Section 2.11 for more detailed discussion of advances in the environmental assessment of these materials), increased scrutiny has fallen on the selection of the activator for use in these binders. This also has cost implications: the activator is usually the most expensive component of an alkali-activated binder, particularly if it has been produced at high purity for use in other industry sectors (which is the case for most commercial alkali silicate solutions), where such high purity may be less important to its use in alkali-activation. So, alternative routes to alkali-activation that do not require the use of large volumes of commercial sodium silicate solutions have received serious recent attention. The production of silicate activators from olivine [6] or from waste glass [7-10], and the use of biomass ashes as an alkaline activator [11], have been established with some success.

The use of near-neutral salts as activators has also seen considerable advances in recent years. This appears to be a pathway that is particularly attractive for production of cements based on ground granulated blast furnace slag, which can be made to react and harden in a useful timeframe by the addition of alkali carbonates or sulfates [12, 13]. In some cases, significant benefits can be gained by using a calcined layered double hydroxide as a carbonate-binding mineral additive [14, 15], to accelerate the reaction of some slags with a modest magnesia content which would otherwise not react sufficiently rapidly with near-neutral salt activators. The combination of calcium hydroxide and potassium carbonate has also been shown to give very good performance as an activator for kaolinite [16], offering a potentially very low-carbon emissions route to the production of affordable binders without needing a clay calcination step.

2.1.2 Precursors

The selection of precursors available for use in alkali-activation has also broadened significantly in recent years, with particular emphasis being placed upon the use of materials for which there is not strong competition in demand from utilization in blends with Portland cement. For example, calcined non-kaolinitic clays [17-20], palm oil fuel ash [21, 22] or other minerals [23-26], have been shown to yield alkali-activated binder systems with technical properties that are attractive in given applications. Various industrial by-products or wastes without current large-scale utilization as supplementary cementitious materials have been tested and validated for use in alkali-activated binders, including red mud [27-29] and various glassy wastes including slags, some of which can benefit from thermal re-processing or modification to improve their reactivity before use [10, 30-35]. Detailed work is also ongoing to better understand the reactivity of fly ashes under alkali-activation conditions [36-39], and to valorize kaolinitic clay resources which are not of sufficient purity for use in other applications such as ceramic whitewares or coatings [40-42]. Common to many of these types of materials, the role of iron in alkali-activation precursors (and in the resulting binders) is beginning to be understood to some degree [19, 43, 44]. However, a detailed description of its reactivity and the structural implications of its inclusion in the binding gel still remain very much elusive. This is an area in which further advances are expected – and needed – in the coming years.

Some of the potential precursors described here and in the broader literature are only available in commercially viable quantities in limited locations - but in the locations where they are available, utilization in alkali-activated binders can be extremely attractive as a local solution to the needs of the construction industry. This ability to achieve local specificity in materials design and specification highlights one of the key strengths of alkali-activation, which is its ability to make use of a wide (and ever-growing) range of materials as precursors. However, it also raises challenges in standardization and specification, as it is almost impossible to write a prescriptive recipe-based standard that covers such a broad set of potential material chemistries. This highlights the need for performance-based specification of alkali-activated binders rather than relying on a prescriptive approach; discussion will return to this point in Section 2.10 in consideration of durability.

2.2. Rheology

An understanding of the rheological properties of alkali-activated cement pastes, mortars and concretes is essential to ascertaining their consistency and workability, and consequently their ease of casting or placement. In addition, the rheological properties of alkali-activated cement-based materials have a strong influence on their microstructure, mechanical properties, and durability. The identification and modeling of rheological characteristics of alkali-activated materials (pastes, mortars and concretes) have been intensively studied since the last ICCC, as this has been identified as an area with major practical importance (and challenges) for the field application of these materials.

The rheological behavior of alkali-activated slag (AAS) pastes, activated with NaOH alone or in combination with Na_2CO_3, was similar to the rheology observed in Portland cement pastes and could be fitted by the Bingham model. Conversely, the AAS pastes activated with waterglass (AAS-Wg) required description by the Herschel-Bulkley model, as shown in Fig. 1 [45]. Moreover, their rheology depends on both the SiO_2/Na_2O ratio of waterglass and the Na_2O concentration of the activator. The early-age formation of a C-S-H type gel in silicate-activated AAS due to the reaction between silicate species in waterglass and Ca^{2+} as it dissolves from slag particles, and the effect of this gel formation on the paste rheology, has been confirmed in several publications [3, 4].

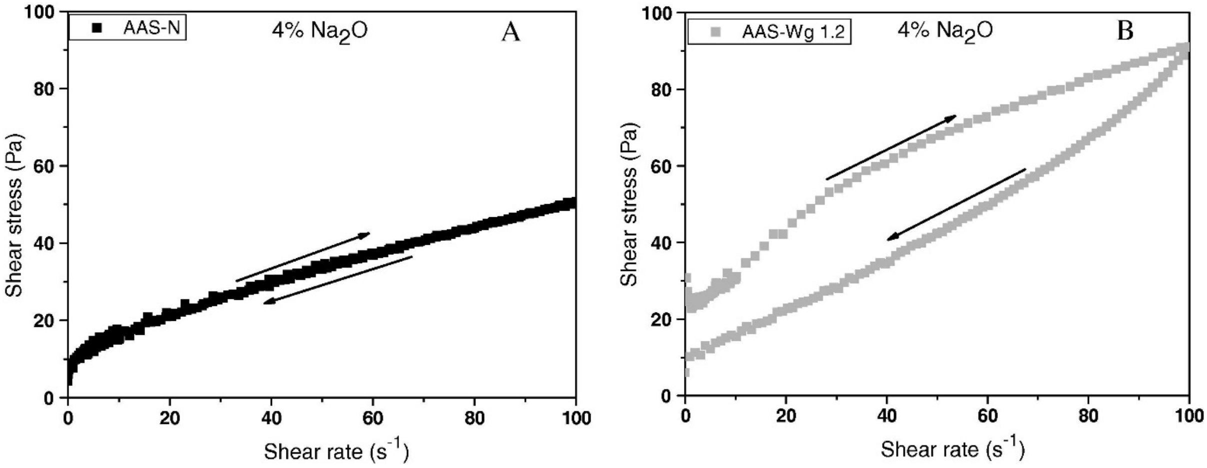

Figure 1. Shear stress versus shear rate curves showing paste hysteresis cycles: (A) NaOH-activated paste (AASN); (B) waterglass-activated paste (SiO_2/Na_2O=1.2 in the activator; AAS-Wg). Reproduced from [45].

The high viscosity of alkali silicate-activated cements, sometimes also accompanied by a high yield stress, is one of the critical challenges that hinder their wide application. Favier et al. [46] identified that this high viscosity was intrinsically due to the use of a viscous alkaline silicate activating solution, not controlled by interparticle contacts. Yang et al. [47] focused on ameliorating the rheological performance of sodium silicate-activated fly ash/slag pastes using fly ash microspheres as an inorganic dispersing agent. Rheology is also temperature-dependent; Mehdizadeh and Najafi Kani [48] determined an "apparent activation energy" parameter from the temperature dependence of the rheology of alkali-activated phosphorous slag (AAPS) paste, based on the Arrhenius viscosity model, and determined an activation energy of 42 (± 3) kJ/mol for the temperature range 10-40°C, which was of a similar magnitude to the equivalent parameter determined for Portland cement pastes.

The nature of the mixing protocol has been identified to be a key determinant in AAS mortar and concrete rheology. In a series of studies, the Bingham model gave a good fit for all the PC and AAS mortars and concretes tested [49, 50]. A longer time of mixing had an adverse effect on rheology, but gave a slight improvement in hardened performance. In AAS-Wg concrete, the application of a longer mixing time can enhance the rheological behaviour and improve the mechanical properties, as the input of mixing energy can partially break down the early-stage microstructure to allow further reaction to continue. A longer mixing time raised the degree of thixotropy in PC and in NaOH-activated slag concretes, which can be attributed to the formation of fine particles induced by over-mixing, but decreased flocculation and lowered the degree of thixotropy in sodium silicate-activated slag concrete.

Alkali-activated materials (AAMs) have also been proven as useful model systems for the testing and validation of mini-slump [51] and creeping sphere [52] rheological measurement methods. Each different approach to rheological testing, including but not limited to these methods, brings access to different shear rate regimes and different shear histories in the sample, which can enrich the understanding of time-dependent rheological processes in a complex fluid. Understanding the time-dependence of the rheology of alkali-activated pastes is not straightforward [53, 54], as these materials tend to be thixotropic in addition to the reversible non-Newtonian aspects of their behavior, but it is often challenging to distinguish true thixotropy from the gel structural evolution that is also taking place during the rheological measurements.

2.3. Chemical Admixtures

Related to the challenges of rheology control in AAMs, it has been identified that it is critically important to improve the use and applicability of admixtures to improve rheology under alkali-activation conditions. Due to the very significant differences in surface chemistry, zeta potential and dissolution mechanisms when comparing alkali-activation to Portland cement hydration [55, 56], it is important to design organic molecular architectures that are specifically applicable in alkali-activated binders. Recent efforts [57, 58] have demonstrated important progress in this regard, including demonstration of an allyl ether-based PCE with short side chains that gave extremely effective plasticizing performance in an NaOH-activated slag paste at a dose as low as 0.05 wt.% [57]. Keulen et al. [59] also showed that a proprietary PCE admixture could dramatically increase both the slump and the slump retention of alkali-activated fly ash-slag blended concretes, as shown in Fig. 2.

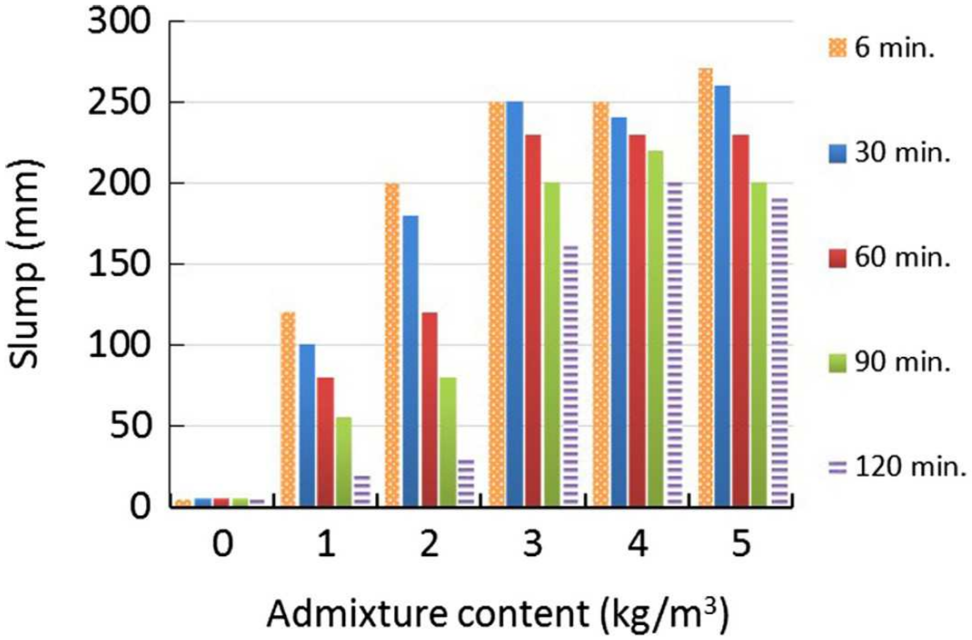

Figure 2. Slump and slump retention of alkali-activated concretes (binder 73.7% fly ash, 25% BFS, 1.3% $Na_2SiO_3{\cdot}5H_2O$ powder; activator 3 M NaOH) as a function of PCE admixture dose. Reproduced from [59].

There has also been important work aimed at improving the open working time of alkali-activated concretes and grouts, which is problematic in some applications due to the relatively rapid workability loss that is shown by some alkali-activated mixes (including in cases where workability can be lost even though setting is not unduly rapid). This will be discussed further in Section 2.4. Many chemical retarders for PC are not compatible with AAMs [60], but citric acid [61], *d*-gluconic acid [62], borate and phosphate [63] have all been described to give useful retardation in specific cases. However, the appropriate selection of a retarder depends critically on the role and content of calcium within the alkali-activation process; high-calcium mixes tend to be more effectively retarded by small organics that can complex Ca^{2+} as it is released from the solid precursor and thus delay the precipitation of C-A-S-H type gels, whereas low-calcium mixes appear to be more amenable to the use of inorganic retarders. Although care is required to select admixtures that can give retardation without loss of some percentage of the final strength development, it is not always straightforward.

2.4. Setting time

The setting time of an alkali-activated material (AAM) is a critical performance parameter that affects its practical application. The practical ability to control setting time of alkali-activated binders can determine the time window available for mixing, transportation, and casting of concrete. However, fast setting is a feature of AAS-Wg based materials; the setting time of this type of binder is often less than 30 min [64]. Setting behavior is affected by many factors, such as raw materials, specimen preparation and process conditions, as well as the use of additives as discussed in section 2.3. Lower-calcium alkali-activated binders have been identified to set through a gel percolation process [65], distinct from the localized precipitation of C-A-S-H type gels that characterizes the early stages of slag alkali-activation. This distinction brings important new abilities to understand and manipulate the setting processes of each binder type.

Li et al. [66, 67] found that the setting times of alkali-activated slag-fly ash and alkali-activated slag-metakaolin pastes were prolonged with increased fly ash or metakaolin contents. Li et al. [64]

summarized the setting times of slag-based AAMs designed in the SiO_2-Al_2O_3-CaO system with a single activator (sodium silicate of modulus 1.4), as shown in Fig. 3. They found a general trend that the setting time decreased with increasing CaO content in the SiO_2-Al_2O_3-CaO system. The role of Ca (and correspondingly also Mg) as a network modifier in the slag glass leads to more rapid dissolution of these precursors, whereas fly ash does not show the same degree of reactivity as it is a more chemically durable glass. However, when comparing blast furnace slags of different chemistry, the ability to use a single indexing parameter to predict reaction kinetics (as measured by isothermal calorimetry) remains elusive [68, 69], as it is becoming clear that many parameters beyond simple glass chemistry play important roles in determining the rate of slag reaction under alkali-activation. An indexing approach that also includes particle size distribution parameters has been proposed for fly ash activation [37], but this will also require further development before it could be considered in any way broadly applicable.

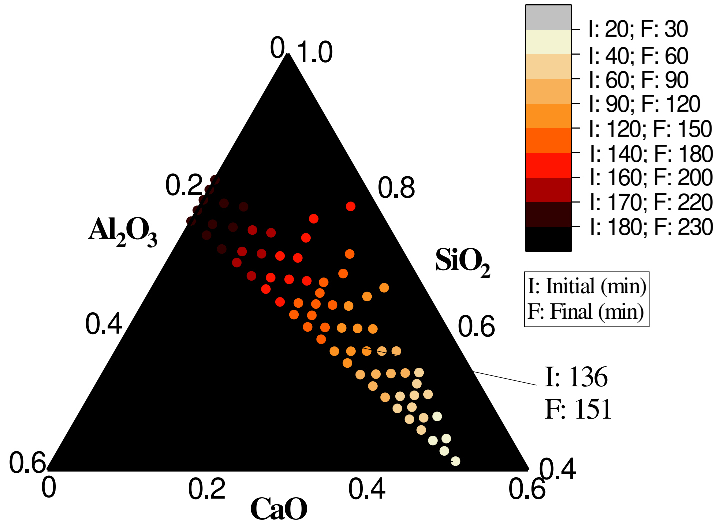

Figure 3 Setting times of AAMs (color scale, in minutes) in the SiO_2-Al_2O_3-CaO solid precursor system [64]

Careful selection and/or combination of activators is another way to manipulate the setting times of AAMs. Shi & Day [70] and Bernal et al. [13, 71] have illustrated that a prolonged induction period, which can take up to 3-5 days in some slag-based AAM systems, can be obtained when sodium carbonate is used as the activator. They showed that the Na_2CO_3 promotes the formation of calcite and mixed sodium-calcium carbonates prior to C-(A)-S-H; and that the fairly modest pH (between 11 and 12) generated from this activator gives a low rate of initial dissolution of the slag [70]. However, high-magnesia blast furnace slags do react relatively rapidly with Na_2CO_3 as an activator [14], and can under some conditions give higher early strength with this activator than with sodium silicate, when using a sufficiently high-MgO slag [72].

Li et al. [66, 67] further investigated the setting time of alkali-activated slags, and found that the setting time was prolonged with an increase in the dose of Na_2CO_3 as activator, especially when considering the final setting time and a slag of moderate MgO content, as shown in Fig. 4. The initial setting time of Na_2CO_3-AAS in that study was more than 300 min, while the final setting time was about 6 days. A wide range of setting time results were also shown in the work of Fernández-Jiménez & Puertas [73] (mortar setting time above 3 d), Kovtun et al. [74] (concrete setting time about 8 h), and Atiş et al. [75] (paste setting time about 3 h). However, a well-balanced mixture of Na_2CO_3, $Na_2O{\cdot}r SiO_2{\cdot}n H_2O$, and/or NaOH can take advantage of the influence of each of the respective anion groups present, leading to the abilty to control and tailor setting time, workability and mechanical properties [71, 76].

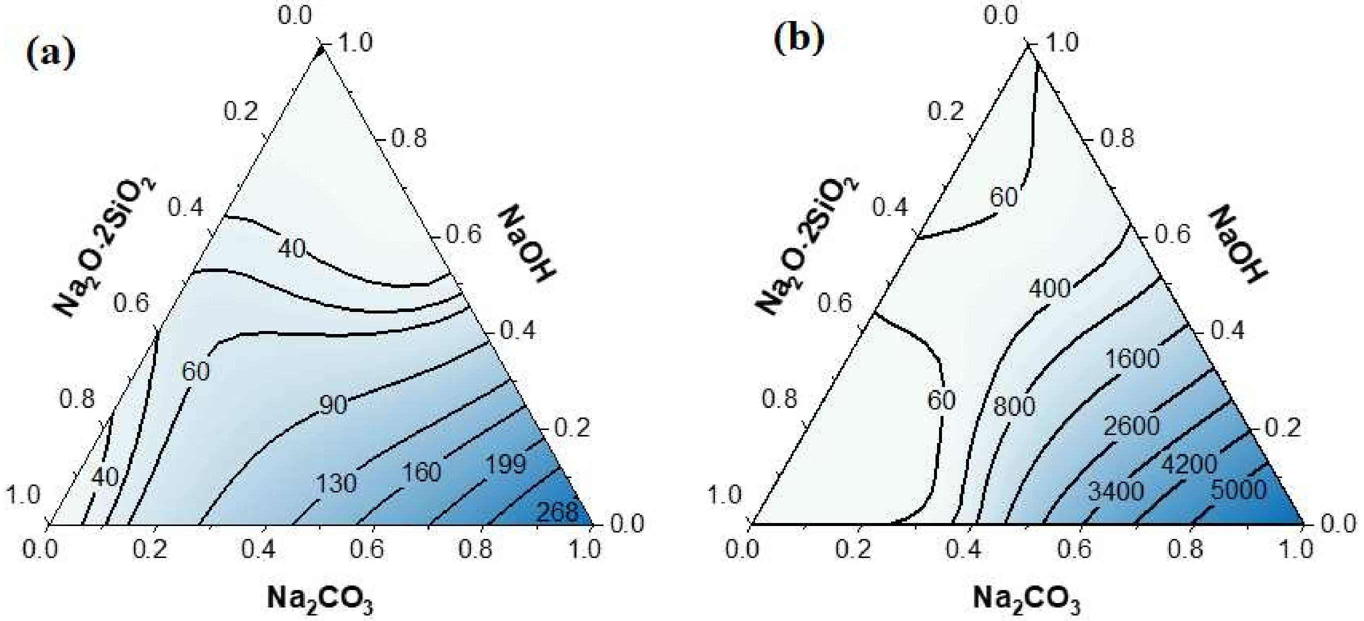

Figure 4. Contours of setting time (min) of alkali-activated slag with Na_2CO_3-NaOH-Na_2SiO_3

activators: (a) Initial setting time, (b) Final setting time [66, 67]

Garg and White [77] investigated how nano-ZnO retards the setting of alkali-activated materials, by pair distribution function (PDF) analysis and isothermal calorimetry. Fig. 5 illustrates the reaction between tetrahydroxozincate ions ($Zn(OH)_4^{2-}$) and calcium ions (Ca^{2+}) in the retardation stage, that can affect the nucleation/growth of the C-(A)-S-H type gel because Ca^{2+} is bound into a calcium zincate phase. In the other hand, nano-ZnO does not significantly influence the alkali-activation reaction of metakaolin-based binders [77], as interactions involving calcium play a pivotal role in dictating the effectiveness of nano-ZnO in retardation of AAMs.

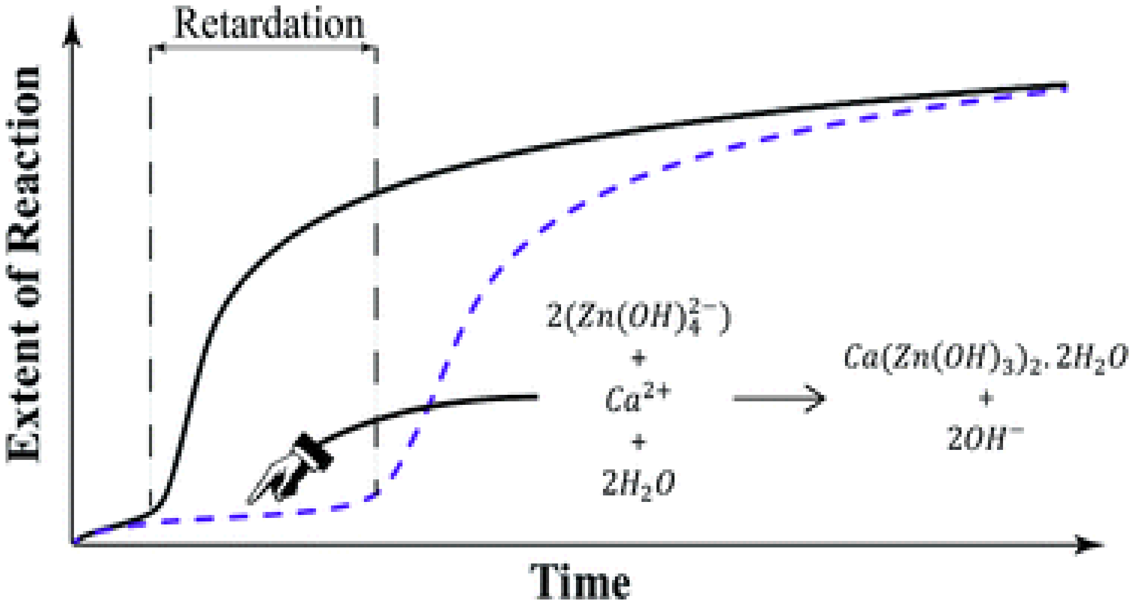

Figure 5. A schematic outline of the retardation process caused by adding nano-ZnO to alkali-activation of slag, sketched based on the discussions in Reference [77]

2.5. Structural characterization

2.5.1 Experimental approaches

In alkali-activated binder systems, as in Portland-based cements, the disordered, complex and multiphase nature of the reaction products that contribute to the main strength gain means that it is difficult to gain a full understanding of the binder characteristics from any small subset of common materials science techniques [2]. Therefore, cementitious materials (and AAMs in particular) provide fertile ground for the development and implementation of new approaches to the experimental characterization of complex materials, and the continued structural characterization of alkali-activated materials is still a key field of investigation. The C-S-H type gel (often represented as C-(N)-A-S-H) and layered double hydroxide (LDH) secondary phases that dominate higher-calcium AAMs, and the alkali-aluminosilicate (N-A-S-H) gel formed in lower-calcium AAMs, are all highly complex in chemistry, but are becoming better understood through the application of both conventional and advanced experimental analytical tools. The use of new analytical techniques as well as novel research routes during the past years has provided valuable insight into the structure of alkali-activated binders, and there is no evidence to suggest that major advances in this area are likely to end any time soon.

There has been much recent focus on the factors affecting aluminum and alkali uptake into the C-S-H structure by analysis of synthetic gels. The full details of this work are beyond the scope of the current review, and an excellent overview was provided in a paper presented at the 2015 ICCC [78]. A low Ca/Si ratio favors the incorporation of Al(IV) into C-S-H gel, whereas a high Ca/Si ratio results in more octahedrally coordinated Al(VI) [79, 80] that is predominately present in "third aluminate hydrate" (TAH) and in AFm phases [81]. High Al and alkali content, as in the case of many AAS binders, leads to co-existence of C-A-S-H and N-A-S-H type products, although these two gels can be very difficult to distinguish and isolate from each other unless detailed structural models are applied to aid in the interpretation of spectroscopic data [82]. Cross-linking within the C-A-S-H type structure has also been identified as playing a key role in the structural description and understanding of the binding phases formed in high-Ca AAMs [82-84]

Nuclear magnetic resonance (NMR) spectroscopy is now well known as a key technique to track the information on the local bonding environments of silicon and aluminum atoms. The structure of C-(N)-A-S-H gel has been described by various groups [83, 85-88]. However, NMR has a limited capacity to assess medium range ordering. X-ray and neutron pair distribution function

(PDF) analysis are now well established as techniques for understanding the gel structure formed in alkali-activated binders, due to the ability of the PDF technique to probe the local atomic structure of disordered materials [89], although the analysis of multi-phase materials by this technique remains very challenging. Gong & White [90] used X-ray total scatting and PDF analysis to study the impact of chemical variability on phase formation in alkali-activated granulated blast-furnace slag (GGBS). The primary reaction product after alkali-activation was C-(N)-A-S-H gel with a highly disordered structure, and PDF analysis revealed that atomic arrangements, as shown in Fig. 6 for the short-range ordering < 5 Å, in the C-(N)-A-S-H gel differed depending on the chemical composition, especially the calcium content, of the raw material. The gel connectivity of C-(N)-A-S-H gel increased with decreased calcium content, as shown in Fig. 6, represented to a first approximation by the intensity of the peak just above 3 Å assigned to Si-Si/Al and Mg-Al correlations. Magnesium in alkali-activated GGBS pastes is primarily incorporated in the secondary reaction product, which is a hydrotalcite-like phase, as will be discussed in more detail below. In-situ X-ray total scattering measurements and PDF analysis are also starting to be widely used in the study of alkali-activated binders, as one of few techniques that can give time-resolved information about gel local structure during setting and hardening [91-93].

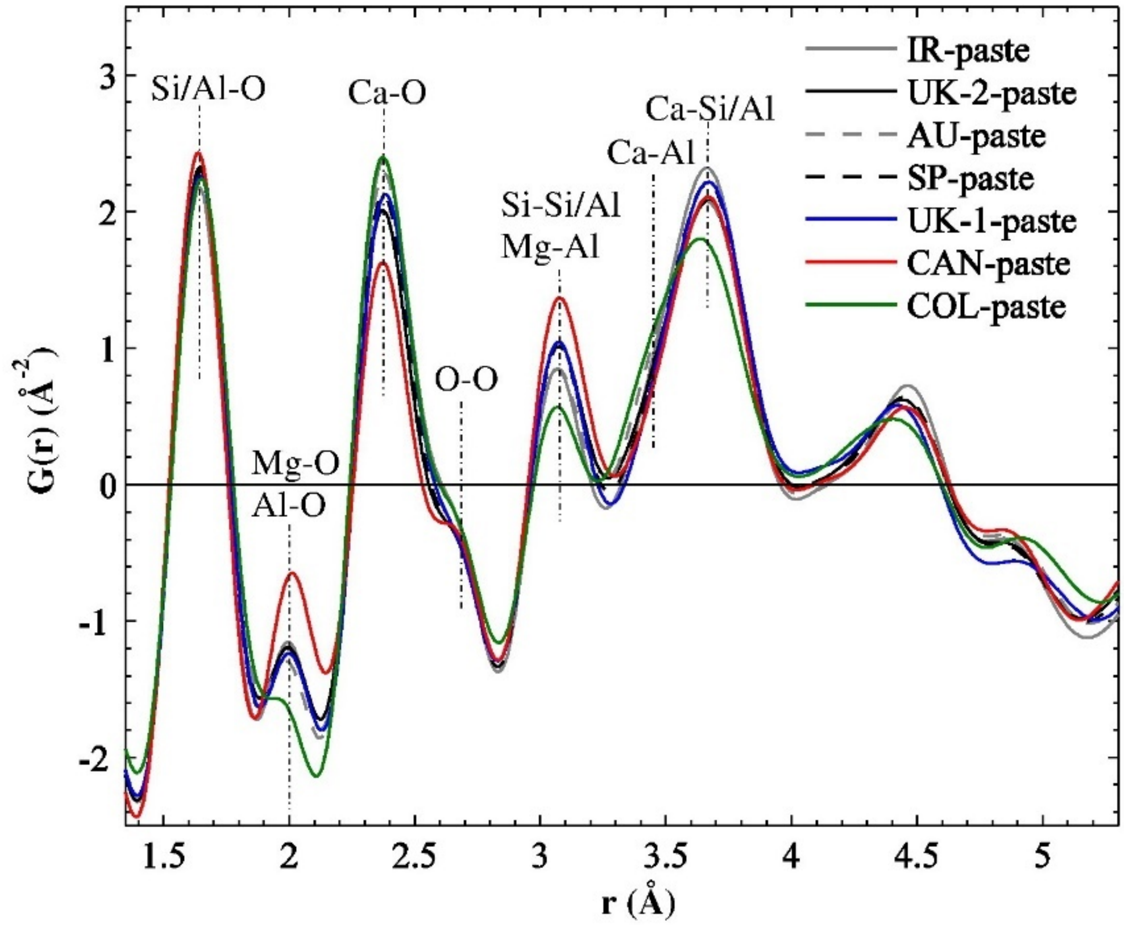

Figure 6. X-ray PDFs of pastes produced from hydroxide-activated granulated blast-furnace slags (slags from different sources as noted in the legend), showing the short-range ordering (< 5 Å) [90].

A method to investigate the chemistry of aluminosilicate-based cementitious binders by alkali-activation of high-purity synthetic amorphous aluminosilicate powder has been proposed by Walkley et al. [94]. The phase evolution and nanostructure development of these materials have been examined after activation [95, 96]. Using this information, a new structural model of alkali aluminosilicate gel (N-A-S-H) gel frameworks has been proposed based on data from solid-state nuclear magnetic resonance spectroscopy (^{17}O, ^{23}Na, and ^{27}Al) [97]. Fig. 7 shows part of the proposed conceptual model for this gel structure, with charge-balancing of the partial negative charges on bridging oxygen associated with tetrahedral Al provided by sodium and by extra-framework Al (Al_{EF}). The alkali aluminosilicate gel predominantly comprises fully coordinated (Q^4 or q^4) Si and Al units. A considerable proportion of Al^{3+} in tetrahedral coordination exists in sites of lower symmetry, where some of the charge-balancing capacity in the gel is provided by extra-framework Al species which have not previously been observed in these materials. Greiser et al. [98] conducted advanced multi-dimensional NMR analysis of N-A-S-H gels derived from various amorphous silica sources and also identified extra-framework Al sites, although contended that their results were consistent with tetrahedral Al_{EF} sites, as also noted by Brus et al. [99] rather than the octahedral Al_{EF} identified by Walkley et al. [97]. There is evidently important further work required to unravel the nanostructural details of the N-A-S-H gel structure, and multi-nuclear and multi-dimensional NMR techniques are expected to underpin and inform these efforts in coming years.

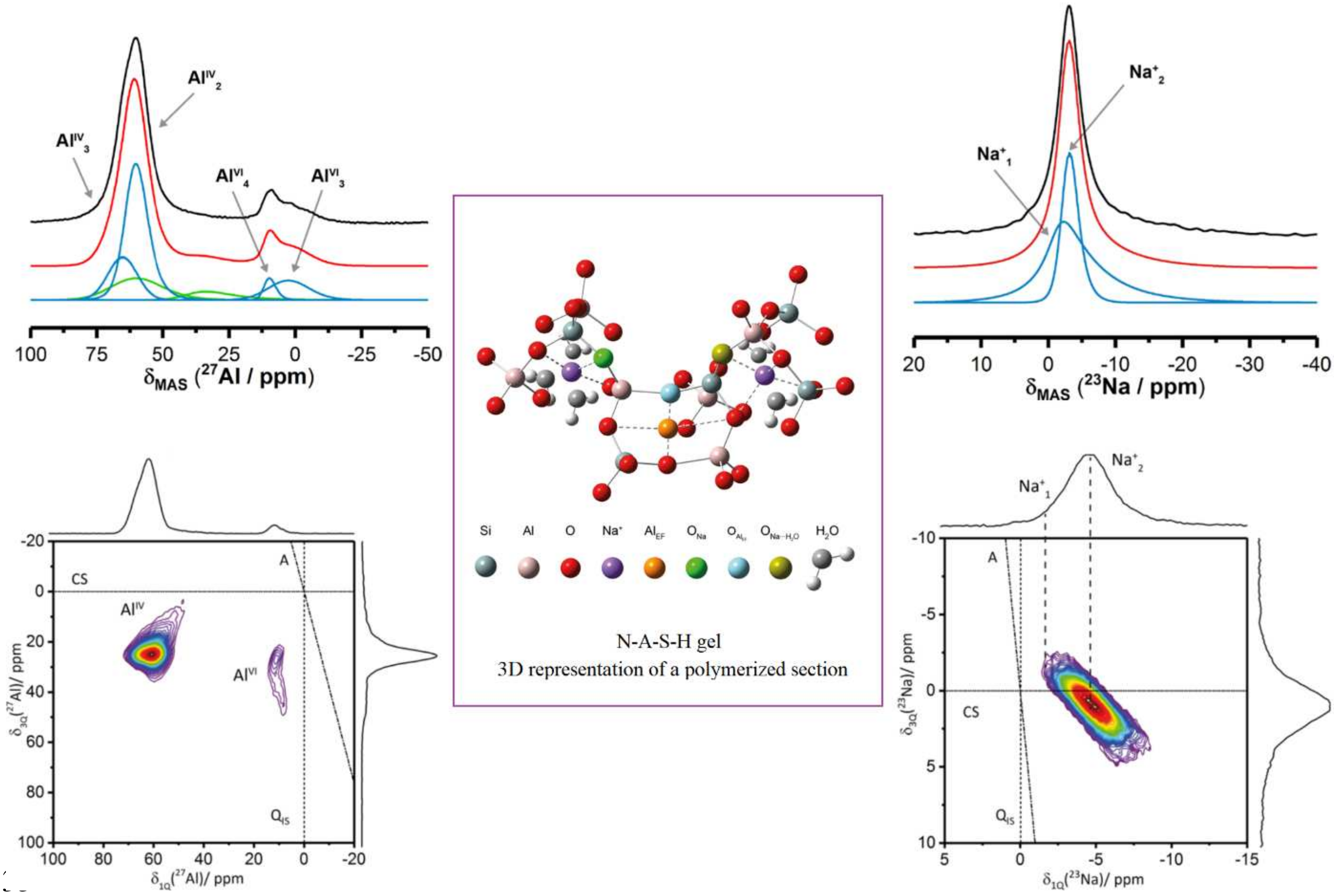

Figure 7. ^{27}Al and ^{23}Na MAS and 3QMAS NMR analysis for the gel of alkali-activated synthetic precursor (Si/Al=2), and a 3D representation of a polymerized section of the N-A-S-H gel showing various constituent environments as marked, adapted with permission from [97]. Copyright American Chemical Society.

Scanning electron microscopy (SEM), together with energy-dispersive X-ray spectroscopy (EDX), has been widely used as a powerful tool by different scholars [91, 100, 101] to track microstructural evolution in alkali-activated binders, including some important work on model systems where “microreactors” were ion-milled into slag grains and the morphology of the reaction products formed by their reaction with different alkaline solutions monitored [102]. Fig. 8 shows examples of the data that were obtained using this approach, where both the concentration and the nature of the alkaline solution led to remarkable differences in the appearance of the reaction products formed. The large platelets of hydrotalcite-like minerals and the globular C-S-H type gel are particularly evident at the highest concentration of KOH tested, but there is a clear progress of the alkali-activation reaction under all conditions depicted.

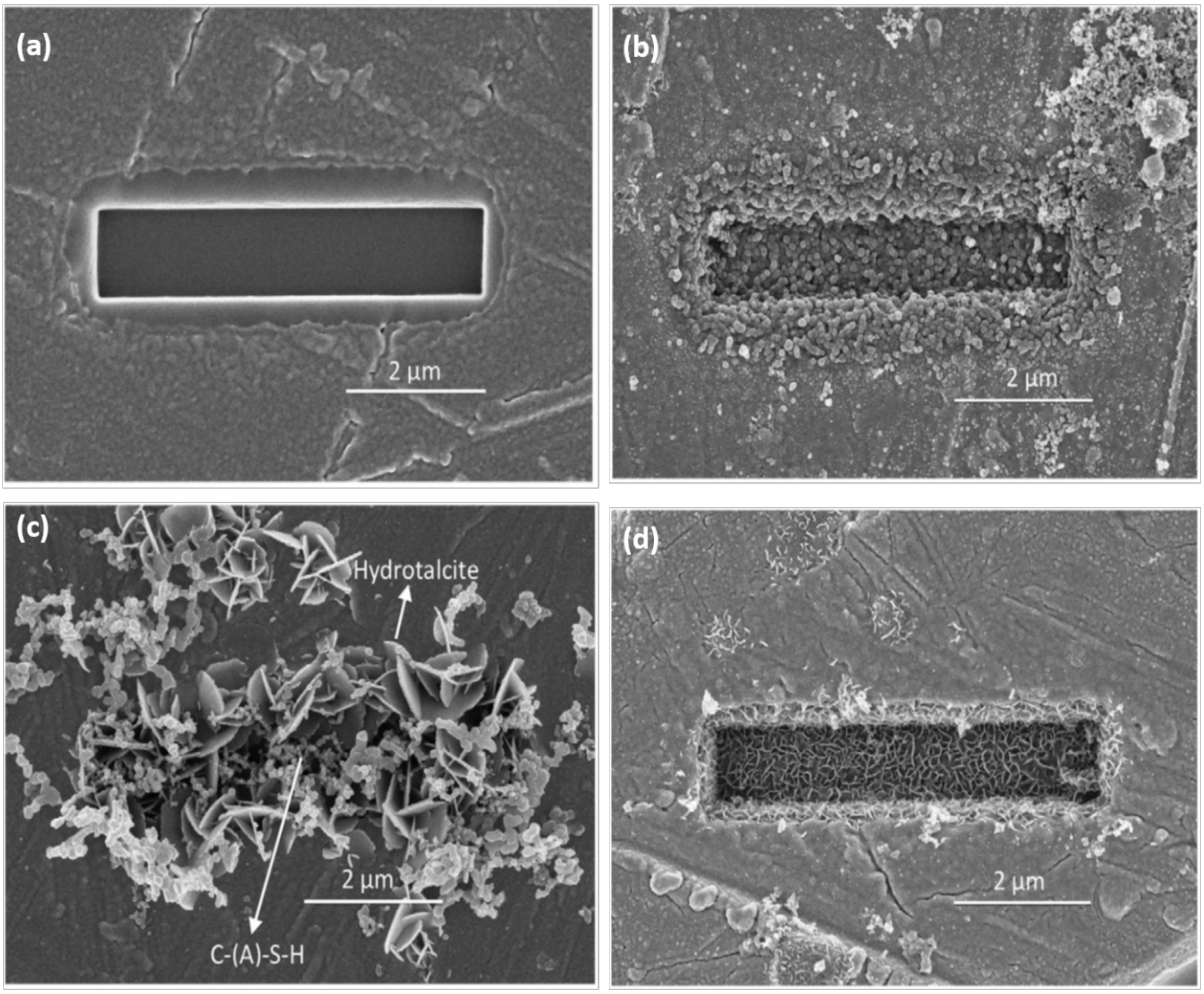

Figure 8 (a) A microreactor ion-milled into a GGBS grain; and microreactors exposed for 2 days to: (b) 0.1 M KOH; (c) 10 M KOH; (d) 1 M NaOH. Reproduced from [102]

The use of SEM as an analytical technique is very well established in the field of cementitious materials, both for imaging and for determination of elemental compositions. Particularly important information has recently been obtained regarding the Mg-Al layered double hydroxide (hydrotalcite-like) phase in alkali-activated slags. Richardson & Li [103] used SEM-EDX to determine the Mg/Al ratio in KOH-activated blast furnace slag paste after 18 years of curing; a ratio of 2.6 was determined, in excellent agreement with calculations based on XRD data for that binder. Ke et al. determined Mg/Al ratios closer to 2.0 for the corresponding Mg-Al LDH phases in Na_2CO_3-activated slag binders [14] and in Na_2SiO_3-activated slag binders [104], also using SEM-EDX, and consistent with older literature including [105] and others. This phase is often described in the cements literature as being simply "hydrotalcite", but in a mineralogical sense, true hydrotalcite has Mg/Al = 3.0 and contains carbonate in its interlayer [106], whereas the LDH phases formed in many alkali-activated binders will be carbonate-free. The carbonate-containing member of the hydrotalcite family with Mg/Al = 2 is correctly called meixnerite, whereas the carbonate-free "M_4AH_{13}" hydrotalcite-group composition, which is probably the most relevant to most alkali-activated binding systems, does not have a formal mineral name. So, the continued description of the Mg-Al LDH phase formed in alkali-activated binders as "hydrotalcite-like" seems satisfactory, but it does need to be clearly identified that this is not true hydrotalcite in the mineralogical sense.

Transmission electron microscopy (TEM) has also been applied to the analysis of alkali-activated binders with some success [103], but sample preparation for this technique remains challenging and the samples are prone to beam damage. Helium ion microscopy (HIM), a technique with some resemblances to SEM but potentially offering higher spatial resolution, was proposed by Morandeau et al. [107] for studying the nanoscale structure of alkali-activated materials. HIM involves imaging of sample surfaces by detecting secondary electrons that are excited from the sample surface by bombardment with helium ions. Spatial resolution is high due to the specific nature of the beam-sample interaction [108]. Hence, in comparison with SEM, this method is well-suited for resolving nanometer-scale surface morphologies and porosity present in rough and irregular fractured samples, including alkali-activated binders. Fig. 9 shows a selection of HIM images of AAS obtained by Morandeau et al. [107]. Finer heterogeneous morphological details have been captured. Two types of C-(N)-A-S-H gel have been identified, with the 'inner' gel showing a foil-like morphology while the 'outer' gel appearing more globular. The use of HIM with EDX analysis can provide new insight into the structure of alkali-activated materials as well as other binder systems, and although the HIM instruments are still expensive, this technique is becoming more widely available in the international community.

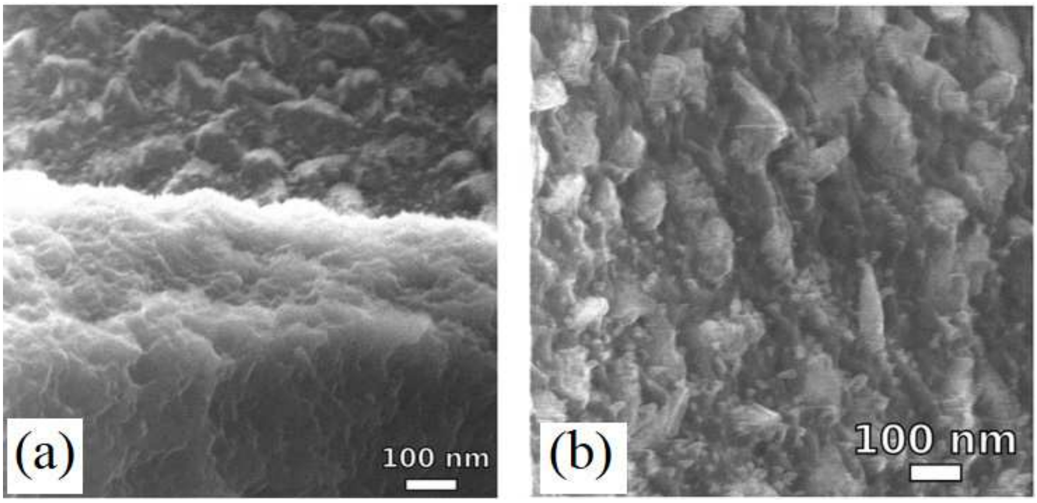

Figure 9. HIM images (a) GGBS particle covered by 'foil-like' C-(N)-A-S-H gel; (b) the surface of the concave spherical void: C-(N)-A-S-H gel. Reproduced from [107].

Scattering and diffraction-based techniques have been used to provide insight into AAMs during the initial [109-111], medium-term [112], and later-age [113] evolution of gel, crystallite, and pore structure in AAMs. The combination of neutron and X-ray scattering, applied in parallel to provide different aspects of the required information, has also given important new insight into the highly-connected nature of the pore structure in metakaolin-based AAMs [114]. The marked differences in pore geometry and its evolution with curing as a function of the nature of the alkali cation present have also been examined using the combination of PDF, small-angle X-ray scattering and electrical impedance methods [115]: the structure-forming (kosmotropic) Na^+ leads to a pore network structure that evolves considerably over a 5-year curing duration, while the pore networks generated through the use of chaotropic (K^+ or Cs^+) alkali cations are much more stable during extended curing periods [115].

Another essential aspect of alkali-activated binder chemistry that has received attention – and answers to some key outstanding questions – in recent years is the exact chemical nature of the green coloration in alkali-activated slag binders (and similarly in high volume Portland-slag blends). There has been much speculation in the past that this coloration is due to the presence of polysulfide species (resulting from the release of sulfide by slag dissolution), but the previous spectroscopic evidence was far from sufficient to fully substantiate this argument. However, Chaouche et al. [118] have recently used synchrotron-based X-ray absorption near edge spectroscopy (XANES) to demonstrate that the blue/green regions of alkali-activated (and Portland cement-blended) slag binders contain the characteristic spectroscopic features of the trisulfur (thiozonide) radical anion S_3^-, the same species that gives color to ultramarine pigments. Consistent with this, Le Cornec et al. [119] have also recently applied vibrational spectroscopy to the analysis of greening effects in 70% GGBS-30% PC blended cements, and identified spectroscopic features consistent with the confinement of various sulfur radical ions (S_2^-, S_3^- and S_4^-) within the interlayer space of LDH phases, proposed to be of the AFm family. They claimed that all three of these polysulfide species were present at similar ratios in the hydration products of various slags tested, which modifies the characteristically blue pigmentation of the S_3^- radical anion (which is the most prominent species in their spectra also), to instead give a green color [119]. This is clearly an important step forward in understanding the fundamental science of AAMs, but also has implications for understanding the role of binder redox chemistry in controlling steel corrosion processes.

2.5.2 Modelling approaches

There have also been notable recent advances made in the modelling of AAM binder chemistry by a variety of modelling approaches at different length scales. At an atomistic level, a number of molecular dynamics (MD) studies have generated model structures claiming to represent N-A-S-H gels. However, the majority of these studies have not included water in a realistic or reasonable manner, and so have generated structures of anhydrous or partially-hydrated glasses rather than anything representative of a N-A-S-H structure that could form by precipitation from an aqueous solution. Features such as edge-sharing tetrahedra and extensive Al^{IV}-O-Al^{IV} bonding, which are not observed to any significant degree in hydrous aluminosilicate minerals, can be viewed as indicators of such an unrealistic structure. An exception to this trend is the work of Lolli et al. [120], who used MD to generate correctly hydrated N-A-S-H gel structures based on three approaches: a “crystalline” structure based on adjusting the sodalite framework to the desired N-A-S-H stoichiometry; a “defective” structure generated by introducing defects into the sodalite framework and allowing this to relax (in the presence of water) using MD, and an “amorphous” structure based on SiO_2 glass adjusted to the desired N-A-S-H stoichiometry. Among these three models, the “defective” structure (Fig. 10) gave the best match to experimental PDF data, and also yielded predictions of nanoscale mechanical properties and porosity that are consistent with the available literature, while complying with the requirements for predominantly Q^4 bonding, the absence of edge-sharing tetrahedra, and agreement with Loewenstein’s principle of Al-O-Al avoidance [121]. This can therefore be considered to be a reasonably representative structural model for N-A-S-H gel at this length scale, and is consistent at a chemical level with the schematic description of the potential site types that was shown in Figure 7.

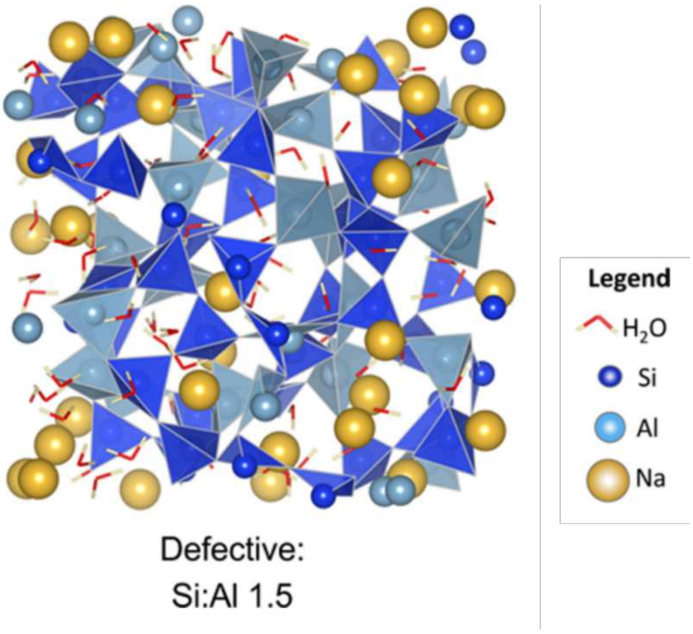

Figure 10. Representation of part of the N-A-S-H gel structure generated by application of molecular dynamics to relax a defective sodalite framework. Reproduced with permission from [120]. Copyright American Chemical Society.

At the mesoscale, Valentini [92] adapted an established code designed for Portland cement hydration simulations to describe the activation of metakaolin by different alkaline solutions, while Yang & White [122] advanced the use of on-lattice coarse-grained Monte Carlo simulations to describe activation of different aluminosilicate precursors. Modeling approaches such as these are computationally intensive and need care in parameterization and specification to ensure that atomic-scale interactions are replicated as accurately as possible on the mesoscale, but also provide unparalleled access to mechanistic and microstructural information on a length scale of up to hundreds of nanometers, which is very difficult to access experimentally in real-time.

Thermodynamic modeling of phase assemblages in AAMs has been an area of particularly important recent developments, where the application of a detailed ideal solid solution model for the C-(N,K)-A-S-H system [123] supported by the availability of improved solubility data [124] has significantly moved forward the state of the art. This has enabled advances in phase assemblage predictions for alkali-activation of blast furnace slag [125-127], including prediction of phase diagrams for a wide range of slag and activator compositions [128]. Solubility information for N-A-S-H gels [129], and improved information for aqueous species in the N-K-A-S-H-Cl system [130], are bringing the opportunity for modelling of some lower-calcium binder systems [131], although much work is still required to develop and validate the necessary range of model constituents to enable full description of the phase assemblages in these binders. In particular, the database of zeolite phases available for inclusion in models of the (N,K)-A-S-H system requires expansion, as there are significant gaps in the literature here, although constrained to some degree by issues of metastability and difficulties in actually defining "solubility" in many instances.

2.6. Microstructure and mechanical properties

The development of a detailed understanding of the microstructure and mechanical properties of AAMs is obviously key to the application of these materials in civil and infrastructure applications. In particular, it is essential to understand whether the engineering design equations that have been established for conventional concretes are also broadly applicable to AAM concretes. A detailed review of the mechanical properties of AAM concretes has been provided recently by Ding et al. [132], and the full scope of that review will not be repeated here. However, it should be noted that in many cases, the general functional forms of relationships that work well in describing the characteristics of Portland cement-based concretes also appear valid for AAM concretes, but some re-fitting of parameters seems necessary.

Analysis of the stress-strain characteristics of AAM concretes has tended to show that these materials show a higher tensile strength, lower modulus of elasticity, and lower Poisson's ratio than conventional Portland cement concretes, as reported by e.g. [133-135] and many others. Thomas and Peethamparan [136] also showed that the specimen size effect in compressive strength testing of AAM concrete cylinders was well described by the established models for Portland cement in the case of AAMs based on GGBS, but observed an unexpectedly strong size effect in AAMs based on fly ash. This was attributed to microcracking effects in the fly ash–based binders; microcracking of AAMs is certainly an area requiring more detailed analysis, and will be revisited below (section 2.8) in the discussion of dimensional stability. The creep of AAM concretes also requires further attention. There are indications that although the early-age creep of these materials resembles that of Portland cement-based concretes, the deceleration of creep over extended timeframes may be less dramatic in AAM concretes, meaning that longer-term creep processes must be taken into account in structural design procedures [137]. AAMs have also been observed to have a higher fracture energy [138, 139] and a more compact interfacial transition zone [138, 140] than comparable Portland cement-based materials, and undergo a more localized cracking process [141]. The strong aggregate-paste bond also gives relatively high fatigue resistance [142, 143].

An important finding underpinning much of the analysis of AAM property-microstructure relationships was the identification by Winnefeld et al. [68] that the degree of reaction of the blast furnace slag precursor appears to be a characteristic parameter which controls strength, across a range of slag sources and activators. It is quite probable that this relationship is critically dependent on the pore structure of the AAM binder; Ranjbar et al. [144] obtained strengths of over 130 MPa by hot-pressing fly ash-based AAMs to reduce porosity, while Rouyer et al. [145] showed a clear relationship between Young's modulus and pore volume of a range of metakaolin-based AAMs. Blyth et al. [146] also showed orders-of-magnitude differences in intrinsic permeability between hydroxide-activated and silicate-activated slag binders, but without a corresponding difference in the Young's modulus, which was attributed to a very marked reduction in the characteristic pore diameter upon silicate activation. Bernal et al. [147] also reported a surprisingly low dependence of mechanical properties on total pore volume in alkali-activated slag mortars, where water/binder ratios of 0.40 and 0.44 gave similar 28-day strengths and identical 56-day strengths. Babaee and Castel [148] used water vapor sorption as a sensitive probe of pore structure in blended fly ash-slag AAMs, distinguishing the very fine pores which dominate slag-rich pastes from the mesoporous nature of fly ash-rich binders. Hu et al. [149]

reported that the compressive strength of alkali-activated slag/fly ash mortar is mainly affected by total porosity and porosity of capillary pores, with sizes ranging from 10 to 10^4 nm. The change of pore structure in the mortar was strongly influenced by the activator silicate modulus, alkali dosage and fly ash content.

2.7. One-part alkali-activated binders

One-part ('just add water') alkali-activated materials can be treated as an important step towards to the commercial-scale development of these low-carbon binders. A new review on one-part AAMs has been published [150] which included systematic analysis of the available literature, so the current paper will not attempt to repeat the full scope of that review, which covered one-part AAMs in respect of raw materials, admixtures, optimum calcination, composition, curing conditions, and mechanical strength. Fig. 11 illustrates the general procedure to prepare one-part AAMs by adding water to a dry mixture of solid alkali-activator and a solid aluminosilicate precursor, including a calcination step if necessary. This technology has been considered as a method to face some technical challenges related to conventional (two-part) AAMs, in particular the question of how to handle large amounts of activator solutions which may be viscous, corrosive, and/or hazardous, on site in a construction application. It should be noted that the pH of most alkali-silicate activators is actually similar to that of fresh Portland cement paste, but the fact that these may need to be stored and handled in large quantities by personnel who are not specialized in chemical handling is nonetheless an important reason to drive forward the development of one-part AAMs.

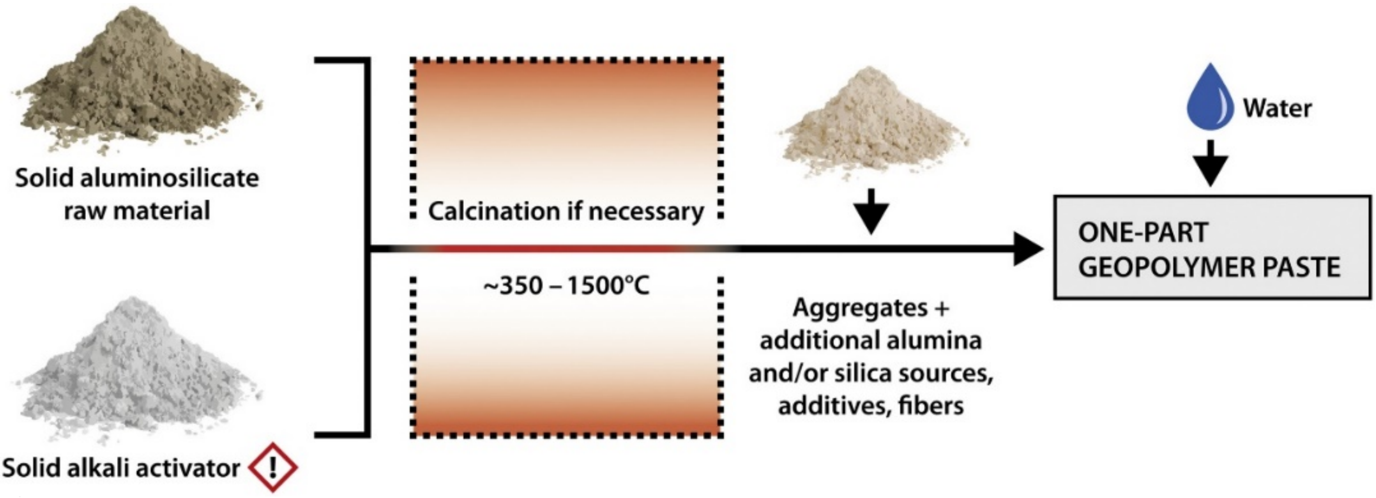

Figure 11. The general procedure of one-part AAM (geopolymer) preparation. From [150].

In one-part alkali-activated binders, any substance that dissolves sufficiently rapidly, and offers alkali cations and provides a high pH environment to facilitate dissolution of the aluminosilicate precursor, can in principle be used as an activator [151]. Sodium metasilicate powders ($Na_2SiO_3 \cdot xH_2O$, $0 \leq x \leq 5$) has been studied as a solid activator in one-part alkali-activated binders [152-154]. Anhydrous sodium metasilicate was reported to contribute to higher compressive strength and better workability than its hydrous counterparts when used to activate fly ash and blast furnace slag-based binders, and is available commercially in the form of spray-dried powders that appear quite amenable to use in alkali-activation processes at an acceptable cost.

Hybrid alkaline cement, where Portland cement and an alkaline activator are added in parallel, can also be regarded as a type of one-part AAM binder. The nanostructural evolution of these cements has been presented by García-Lodeiro et al. [155] via a descriptive model. Fernάndez-Jiménez et al. [156] investigated the hydration mechanisms of fly ash-based alkaline hybrid cement as a function of the nature of the activator as it was supplied in different forms (solid and liquid). When solid sodium sulfate was used as the activator in hybrid binder systems, slightly higher mechanical strength and less AFt and AFm phases were obtained than when it was added as a liquid. Both early age reaction kinetics and the nature of reaction products were influenced by the form of addition of the activator.

Various different precursors, and combinations of precursors, have been validated for use in one-part AAM binders. In addition to the more commonly used GGBS [157, 158], fly ash [159, 160] and calcined clays [161], there has also been meaningful work dedicated to the development of one-part AAMs from industrial waste silicas and $NaAlO_2$ [162][163], and red mud [164, 165]. In many of these binder systems, a careful balance needs to be drawn between adding sufficient alkalis to enable rapid strength development, and avoiding the excessive alkali levels that may lead to efflorescence. Ongoing work to understand the causes and implications of efflorescence in both one-part and two-part AAM binder systems [166-168] is certainly necessary to underpin the development and deployment of one-part AAMs.

Qu et al. [169] produced a pre-industrial hybrid alkaline cement, manufactured in a Latin American plant on a scale of around 20 tons. The proportions used were 30 % Portland clinker + 32.5 % blast furnace slag + 32.5% fly ash + 5% solid activator (the main salt is Na_2SO_4). This hybrid alkaline cement was showed to react with water at ambient temperature and reached a compressive strength around 32 MPa at 28 days, with acceptable setting time and early strength. Further, the cement paste was tested at up to 1000°C, and showed better high-temperature resistance than Portland cement due to the recrystallization of new poorly hydraulic phases, mainly in gehlenite- and rankinite-type phases [170, 171]. Velandia et al. [172] also demonstrated the production of concretes with good performance using a hybrid fly ash-Portland-Na_2SO_4 binder, and provided extensive data about the durability performance of these concretes, including correlations between key durability parameters and compressive strength at ages of up to 1 year.

2.8. Dimensional stability

The dimensional stability of any cementitious binder is a critical factor in determining its use in engineering applications, as concretes are required to neither shrink nor expand excessively in service. The relatively low level of bound water present in AAMs, particularly those with low calcium content, has been observed to cause some susceptibility to drying shrinkage, as has recently been reviewed by Mastali et al. [173]. This area has attracted a high degree of attention in the literature in recent years, as the importance of understanding and controlling shrinkage has become more and more evident. Low-calcium AAMs do not self-desiccate during curing in the same manner as does Portland cement during its hydration [174], as there is not such a strong chemical driving force withdrawing water from the pore fluid into solid phases. However, they do undergo autogenous shrinkage which can lead to early-age cracking if not appropriately controlled [175].

Higher-calcium AAMs such as sodium-silicate activated GGBS can self-desiccate, in part due to the formation of hydration products, and also because the high ionic strength of their pore solution reduces water activity to draw the relative humidity below 100% [176]; this latter effect is likely to be the cause of any observed self-desiccation effects in lower-calcium binders that do not chemically incorporate water of hydration. Ye & Radlińska [177] proposed that the drying shrinkage of alkali-activated GGBS involves densification of the C-(N)-A-S-H as its structure is damaged by reductions in relative humidity, as neither the moisture loss nor the drying shrinkage were reversible upon soaking of dried specimens. Shrinkage mitigation strategies similar to those that are implemented in conventional Portland cement have been evaluated recently for application in AAS {Ye, 2017 #741}. Chemical shrinkage of alkali-activated GGBS and GGBS-rich blends has been studied experimentally [178] and also identified through thermodynamic modeling [125, 127]. Thomas et al. [179] identified a beneficial role for heat curing in reduction of drying shrinkage, while Gao et al. [180] applied a particle packing model at paste scale to optimize blends of GGBS and fly ash for minimum porosity and shrinkage. The shrinkage properties of alkali-activated binders based on different blended precursors have also been reported [181, 182]. Shrinkage-reducing admixtures [183-186] and super-absorbent polymers [187-189] have also shown some effectiveness in reducing drying shrinkage, as has the tailored design of blended activators [190]. While shrinkage control in AAMs does remain an area of open research, with many questions yet to be answered, the fact that this broad range of approaches have all shown some potential for success is a strong indication that this is not an intractable issue.

2.9. Durability

The durability of alkali-activated binders, and concretes produced from them, has been reviewed in various publications [151, 191-193]. In most cases, AAMs have been tested according to methods devised and validated for the testing of Portland cement-based binders; there are ongoing discussions around whether this is entirely appropriate, including through the work of a RILEM Technical Committee [194, 195], and it appears that in the majority of cases there are details of the standard testing methodologies that will require modification if they are to give truly meaningful results for AAMs. Sample preconditioning has been highlighted as an area requiring particular care when designing tests for AAMs, as some of these materials can be damaged by the preconditioning regimes that are often applied to Portland cement-based materials before testing, particularly when very vigorous drying is applied [93, 196-198]. A performance-based specification designed specifically for application to AAMs has been released in the UK, based on minimal adaptations to established Portland cement testing methodologies [199], and efforts are also ongoing in other countries and through multinational collaborative programs; it is expected that this will be an area of rapid development in the coming years.

It has long been identified that binder carbonation under exposure to CO_2 is an area of durability that requires careful consideration when designing and specifying AAMs. Early accelerated testing at high CO_2 partial pressures appeared to show that alkali-activated binders would be very susceptible to carbonation, but this was not directly matched by observations under natural conditions. The reasons for the sometimes very poor performance of AAMs under accelerated carbonation exposure is now understood to be related to specific changes in the carbonate-bicarbonate equilibrium of the AAM pore solution at elevated CO_2 partial pressures [200]. This can give an unrepresentative reduction in pH compared to natural carbonation exposure, which has been shown to give a much less marked reductions in pH [201, 202]. Relative humidity control during carbonation testing has also been shown to be highly influential in determining the observed rate of carbonation [203].

The carbonation of AAMs has been shown to be strongly dependent on binder microstructure, and particularly the degree of microstructural evolution and pore network refinement achieved prior to the start of carbonation exposure, which can be influenced by curing, as well as various mix design parameters such as the activator dose [204-207]. The presence of hydrotalcite-type LDH phases has been identified as being particularly crucial in enabling carbonation resistance, whether these are produced directly as a result of activation of an Mg-containing precursor, or due to the addition of a supplemental Mg source (or calcined LDH as a seeding/templating agent) [208] [15, 209, 210]. The mechanisms of carbonation shrinkage in alkali-activated slag binders have also been identified [211]. Together, these new aspects of insight provide essential steps toward designing AAMs that can appropriately resist carbonation in service, and also in understanding the connections between accelerated and natural carbonation mechanisms to enable the design of appropriate laboratory tests for the prediction of field performance. Electrochemical examinations of carbonated AAM concrete showed that the binders have been capable of keeping the reinforcement in a passive condition even with the lowered pH caused by the accelerated carbonation [212, 213], but this does necessitate further investigation.

In many steel-reinforced concrete applications, the service life of a structure or element is governed by the ability of the concrete to protect the steel from chloride-induced corrosion. The rate and mechanisms of chloride transport in AAMs have been reviewed in detail by Osio-Norgaard et al. [214]. Thomas et al. [215, 216] have provided a comparison of chloride test methods as applied to these materials. Hu et al. [144] found that some alkali could leach out during specimen saturation before the electrically accelerated chloride transport test, and that the water-to-specimen ratio could have a critical effect on the passed charges, but not on the chloride migration coefficient of the specimens. This is an active area of work in international organizations including RILEM and the European Federation for Corrosion, who have established working groups to investigate chloride transport and corrosion initiation in AAMs, with a particular view toward the development of more appropriate testing methods. Noushini and Castel [217] have recently discussed the development of performance-based criteria for AAM concretes based on chloride ponding and electrochemically accelerated tests, which is an essential step toward performance-based standardization of AAMs. For electrochemical testing, it also appears likely that the proportionality constants applied in the relationships that are commonly used to obtain material parameters from polarization curves (Tafel slopes) for Portland cement will need to be re-assessed for AAMs, as there appear to be significant deviations from the classical electrochemistry of Portland cement when considering the particular pore fluid chemistry of AAMs [218].

Chloride binding, particularly by hydrotalcite-type LDH phases, has been identified by some authors to be very influential in determining chloride transport through AAMs [219, 220], although other authors did not identify strong evidence for chloride binding in alkali-activated slag concretes [215, 221]. There is a clear need for further developments to resolve this open question, which is of fundamental importance to service life prediction for reinforced AAMs under chloride exposure.

Ma et al. [222] linked chloride diffusivity, electrical resistivity, and corrosion testing of reinforced alkali-activated concretes, and highlighted the importance of sulfide (provided by blast furnace slag when used as a precursor in AAMs) in defining the corrosion rate post-initiation. The role of sulfide has also been identified in studies of steel corrosion in simulated alkali-activated slag pore solutions [223-225] [226], and in various types of mortar specimens [227-229]. The very high pore solution pH of some AAM binders has also been shown to generate unconventional threshold-like relationships in chloride initiation, and also to give chemical protection of steel reinforcement even at high chloride concentrations [230-232]. Mundra et al. [226] also developed a classification scheme for alkali-activated and slag-blended binders as shown in Fig. 12.

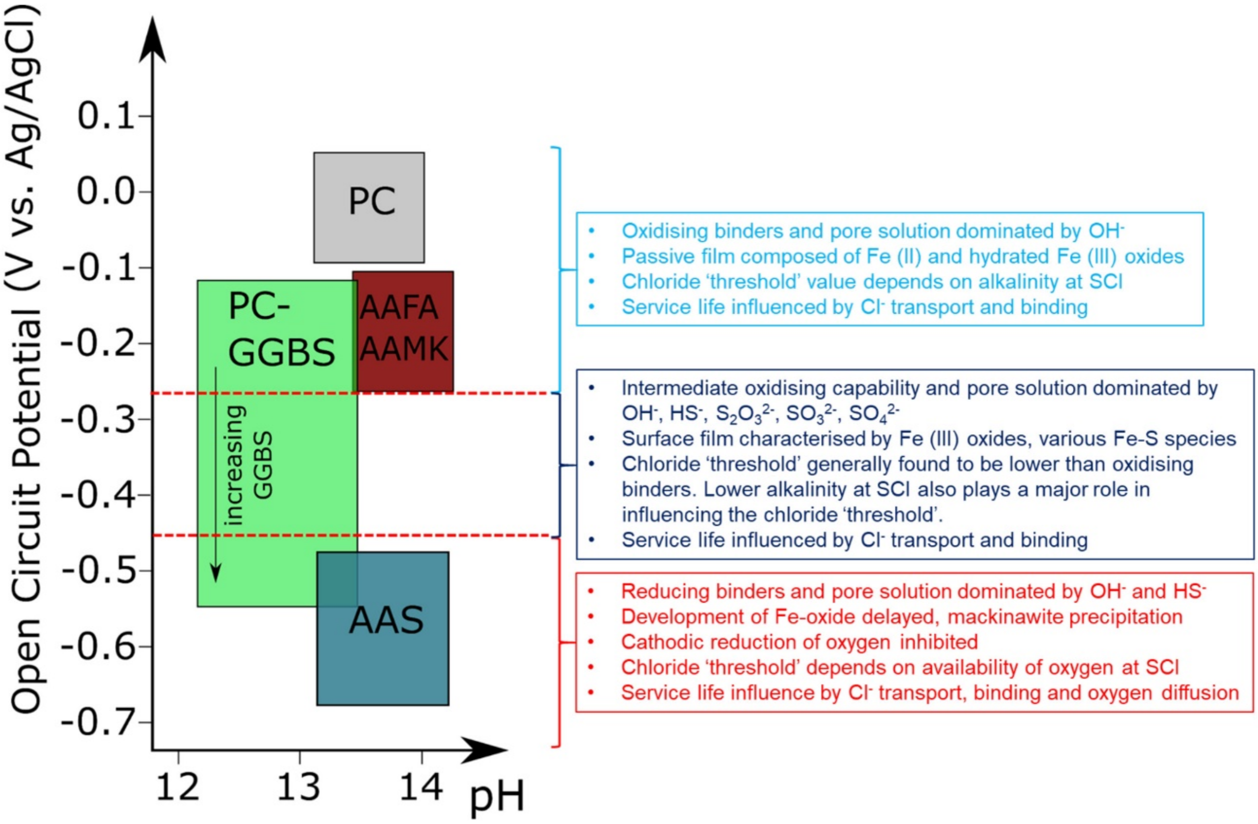

- Oxidising binders and pore solution dominated by OH^-
- Passive film composed of Fe (II) and hydrated Fe (III) oxides
- Chloride 'threshold' value depends on alkalinity at SCI
- Service life influenced by Cl^- transport and binding

- Intermediate oxidising capability and pore solution dominated by OH^-, HS^-, $S_2O_3^{2-}$, SO_3^{2-}, SO_4^{2-}
- Surface film characterised by Fe (III) oxides, various Fe-S species
- Chloride 'threshold' generally found to be lower than oxidising binders. Lower alkalinity at SCI also plays a major role in influencing the chloride 'threshold'.
- Service life influenced by Cl^- transport and binding

- Reducing binders and pore solution dominated by OH^- and HS^-
- Development of Fe-oxide delayed, mackinawite precipitation
- Cathodic reduction of oxygen inhibited
- Chloride 'threshold' depends on availability of oxygen at SCI
- Service life influence by Cl^- transport, binding and oxygen diffusion

Figure 12. Overview of the classification of cements, particularly of AAMs, based on internal redox conditions, and the parameters influencing the onset of steel pitting and the service-life of these binders. AAFA = alkali-activated fly ashes, AAMK = alkali-activated metakaolin. Adapted from [226], under Creative Commons license conditions.

Questions around alkali-silica reactions, analogous to those which can lead to damaging expansion in Portland cement binders with reactive aggregates, also arise regularly in discussions of AAMs because of the high levels of alkali present in these binders. However, the results of testing with a broad range of binder-aggregate combinations have shown that alkali-silica reactions do not appear to be particularly problematic in AAMs with aggregates of 'normal' reactivity [233]. It is possible to induce alkali-silica reaction expansion under accelerated conditions and with the use of a reactive aggregate [234, 235], but in the majority of cases, AAM mortars show less expansion than plain PC mortars with the same reactive aggregates [234, 236-238]. The relatively high Al concentration in the pore solution of AAMs, and in some cases also the lack or near-absence of dissolved Ca, appears to be important in restricting alkali-silica damage [234, 237, 239].

The freeze-thaw and frost-salt resistance of AAMs do appear to merit further attention, as the literature on this topic contains many case studies but lacks consistent or systematic analysis across the class of materials in general. Sulfate attack on AAMs has also been studied according to a number of test methods, largely because such testing is often requested by specifiers or end-users as sulfate attack can be problematic for Portland cement-based materials. However, the fundamental mechanism of Portland cement sulfate attack, with expansive processes involving the monosulfate-AFm phase, is not possible in most AAMs as this phase is absent from the hydrate products. Sulfuric acid attack on AAMs is, however, a relevant mechanism related to use in sewer infrastructure and other highly aggressive environments [240, 241], and the performance of AAMs (particularly those with low Ca content [242, 243]) under such conditions has been observed to significantly exceed that of most other cementitious binders [242, 244]. Organic acid resistance has also been reported to be a strength of low-calcium AAMs, as small organic acids damage calcium-rich binders through complexation and removal of Ca^{2+} ions, but this mechanism is much less significant for AAMs that do not rely on calcium as a key binder constituent [245, 246].

Testing of AAM durability in the field has generally shown results that are consistent with laboratory trials under non-accelerated or minimally-accelerated conditions; the materials that have been put into service under varying conditions have in many cases served very well, including concretes dating back to the 1950s [151, 247, 248], and more recent demonstration or full-scale infrastructure projects [249-252] including an airport in Australia that was constructed largely from alkali-activated concretes [253]. Such projects are essential in building stakeholder acceptance of AAM technology, and in using the experience gained to guide standards development, to ensure that the materials selected, specified and used are fully fit for purpose [254].

2.10. Applications of alkali-activated materials

Alkali-activated binders are finding rapidly increasing uptake in a growing range of applications, and this section will provide a very brief overview of some of these. The primary route to market for these materials in the short term will almost certainly be as a binder in concretes, and increasingly sophisticated approaches to the design and use of AAM concretes (rather than just directly applying protocols used for Portland cement concretes) are being published for concretes based on alkali-activated GGBS [60, 255-257], fly ash [258-260], metakaolin [261], and various blends of these materials [259].

AAMs, including particularly the lower-calcium "geopolymer"-type materials, are also attracting attention as matrices for the conditioning and immobilization of radioactive wastes; the ability of these materials to host, and bind, radioisotopes of cesium and strontium has been demonstrated and analyzed in some detail [262-264]. The effective immobilization of cesium in Portland cement-based matrices is well known to be challenging, and so the availability of a cementing system that can restrict its movement is highly desirable. There have been important recent investigations of the potential for compatibility of AAM matrices with complex waste streams containing multiple radioisotopes [265, 266], with oily wastes [267, 268], with ion exchange media [269, 270], and with graphitic or metallic wastes [271-273]. AAM matrices have also been demonstrated to show generally good stability under irradiation [274-276], and a hydrogen radiolytic yield that depends on water content and pore structure [274].

The ability to produce lightweight AAMs has been investigated by numerous groups, as reviewed recently by Bai & Colombo [277] and by Zhang et al. [278]. Successful approaches have included various types of templating by organic foams or emulsions [160, 267, 268, 279-281], foaming by peroxide addition [282] or by metal powders [283] and the use of lightweight aggregates [284]

AAMs have also been tested – and in some cases validated – in a broad range of 'niche' applications in recent years; a non-exhaustive selection of these includes:

- Well cementing in hydrocarbon and geothermal industries [285-287]
- Chromatographic substrates [288]
- Manufacture of composites [289, 290], including strain-hardening and/or ductile “engineered composite” materials [291-293]
- Repair mortars [294]
- Materials for additive manufacturing or “3D printing” through various extrusion-based and powder bed processes (Fig.13 [295]) [296-298]
- Moderate-temperature refractories or fire-resistant construction materials [299-302]

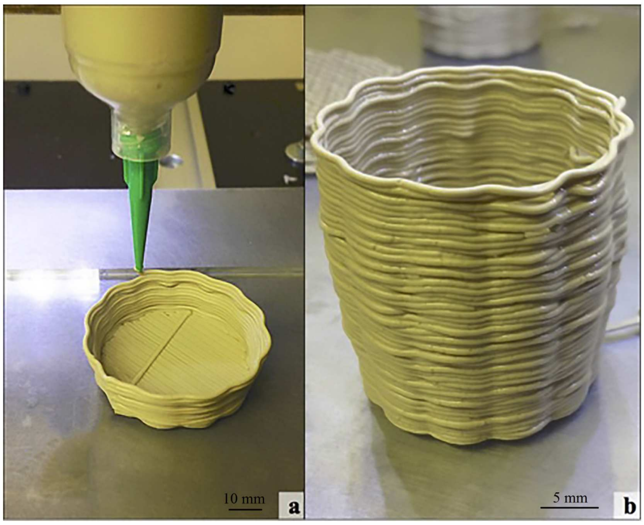

Figure 13. Additive manufacture of a vase from a metakaolin-based AAM, by extrusion. Reproduced from [295].

2.11. LCA and environmental aspects

When considering any type of cement as a potentially “eco-friendly” or “low-carbon” alternative to established technologies, it is essential that the actual environmental footprint of both the conventional and innovative materials are sufficiently well understood and quantified, to enable a fair comparison to be made. However, this is an area in which most current research publication practice in the field of alternative cements falls well short of providing the information needed for informed decision-making. This is potentially in part because of the trend for technical authors to justify the importance of their work (to funders, editors or other stakeholders) by ‘advertising’ the class of materials they prefer to study, and in part because the rigorous comparative environmental assessment of two construction materials is actually a highly specialized and challenging research task in itself. In the specific context of AAMs, Habert & Ouellet-Plamondon [303] have provided some very insightful discussion and assessment of data sources, and highlighted in particular the importance of understanding and controlling the environmental footprint of the alkali activator when designing and specifying an AAM mix design.

Another critical aspect of the assessment of sustainability is the need to conduct a locally-specific determination of energy supply and transport options, and their costs and environmental footprints, as these will differ very strongly between locations worldwide. This means that it is impossible to conduct a valid, generic assessment of the emissions footprint of an AAM at a useful level of precision, without knowing where in the world it will be used. The emissions attributed to electricity generation differ widely from (e.g.) hydroelectric to nuclear to coal sources, and AAMs are much more dependent on electrical energy in production than is Portland cement. This opens some attractive possibilities when considering binder production using a decarbonized electricity supply [304], which may be a strong point in favor of the use of AAMs in regions where low-carbon electricity is available.

The trend in the academic literature recently has therefore been toward regionally-specific (or very localized) assessments of AAMs for use in particular applications or concrete/mortar products in the Americas [305-307], Europe [308-310], and Australasia [311, 312]. The general trend observed in these studies is that AAMs offer greenhouse emissions savings compared to a Portland cement baseline, and usually on the order of 40-60%, but somewhat increased the environmental impact in other non-greenhouse categories, such as abiotic depletion, ozone layer depletion, fresh and marine water ecotoxicity, and human toxicity, that are considered in the life-cycle assessment process. It has also been identified that there is a strong need for more refined and updated life-cycle inventory data for activator constituents including sodium silicate [303, 305, 313], as the currently available international databases do not reflect current production practice or processes. The assessment of recyclability [314, 315] and release of potentially problematic elements (toxic or naturally occurring radioactive materials) [316-318] from AAMs in service has also received some attention as an essential constituent of a full cradle-to-grave or cradle-to-cradle environmental assessment. This will doubtless gain further importance as non-carbon emissions become more of a focus in material and product assessments worldwide, while the sources and characteristics of waste materials used in AAM production become ever more diverse.

The other critical aspect that needs to be considered in environmental analysis of AAMs is durability (at both material and element/structure scale), and this was discussed in Section 2.9 above. Considering all of these aspects together, and to conclude the discussion of AAMs, it should be identified that AAMs are becoming a mature class of materials whose nature and properties are increasingly well understood, and which offer numerous attractive opportunities to exercise their desirable technical and environmental characteristics for the benefit of society. They should not in any way be viewed as a panacea for all problems in the construction materials sector, and nor are they likely to be universally suitable as a replacement for Portland cement-based binders across the full range of applications in which cements are used, for both technical and logistical (materials-supply) reasons. However, as a constituent of the future toolkit of cements, AAMs do bring very significant value.

In the following sections, the focus of this review will turn to some other types of cementing systems, which are not yet as widely deployed as AAMs, but which can also form valuable components of the cements toolkit.

3. Carbonate Binders

The concept of carbonatable binders is based on the fact that some raw materials can harden through carbonation. Carbonated cementitious binders have attracted wide attention in recent years, attributed to their rapid strength gain and the sequestration of CO_2 when exposed to a CO_2 rich environment [319, 320]. This section will discuss carbonated calcium silicate, carbonated Portland cement, MgO-based cement and carbonated waste-derived binders. These four binder types react with water and CO_2, yielding strong cementing materials.

3.1. Carbonated calcium silicate binders

Tricalcium silicate (C_3S), β-dicalcium silicate (β-C_2S), γ-dicalcium silicate (γ-C_2S), tricalcium disilicate (C_3S_2) and monocalcium silicate (CS) can react with CO_2 and form strong monolithic matrices [321-323]. Ashraf & Olek [324] reported that the carbonation of pure calcium silicates consists of two distinct processes: an initial phase-boundary controlled process, and then a subsequent product layer diffusion controlled process. The reaction rate constant was found to vary based on the calcium silicate phases; β-C_2S has the highest reaction rate, followed by C_3S, γ-C_2S, C_3S_2 and finally CS.

The carbonation products of pure calcium silicate are calcium carbonate and Ca-modified silica gel or silica gel [323, 325, 326]. The calcium carbonate crystals resulting from carbonation of C_3S, C_2S, C_3S_2 and CS include the polymorphs calcite, aragonite, and vaterite [326, 327]. The presence of a ^{13}C CP/MAS NMR signal in carbonated C_3S, C_2S, and C_3S_2 phases can be attributed to the additional formation of amorphous calcium carbonate (ACC), as shown schematically in Fig. 14. However, ACC is not formed in carbonated CS under the same environmental conditions, Fig.14 [326]. The presence of poorly crystallized forms of $CaCO_3$ tends to increase the strength of the carbonated calcium silicate matrices [328]. Furthermore, the values of the elastic modulus of $CaCO_3$-rich binders can vary over a relatively wide range due to the presence of different polymorphs of $CaCO_3$ crystals [327].

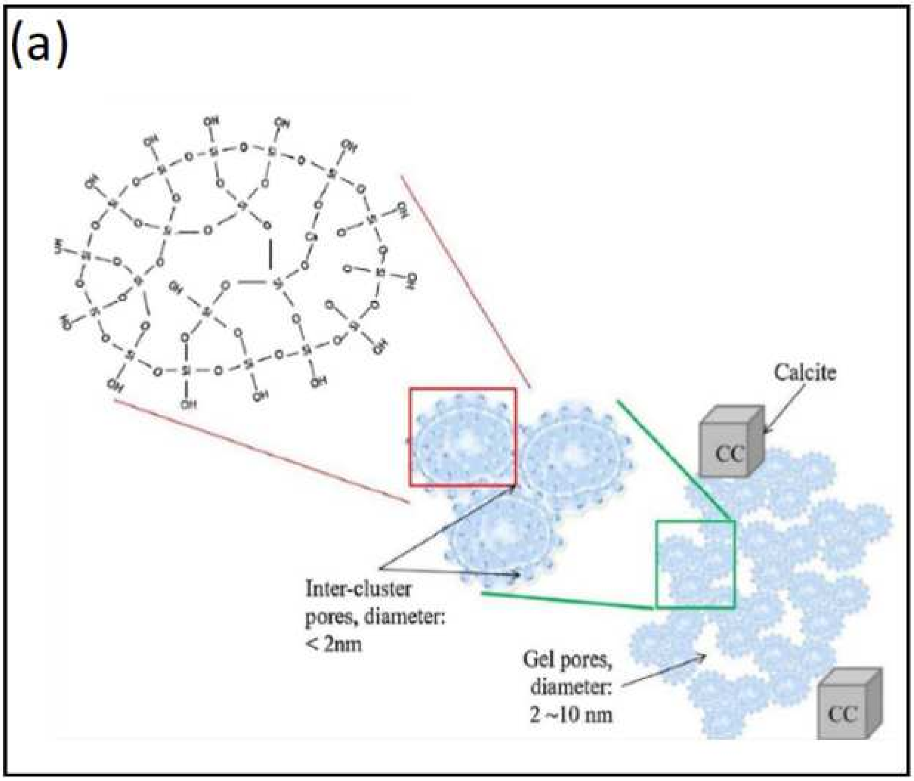

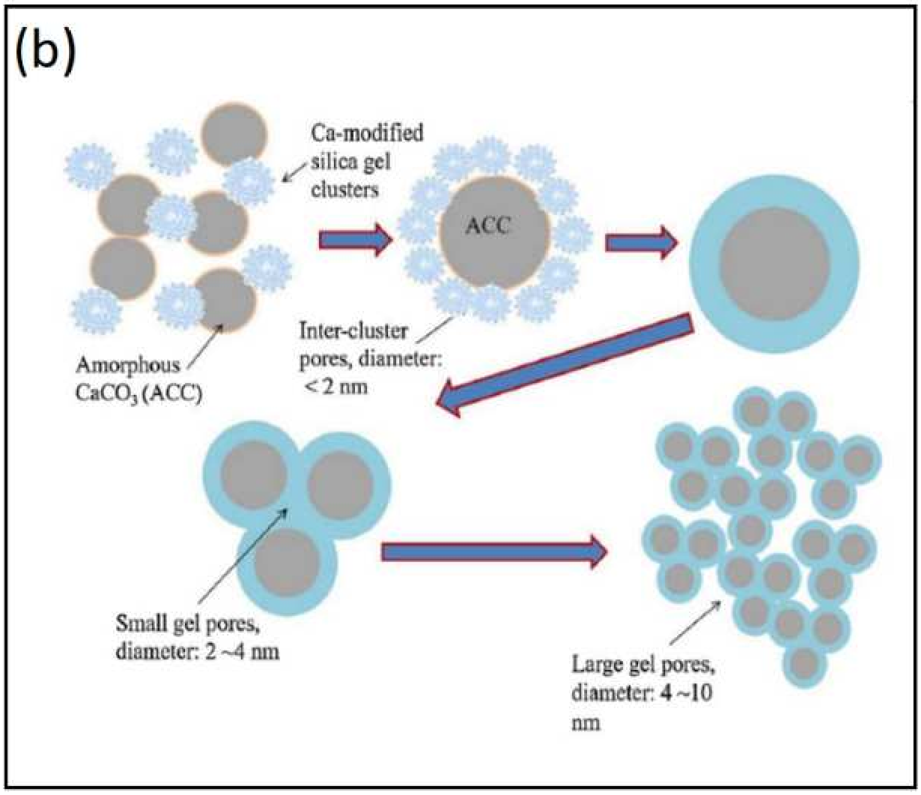

Figure 14. Proposed distribution of the pores (smaller than 10 nm) in carbonated calcium silicate matrixes a) without the presence of amorphous calcium carbonate (ACC) and b) in the presence of

amorphous calcium carbonate (ACC), adapted from [319].

As shown in Fig. 15, the degree of polymerization of Ca-modified silica gel (which is essentially defined by the inverse of the Ca/Si ratio) is nearly the same for all the carbonated calcium silicates discussed, except for the carbonated C_3S, which has a slightly lower degree [326]. However, all the calcium silicates reach a similar overall carbonation level due to the retardation of the carbonation reaction after formation of nearly the same amounts of $CaCO_3$ (Fig. 16), indicating that effect is related to blockage of the surfaces of potentially reactive particles by the precipitated carbonates.

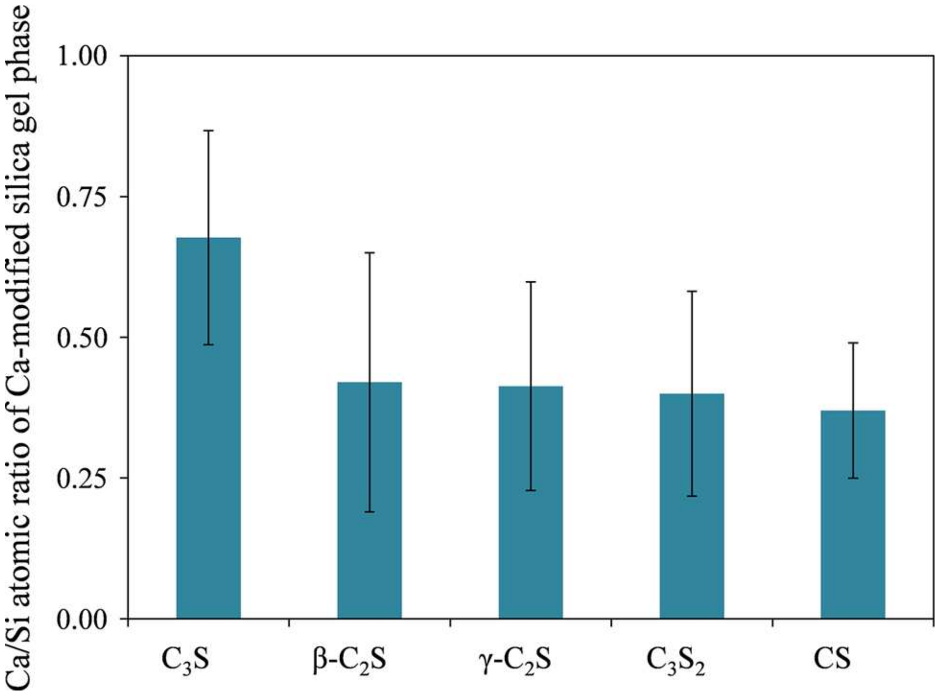

Figure 15. Average Ca/Si atomic ratios of Ca-modified silica gel phase formed during the carbonation reaction of the calcium silicate samples [321].

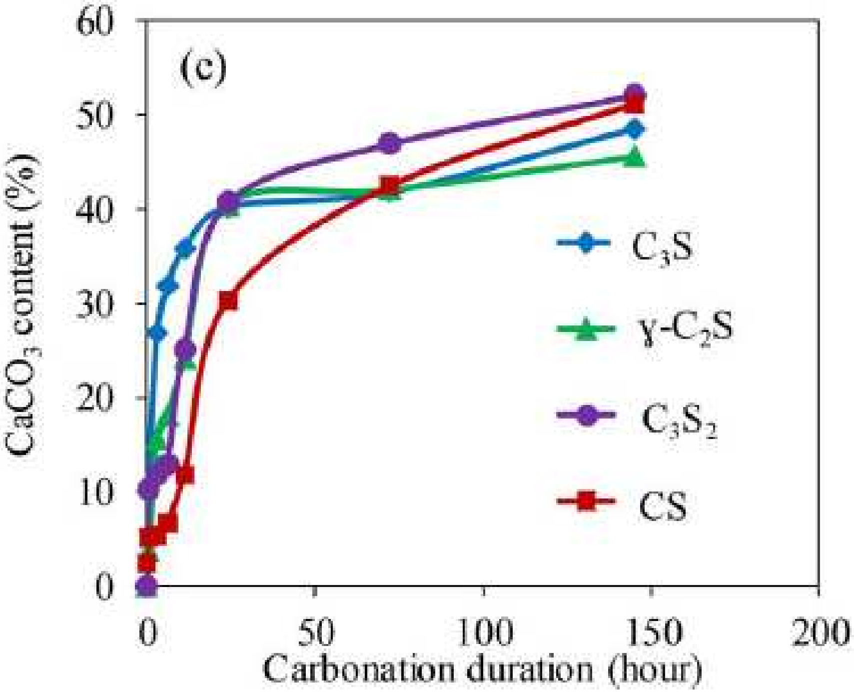

Figure 16. $CaCO_3$ contents (by mass, %) as a function of carbonation duration for different calcium silicate phases [326].

Among these calcium silicates, carbonation of C_2S has attracted more attention due to the different crystal polymorphs that it can take, particularly β-C_2S and γ-C_2S, as γ-C_2S can be produced at much lower synthesis temperatures than the conventional hydraulic calcium silicate phases. Chang et al. found β-C_2S and γ-C_2S to absorb 9.2% and 18.3% of their theoretical levels of CO_2 after 2 h of carbonation, respectively [328], but β-C_2S showed the twice the compressive strength compared to γ-C_2S. A similar result was reported by Guan et al., who found that the compressive strength of carbonated γ-C_2S was 52.4 MPa after 2 h carbonation [329]. Calcite and aragonite are the main crystals formed by carbonation of γ-C_2S, and amorphous Ca-modified silica gel lacking long-range order was also formed [329-331]. Mu et al. [327] proposed a conceptual model of the carbonation process of a γ-C_2S particle, as shown in Fig. 17.

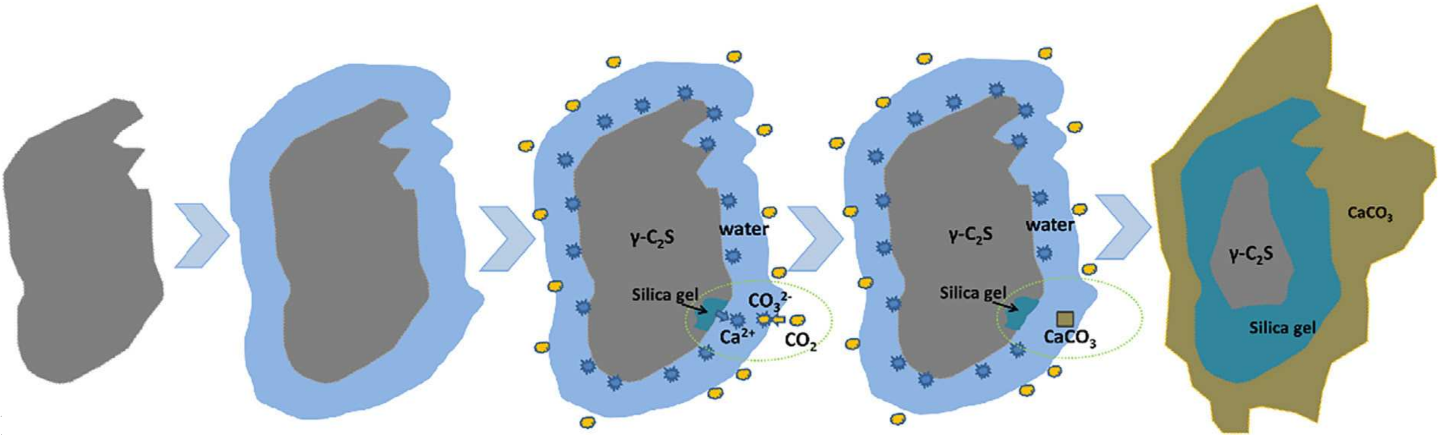

Figure 17. A conceptual carbonation model diagram of γ-C_2S particle. From [327]

3.2. Carbonated Portland cement (PC) binders

It is well known that accelerated early-age carbonation of Portland cement binders can result in rapid strength gain and lower permeability. This is because the carbonation reaction leads to a reduction in total porosity through the formation of carbonation products that occupy more space than the portlandite that they are replacing. Shi et al. [332] proposed the use of pre-conditioning to improve the accelerated carbonation of PC binders; the compressive strength of carbonated concrete after proper pre-conditioning then 2 h of CO_2 exposure is similar to that of the concrete after 24 h of steam curing. Furthermore, the carbonated concrete exhibits a similar compressive strength to that of steam-cured concrete during winter weathering exposure [333]. Shi et al. [334, 335] suggested that pre-conditioning environments have the most crucial effect on the effectiveness of CO_2 curing. Additionally, the temperature of the samples rises very quickly once the samples are exposed to CO_2; this could reach a peak value of 70 °C during the first 15-20 min, then goes down gradually with time.

Kenward et al. [336] studied hydration of an oil-well cement in the presence and the absence of pure CO_2 gas. The carbonate formed was initially amorphous calcium carbonate that was not detectable by XRD, but this changed to crystalline calcite detectable by XRD within 24 h. The addition of carbon dioxide did result in performance benefits.

Shah et al. [331] have suggested that the precipitation of the three polymorphs of calcium carbonate (calcite, vaterite, and aragonite) takes place in carbonated PC, while Castellote et al. [333] only detected calcite in carbonated PC. $CaCO_3$ polymorphism is sensitive to pore fluid chemistry, carbonation conditions and duration, and may also involve amorphous phases as noted in Section 3.1, so this is a complex area requiring further analysis. Based on thermogravimetric analysis, the main mass loss from carbonated PC pastes takes place between 600°C and 950°C. The poorly crystalline carbonates, preferentially associated with C-S-H carbonation, decomposed at a temperature below 600°C, while the decomposition temperature of well crystallized $CaCO_3$ is above 600 °C [320, 337, 338]. The carbonated PC was strongly decalcified to form these $CaCO_3$ phases along with a Ca-modified silica gel, identified via the decrease of the Q^1 and Q^2 sites, and increase in Q^3 and Q^4 sites, according to ^{29}Si MAS NMR analysis. ^{27}Al MAS NMR spectroscopy confirmed that the aluminum-bearing phases, containing mainly AlO_6 (ettringite and AFm) and AlO_4 sites (C-A-S-H) were dissolved to form an alumino-silicate amorphous gel (with Al as AlO_4), characterized by a broad resonance that was always positioned at the same chemical shift (55 ppm) [339].

3.3. Magnesium-based cement (MC) binders

In recent decades, the use of reactive magnesium oxide (MgO) in PC has received more and more attention. Carbonation of magnesium-rich cements improves the compressive strength of these cementitious materials, which is attributed to the densification of materials caused by the formation of nesquehonite ($MgCO_3 \cdot 3H_2O$), dypingite ($Mg_5(CO_3)_4(OH)_2 \cdot 5H_2O$) and artinite ($Mg_2(OH)_2CO_3 \cdot 3H_2O$) [340, 341]. Mo et al. [342] suggested that a large amount of calcite and a relatively smaller amount of aragonite are the calcium carbonates formed, while magnesian calcite is formed due to the incorporation of Mg^{2+} in the carbonated phase, and nesquehonite is formed only in pastes containing at least 40% reactive MgO. Nesquehonite has been identified as the key binding phase in other potential carbonated magnesia-based binders [343].

Figure 18 shows the morphology of carbonated magnesia cement [344]. The needle-like nesquehonite and disk/rose-like hydromagnesite/dypingite, which are the main sources of strength development in these cement formulations, are observed. The disk/rose-like hydromagnesite/dypingite crystals that formed due to the carbonation process could be distinguished from the hydromagnesite seeds included within the initial mix, which possesses a ground ball-like morphology.

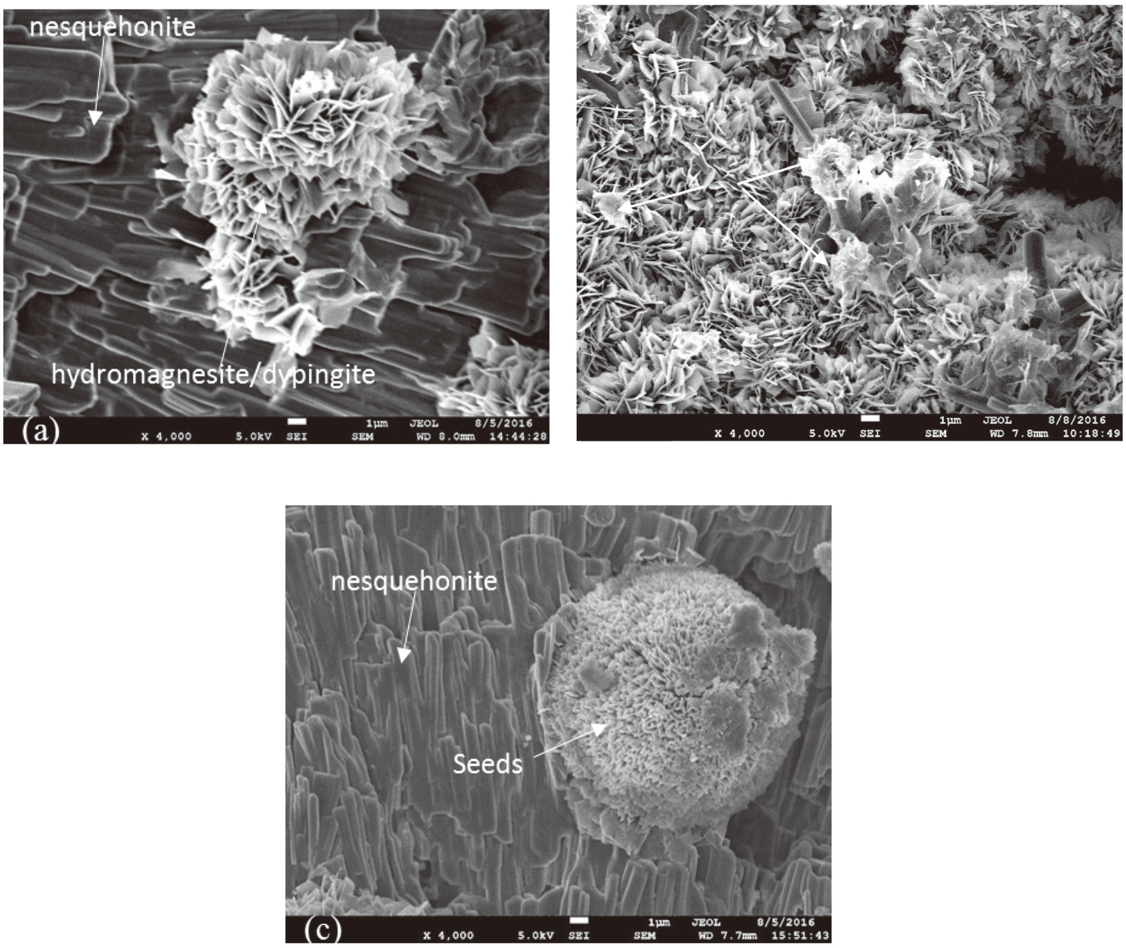

Figure 18. SEM images of H_2O samples after carbonation: (a) $H_2O{\cdot}S0$, (b) $H_2O{\cdot}S0.5$ and (c) $H_2O{\cdot}S1.0$. From [344].

The area of magnesia-based cements is very diverse, and includes cements which harden and gain strength by various combinations of carbonation and other chemical reactions, as reviewed in detail recently by Walling & Provis [345]. These cements are proposed for use in many applications ranging from large-scale construction to nuclear waste immobilization, and in some cases offer the possibility for notable CO_2 emissions savings compared to conventional Portland cement. The supply of MgO is constrained in some areas due to cost or resource availability, but this is not universally the case, and materials of very good technical and environmental performance can certainly be produced using this chemistry.

3.4. Carbonated waste-derived binders

Steel slag is a broad classification for several types of industrial by-products produced during the steel making process, which may be regarded as a waste-derived binder precursor [346-348]. Generally, the components of steel slag include hydraulic calcium silicates (C_3S, β-C_2S), non-hydraulic calcium silicates (e.g. γ-C_2S, CS), and free CaO, each of which can react with CO_2. Formation of calcium carbonate in the form of calcite and aragonite in the carbonated steel slag binders causes microstructural densification associated with a reduction in the total porosity, and hence improves the compressive strength. A carbonated steel slag binder was observed to show a shift in its dominant pore diameter from 0.3-3 μm before carbonation, to <0.1 μm in the carbonated paste [349]. The free CaO in the steel slag is partially or completely consumed due to the reaction with CO_2, which improves the volume stability of the binder [350, 351]. Calcium carbonate (as calcite and aragonite) is the main carbonate product formed, and portlandite and calcium silicate seem to be more carbonation-reactive than the Fe-bearing phases that are also present [349]. Monkman et al. [352] reported the possibility of using a carbonated ladle slag as a fine aggregate. After carbonation, calcium carbonates and spurrite were detected as new phases by XRD, together with the consumption of hydrogarnet and calcium hydroxide. Mortars made with the slag sand demonstrated strengths comparable to mortars made with conventional river sand.

High calcium fly ashes have an attractive capacity to be used for mineral sequestration of CO_2 under controlled conditions [353, 354]. A recent study show that Ca-rich fly ashes react readily with gas-phase CO_2 to produce robustly cemented solids which can achieve a compressive strength of around 35 MPa and take up 9% CO_2 under optimized conditions [355]. Mahoutian and

Shao [356] implemented a low temperature process to produce a binder material from blends of fly ash and ladle slag. CO_2 gas (99.5% purity) was used for carbonation of the synthesized cement for 2 hours and showed that the early age carbonation curing increased the subsequent hydration strength.

4. Belite-Ye'elimite Binders

Ye'elimite, or calcium sulfoaluminate ($Ca_4Al_6O_{12}SO_4$), is the main mineral in CSA cement clinker, and has a crystallographic structure belonging to the sodalite family [357]. CSA cements have been developed on a commercial basis and used in real applications, primarily in China, since the 1970s [358]. These cements are normally used as components in specialty applications because of their higher price compared to Portland cement. However, as low-carbon binders, the interest in these binders from the cement industry continues to increase because it is closer to the objective of 'eco-friendly' than many of the other low-carbon binder systems that are still under R&D [359, 360]. The highly innovative production of ye'elimite-containing clinkers burning waste elemental sulfur as fuel, meeting both energy and materials supply demand in a single step, has also been demonstrated in a full-scale kiln [361], with the potential for further scale-up.

Ye'elimite reacts very quickly with water and contributes to the development of early strength of this binder, forming monosulfate, ettringite, and amorphous aluminum hydroxide as major hydrates. Various other reaction products can be obtained, such as strätlingite, monocarboaluminate, and gibbsite depending on the minor phases in the CSA cement [362, 363]. Normally calcium sulfates are used to adjust the binder hydration reactions, and to promote the formation of ettringite rather than monosulfate [364, 365]. Dicalcium silicate (belite) and ferrites are present as additional main mineralogical components of CSA cements. In this paper, the authors will focus on some belite-ye'elimite binders containing more belite than ye'elimite, which is different from CSA cements that contain more ye'elimite than belite. Both belite and ye'elimite are lower energy minerals compared with tricalcium silicate (alite), which are suitable for low energy and low-carbon clinker cement production and applications.

4.1. Belite-ye'elimite-ferrite binders

Belite-ye'elimite-ferrite (BYF) binders, also known as calcium sulfoaluminate or sulfobelite cement [359, 360], have belite as the main phase (45-75%), and ye'elimite as a second component (20-45%). This approach to manufacturing BYF binders allows the use of less expensive Al-rich raw materials, due to the lower ye'elimite content in the clinker compared to 'conventional' CSA cements which require a higher-purity Al source. The recent main research interest in this type of binder is related to the understanding of ye'elimite hydration, that should be carefully controlled to achieve desired rheology and setting time, and also on achieving more reactivity of the belite component that contributes to the later growth in strength. BYF binders are not yet in large-scale industrial production, but have been developed to pilot scale by some cement companies under certain national and multi-national projects.

A study by Cuesta et al. [366] on the early hydration mechanisms of synthetic ye'elimite revealed that the polymorphism of ye'elimite (orthorhombic stoichiometric and pseudo-cubic solid-solution ye'elimite) influenced the hydration kinetics, together with the w/c ratio and the solubility of the additional sulfate sources.

Recently, new data on the hydration of BYF cements have been published by Álvarez-Pinazo et al. [367]. 'Non-active' clinker (containing β-belite and orthorhombic ye'elimite) and 'active clinker' (containing α'_H-belite and pseudo-cubic ye'elimite) have been studied with different calcium sulfate sources. The findings of this study showed that the active-clinker mortar developed higher compressive strengths than non-active-clinker mortars, independent of the choice of sulfate source, and it formed higher quantities of ettringite during hydration and less AFm compared to non-active cements. Another interesting finding that should be mentioned is that the paste with basanite ($CaSO_4\cdot0.5H_2O$) as the sulfate source showed the highest viscosity values and a hysteresis cycle attributed to fast setting, more so than gypsum- and anhydrite-containing pastes; this behavior can be adjusted by adding a small amount of polycarboxylate-based superplasticizer (SP) (0.05 wt%) without changing the phase assemblage [368, 369] (Fig. 19). This offers a possibility to add a superplasticizer normally used in Portland cement binders to control the rheological behaviour of BYF cements.

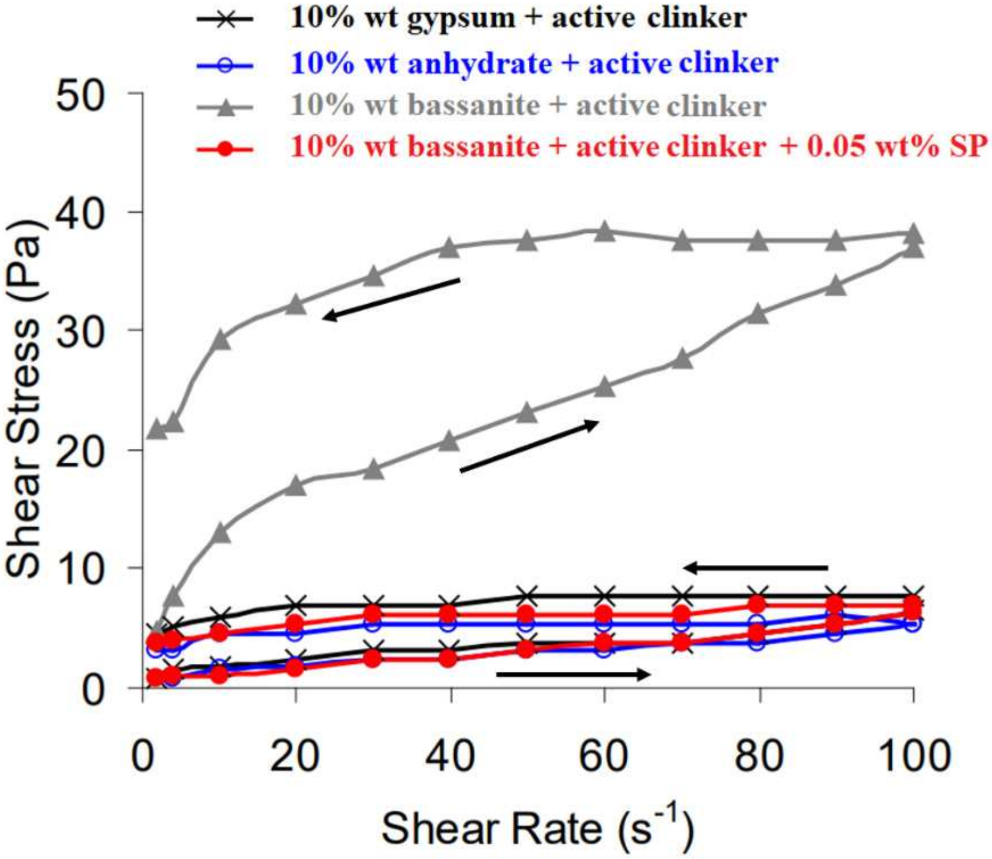

Figure 19. Flow curves of different BYF clinkers with different additional sulphate sources (re-drawn based on [367])

Morin et al. [370] studied five different BYF cements by experimental analysis and thermodynamic modeling to track the hydration kinetics and phase assemblage, which were influenced by the quantity of anhydrite, the w/c ratio, and the clinker fineness. The results indicated that with increasing addition of anhydrite, belite hydration was delayed, which contributed to the formation of a strength plateau between early ye'elimite hydration and later belite and ferrite hydration. Also, a higher fineness of cement together with increased w/c ratio leads to higher belite hydration kinetics. Those authors proposed that the question of whether there is enough water provided to form all hydration products strongly influences the hydration of belite and ferrite phases.

4.2. Belite-alite-ye'elimite binder

Because some belite-ye'elimite-ferrite cements present quite low mechanical strength due to their high content of belite with slow reactivity, methods to improve early strength have been sought. One such approach is a clinkering method aiming to introduce a reactive alite phase into the belite-ye'elimite binder system, as an alternative way to improve the mechanical strength. However, the temperature incompatibility between alite formation (above ~1300 °C) and ye'elimite decomposition (between 1300 and 1350 °C) brings difficulty in achieving the coexistence of alite and ye'elimte phases in clinkering processes. However, this problem can be solved and controlled by addition of minor quantities of CaF_2 [371] or other oxides, such as ZnO, B_2O_3, or Na_2O, in the raw meal [372].

Chitvoranund et al. [373] prepared a clinker by firing limestone, tuff, gypsum and calcium fluoride (used as mineraliser) in a laboratory furnace at 1300 °C for 45 min, which requires a synthesis temperature 150–200°C lower than traditional PC clinker. The minerals present in the clinker included alite (48.3%), belite (1.5% α'-C_2S + 10.3 % β-C_2S + 2.2% γ-C_2S), ye'elimite (9.6%), and ferrite (12.9%). Later, the ground clinker was mixed with 5% anhydrite to make a so-called alite-calcium sulfoaluminate cement. The hydration products were mainly C-S-H, ettringite, monosulfate, and portlandite, and hydration rates are rapid. Thermodynamic modeling revealed that the cement reacted strongly within the first 10 days of hydration, then the reaction process slowed down and was almost completed by 100 days. Ferrite exhibited reactivity in the presence of C_3S, and was consumed to give monosulfoaluminate and katoite. The compressive strength of mortars developed quite rapidly, from 10 MPa at 1 day to 35 MPa at 28 days. The release of CO_2 from this approach to clinker production is estimated at about 11-12 % less than conventional

Portland cement without the consideration of other factors.

In another study by Londono-Zuluaga et al. [374], a novel clinkering process to prepare belite-alite-ye'elimite (BAY) binders has been optimized (900 °C/30 min – 1300 °C/15 min) and scaled-up to 2 kg scale. This process involved as raw meal a mix of natural limestone, sand, iron oxide (a byproduct of the sulfuric acid industry), gypsum, and kaolin. The main mineralogical composition of their final scaled-up BAY clinker was 60.6 % belite, 14.3 % of alite and 10.4% ye'elimite, on a mass basis. BAY cements were prepared by mixing the scaled-up clinker with 12 wt.% anhydrite. The analysis of hydration highlighted that the main reaction products are ettringite, AFm phases (monosulfoaluminate and strätlingite), katoite, and C-S-H. Ye'elimite reacted with anhydrite to be completely consumed within 1 day, alite and ferrite almost fully reacted after 7 days, and belite showed a typical slower hydration behavior. Portlandite was not detected in the pastes at testing ages of 1, 7 and 28 days; it was speculated to be consumed to form katoite, AFt phases or monosulfoaluminate. The compressive strength of BAY mortars was recorded to be higher than that of a BYF binder prepared by the same group, at any testing age, most likely due to the presence of alite. The influence of fly ash blending in BAY cements has been also reported by the same authors [375]: with the addition of fly ash, the compressive strengths of mortars increased to 68, 73 and 82 MPa, for mortars with 0, 15 and 30 wt.% replacement of BAY cement by fly ash respectively, at 180 days. The main hydration products were AFt, AFm phases, katoite, and C-S-H for all systems studied. Utilizing a small amount of superplasticizer makes it possible to prepare BAF pastes with low viscosity values. The reactivity of belite appeared to have been inhibited by the high addition of fly ash, and other than the strength increase, no clear evidence of pozzolanic chemical reaction with fly ash in BAY systems was obtained. These do appear to be a promising class of cements for future large-scale utilization. Zhou et al. [376] investigated the influence of the ferrite phase in a similar binder system on its hydration and mechanical properties.

4.3. Belite-ye'elimite-ternesite binder

Belite-ye'elimite-ternesite binders have been treated as another interesting alternative material for reducing CO_2 emissions. The HeidelbergCement Technology Center (HTC) has worked for several years to develop new and innovative techniques of production approaches for this binder, and have published some patents related to this type of cement in recent years.

Ternesite ($C_5S_2\hat{S}$) was first found in Germany as a natural mineral in the 1990s. It is also found in the crust covering the areas of Portland cement kilns where the temperature is lower than 1250 °C. The advantages of ternesite-containing clinkers are quite clear due to the lower clinkering temperature. For a long time, this phase has been regarded as a non-hydraulic material, until it was recently found to be reactive with aluminum hydroxide. According to Ben Haha et al. [377], aluminum hydroxide can be used to activate ternesite to form ettringite, strätlingite and C-S-H in different proportions, depending on the reactivity and reaction degree. Work by Montes et al. [378], focusing on how other calcium aluminates activate the hydration of ternesite, has also been published recently. Synthetic C_3A, $C_{12}A_7$, CA and $C_4A_3\hat{S}$ (ye'elimite) phases were blended with ternesite separately, then the hydration reactions of the blends were studied through various techniques. Ternesite was activated in all the blends with aluminates, with descending effectiveness order $C_{12}A_7 \approx CA > C_3A >>> C_4A_3\hat{S}$. Also, the presence of ternesite changes the hydration products of these aluminates. However, ternesite was less consumed in the samples mixed with ye'elimite due to the sulfate common ion effect. Even though in this study some calorimetric evidence of an activating effect was recorded, ternesite could not be regarded as having been activated by ye'elimite as no strätlingite was detected. The characteristics of ternesite as a component of belite-ye'elimite (sulfobelitic) binders was later discussed by Blanco and Carmona [379] who noted that ye'elimite and ternesite can co-exist in the $CaO-SiO_2-Al_2O_3-CaSO_4$ system.

A single-stage process to produce ternesite-containing clinkers (belite and ternesite-rich calcium sulphoaluminate) has been proposed by Hanein et al. [380], based on some important new work in determining and defining the high-temperature thermodynamics of sulfur-containing clinkerization processes [381]. The clinker was obtained in a pilot plant where the partial pressure of O_2 and SO_2 was controlled in the kiln. The target operation temperature was set up to 1260 °C in order to make the process to reach steady state rapidly, corresponding with their thermodynamic calculations that the upper limit stability temperature for ternesite is ~1290 °C. The results also clearly confirmed that ternesite can be synthesized in a dry atmosphere.

5. Conclusions and Final Remarks

The development and use of low-carbon binders as an alternative to Portland cement-based materials, aiming to reduce the carbon footprint associated with construction and other applications, has made notable progress in recent years. In summary:

a) Alkali-activated binders are very important and high-potential alternative materials, which are now deployed on a commercial scale in several nations in the world. Recently the development of understanding on the rheological behavior, setting properties and structural characterization of alkali-activated binders has advanced rapidly. Progress in formulation of one-part alkali-activated binders has further approached large-scale production and application. However, the development and optimization of mix designs based on different raw materials and activators has not yet been systematically understood. Durability performance appears very good in most areas but needs more detailed work on test method validation and standardization. Environmental assessment of these materials should also be improved.

b) Carbonatable binders, regarding as a new approach to address concerns over CO_2 emissions, still are in a development route. The technology has been advanced recently, especially in the understanding of accelerating and controlling the carbonation hardening process. The limitations for these binders in application are also becoming clear, for instance the CO_2-rich atmospheres required for curing, and the pH reduction that means that use in reinforced elements will be challenging. However, these binders which may offer very high CO_2 savings if a circular CO_2 economy develops [360] still deserve serious attention as alternative low-carbon materials.

c) Belite-ye'elimite binders: this is a relatively new approach to produce alternative cementitious materials compared to the conventional CSA cements, targeting a high belite content in the clinkers. Although belite-ye'elimite-based binders are still under development and have not reached the full scale-up stage, the clinkering process, understanding of hydration, and the formulation of binders has developed greatly, not only in the scientific community but also in the cement industry. Good mechanical strength was obtained by hydrating this type of binder. The control of the rheological behavior and setting time have also been investigated. However, this binder system and technology is not yet commercialized or standardized. The clinkering process, which depends on different raw materials, should be optimized for large-scale production.

Acknowledgements

The financial support of this work from the National Natural Science Foundation of China under contract No. 51638008 is greatly appreciated.

References

[1] C. Shi, A. Fernández-Jiménez, A. Palomo, New cements for the 21st century: The pursuit of an alternative to Portland cement, Cem. Concr. Res., 41 (2011) 750-763.

[2] J.L. Provis, A. Palomo, C. Shi, Advances in understanding alkali-activated materials, Cem. Concr. Res., 78 (2015) 110-125.

[3] C. Shi, D. Roy, P. Krivenko, Alkali-activated cements and concretes, Taylor & Francis, 2006.

[4] F. Pacheco-Torgal, J. Labrincha, C. Leonelli, A. Palomo, P. Chindaprasit, Handbook of alkali-activated cements, mortars and concretes, Elsevier, 2014.

[5] J.L. Provis, Alkali-activated materials, Cem. Concr. Res., 114 (2018) 40-48.

[6] X. Gao, Q.L. Yu, A. Lazaro, H.J.H. Brouwers, Investigation on a green olivine nano-silica source based activator in alkali activated slag-fly ash blends: Reaction kinetics, gel structure and carbon footprint, Cem Concr. Res., 100 (2017) 129-139.

[7] R. Vinai, M. Soutsos, Production of sodium silicate powder from waste glass cullet for alkali activation of alternative binders, Cem Concr. Res., 116 (2019) 45-56.

[8] N. Toniolo, A. Rincón, J.A. Roether, P. Ercole, E. Bernardo, A.R. Boccaccini, Extensive reuse of soda-lime waste glass in fly ash-based geopolymers, Constr. Build. Mater, 188 (2018) 1077-1084.

[9] M. Torres-Carrasco, M.T. Tognonvi, A. Tagnit-Hamou, F. Puertas, Durability of alkali-activated slag concretes prepared using waste glass as alternative activator, ACI Mater. J., 112 (2015) 791-800.

[10] Y. Liu, C. Shi, Z. Zhang, N. Li, An overview on the reuse of waste glasses in alkali-activated materials, Resourc. Conserv. Recyc., Accepted for publication (2019).

[11] A. Peys, H. Rahier, Y. Pontikes, Potassium-rich biomass ashes as activators in metakaolin-based inorganic polymers, Applied Clay Science, 119 (2016) 401-409.

[12] S.A. Bernal, Advances in near-neutral salts activation of blast furnace slags, RILEM Tech. Lett., 1 (2016) 39-44.

[13] S.A. Bernal, J.L. Provis, R.J. Myers, R. San Nicolas, J.S.J. Van Deventer, Role of carbonates in the chemical evolution of sodium carbonate-activated slag binders, Mater. Struct., 48 (2015) 517-529.

[14] X. Ke, S.A. Bernal, J.L. Provis, Controlling the reaction kinetics of sodium carbonate-activated slag cements using calcined layered double hydroxides, Cem Concr. Res., 81 (2016) 24-37.

[15] X. Ke, M. Criado, J.L. Provis, S.A. Bernal, Slag-based cements that resist damage induced by carbon dioxide, ACS Sust. Chem. Eng., 6 (2018) 5067-5075.

[16] M. Esaifan, H. Khoury, I. Aldabsheh, H. Rahier, M. Hourani, J. Wastiels, Hydrated lime/potassium carbonate as alkaline activating mixture to produce kaolinitic clay based inorganic polymer, Appl. Clay Sci., 126 (2016) 278-286.

[17] L. Valentini, S. Contessi, M.C. Dalconi, F. Zorzi, E. Garbin, Alkali-activated calcined smectite clay blended with waste calcium carbonate as a low-carbon binder, J. Cleaner Prod., 184 (2018) 41-49.

[18] J. Dietel, L.N. Warr, M. Bertmer, A. Steudel, G.H. Grathoff, K. Emmerich, The importance

of specific surface area in the geopolymerization of heated illitic clay, Appl. Clay Sci., 139 (2017) 99-107.

[19] R.C. Kaze, L.M. Beleuk à Moungam, M.L. Fonkwe Djouka, A. Nana, E. Kamseu, U.F. Chinje Melo, C. Leonelli, The corrosion of kaolinite by iron minerals and the effects on geopolymerization, Appl. Clay Sci., 138 (2017) 48-62.

[20] M. Lassinantti Gualtieri, M. Romagnoli, S. Pollastri, A.F. Gualtieri, Inorganic polymers from laterite using activation with phosphoric acid and alkaline sodium silicate solution: Mechanical and microstructural properties, Cem Concr. Res., 67 (2015) 259-270.

[21] N. Nadziri, I. Ismail, S. Hamdan, Binding gel characterization of alkali-activated binders based on palm oil fuel ash (POFA) and fly ash, J. Sust. Cem.-Based Mater., 7 (2018) 1-14.

[22] G. Sukmak, S. Horpibulsuk, M. Setkit, S. Kassawat, A. Arulrajah, Palm oil fuel ash-soft soil geopolymer for subgrade applications: strength and microstructural evaluation, Road Mater. Pave. Des., 20 (2019) 110-131.

[23] H. Sreenivasan, P. Kinnunen, E.-P. Heikkinen, M. Illikainen, Thermally treated phlogopite as magnesium-rich precursor for alkali activation purpose, Miner. Eng., 113 (2017) 47-54.

[24] E. Najafi Kani, A. Allahverdi, J.L. Provis, Calorimetric study of geopolymer binders based on natural pozzolan, J. Therm. Anal. Calor., 127 (2017) 2181-2190.

[25] H.S. Hassan, H.A. Abdel-Gawwad, S.R. Vásquez-García, I. Israde-Alcántara, N. Flores-Ramirez, J.L. Rico, M.S. Mohammed, Cleaner production of one-part white geopolymer cement using pre-treated wood biomass ash and diatomite, J. Cleaner Prod., 209 (2019) 1420-1428.

[26] A. Nana, J. Ngouné, R.C. Kaze, L. Boubakar, S.K. Tchounang, H.K. Tchakouté, E. Kamseu, C. Leonelli, Room-temperature alkaline activation of feldspathic solid solutions: Development of high strength geopolymers, Constr. Build. Mater, 195 (2019) 258-268.

[27] P. Krivenko, O. Kovalchuk, A. Pasko, T. Croymans, M. Hult, G. Lutter, N. Vandevenne, S. Schreurs, W. Schroeyers, Development of alkali activated cements and concrete mixture design with high volumes of red mud, Constr. Build. Mater, 151 (2017) 819-826.

[28] Y. Hu, S. Liang, J. Yang, Y. Chen, N. Ye, Y. Ke, S. Tao, K. Xiao, J. Hu, H. Hou, W. Fan, S. Zhu, Y. Zhang, B. Xiao, Role of Fe species in geopolymer synthesized from alkali-thermal pretreated Fe-rich Bayer red mud, Constr. Build. Mater, 200 (2019) 398-407.

[29] N. Ye, J. Yang, S. Liang, Y. Hu, J. Hu, B. Xiao, Q. Huang, Synthesis and strength optimization of one-part geopolymer based on red mud, Constr. Build. Mater, 111 (2016) 317-325.

[30] A. Peys, C.E. White, D. Olds, H. Rahier, B. Blanpain, Y. Pontikes, Molecular structure of $CaO–FeO_x–SiO_2$ glassy slags and resultant inorganic polymer binders, J. Am. Ceram. Soc, 101 (2018) 5846-5857.

[31] S. Zhang, A. Keulen, K. Arbi, G. Ye, Waste glass as partial mineral precursor in alkali-activated slag/fly ash system, Cem Concr. Res., 102 (2017) 29-40.

[32] P. Kinnunen, H. Sreenivasan, C.R. Cheeseman, M. Illikainen, Phase separation in alumina-rich glasses to increase glass reactivity for low-CO_2 alkali-activated cements, J. Cleaner Prod., 213 (2019) 126-133.

[33] L. Kriskova, Y. Pontikes, F. Zhang, Ö. Cizer, P.T. Jones, K. Van Balen, B. Blanpain, Influence of mechanical and chemical activation on the hydraulic properties of gamma dicalcium silicate, Cem Concr. Res., 55 (2014) 59-68.

[34] S. Onisei, A.P. Douvalis, A. Malfliet, A. Peys, Y. Pontikes, Inorganic polymers made of

fayalite slag: On the microstructure and behavior of Fe, J. Am. Ceram. Soc, 101 (2018) 2245-2257.

[35] P.L. Lopez Gonzalez, R.M. Novais, J. Labrincha, B. Blanpain, Y. Pontikes, Modifications of basic-oxygen-furnace slag microstructure and their effect on the rheology and the strength of alkali-activated binders, Cem. Concr. Compos., 97 (2019) 143-153.

[36] J. Shekhovtsova, I. Zhernovsky, M. Kovtun, N. Kozhukhova, I. Zhernovskaya, E. Kearsley, Estimation of fly ash reactivity for use in alkali-activated cements - A step towards sustainable building material and waste utilization, J. Cleaner Prod., 178 (2018) 22-33.

[37] Z. Zhang, J.L. Provis, J. Zou, A. Reid, H. Wang, Toward an indexing approach to evaluate fly ashes for geopolymer manufacture, Cem Concr. Res., 85 (2016) 163-173.

[38] J.E. Oh, Y. Jun, Y. Jeong, P.J.M. Monteiro, The importance of the network-modifying element content in fly ash as a simple measure to predict its strength potential for alkali-activation, Cem. Concr. Compos., 57 (2015) 44-54.

[39] C.R. Shearer, J.L. Provis, S.A. Bernal, K.E. Kurtis, Alkali-activation potential of biomass-coal co-fired fly ash, Cem. Concr. Compos., 73 (2016) 62-74.

[40] M.A. Longhi, E.D. Rodríguez, S.A. Bernal, J.L. Provis, A.P. Kirchheim, Valorisation of a kaolin mining waste for the production of geopolymers, J. Cleaner Prod., 115 (2016) 265-272.

[41] A. McIntosh, S.E.M. Lawther, J. Kwasny, M.N. Soutsos, D. Cleland, S. Nanukuttan, Selection and characterisation of geological materials for use as geopolymer precursors, Adv. Appl. Ceram., 114 (2015) 378-385.

[42] I. Balczár, T. Korim, A. Kovács, É. Makó, Mechanochemical and thermal activation of kaolin for manufacturing geopolymer mortars – comparative study, Ceram. Int., 42 (2016) 15367-15375.

[43] S. Simon, G.J.G. Gluth, A. Peys, S. Onisei, D. Banerjee, Y. Pontikes, The fate of iron during the alkali-activation of synthetic (CaO-)FeO_x-SiO_2 slags: An Fe K-edge XANES study, J. Am. Ceram. Soc, 101 (2018) 2107-2118.

[44] K.C. Gomes, G.S.T. Lima, S.M. Torres, S. De Barros, I.F. Vasconcelos, N.P. Barbosa, Iron distribution in geopolymer with ferromagnetic rich precursor, Mater. Sci. Forum, 643 (2010) 131-138.

[45] F. Puertas, C. Varga, M.M. Alonso, Rheology of alkali-activated slag pastes. Effect of the nature and concentration of the activating solution, Cem. Concr. Compos., 53 (2014) 279-288.

[46] A. Favier, J. Hot, G. Habert, N. Roussel, J.-B. d'Espinose de Lacaillerie, Flow properties of MK-based geopolymers pastes. A comparative study with standard Portland cement pastes, Soft Matter, 10 (2014) 1134-1141.

[47] T. Yang, H. Zhu, Z. Zhang, X. Gao, C. Zhang, Q. Wu, Effect of fly ash microsphere on the rheology and microstructure of alkali-activated fly ash/slag pastes, Cem. Concr. Res., 109 (2018) 198-207.

[48] H. Mehdizadeh, E. Najafi Kani, Rheology and apparent activation energy of alkali activated phosphorous slag, Constr. Build. Mater., 171 (2018) 197-204.

[49] M.M. Alonso, S. Gismera, M.T. Blanco, M. Lanzón, F. Puertas, Alkali-activated mortars: Workability and rheological behaviour, Constr. Build. Mater., 145 (2017) 576-587.

[50] F. Puertas, B. González-Fonteboa, I. González-Taboada, M.M. Alonso, M. Torres-Carrasco, G. Rojo, F. Martínez-Abella, Alkali-activated slag concrete: Fresh and hardened behaviour, Cem. Concr. Compos., 85 (2018) 22-31.

[51] Z. Tan, S.A. Bernal, J.L. Provis, Reproducible mini-slump test procedure for measuring the yield stress of cementitious pastes, Mater. Struct., 50 (2017) #235.

[52] A. Kashani, J.L. Provis, B.B.G. van Deventer, G.G. Qiao, J.S.J. van Deventer, Time-resolved yield stress measurement of evolving materials using a creeping sphere, Rheol. Acta, 54 (2015) 365-376.

[53] V. Benavent, P. Steins, I. Sobrados, J. Sanz, D. Lambertin, F. Frizon, S. Rossignol, A. Poulesquen, Impact of aluminum on the structure of geopolymers from the early stages to consolidated material, Cem Concr. Res., 90 (2016) 27-35.

[54] P. Steins, A. Poulesquen, O. Diat, F. Frizon, Structural evolution during geopolymerization from an early age to consolidated material, Langmuir, 28 (2012) 8502-8510.

[55] D. Marchon, U. Sulser, A. Eberhardt, R.J. Flatt, Molecular design of comb-shaped polycarboxylate dispersants for environmentally friendly concrete, Soft Matter, 9 (2013) 10719-10728.

[56] A. Kashani, J.L. Provis, G.G. Qiao, J.S.J. van Deventer, The interrelationship between surface chemistry and rheology in alkali activated slag paste, Constr. Build. Mater, 65 (2014) 583-591.

[57] T. Conte, J. Plank, Impact of molecular structure and composition of polycarboxylate comb polymers on the flow properties of alkali-activated slag, Cem Concr. Res., 116 (2019) 95-101.

[58] A. Kashani, J.L. Provis, J. Xu, A.R. Kilcullen, G.G. Qiao, J.S.J. van Deventer, Effect of molecular architecture of polycarboxylate ethers on plasticizing performance in alkali activated slag paste, J. Mater. Sci, 49 (2014) 2761-2772.

[59] A. Keulen, Q.L. Yu, S. Zhang, S. Grünewald, Effect of admixture on the pore structure refinement and enhanced performance of alkali-activated fly ash-slag concrete, Constr. Build. Mater, 162 (2018) 27-36.

[60] N. Li, C. Shi, Z. Zhang, D. Zhu, H.-J. Hwang, Y. Zhu, T. Sun, A mixture proportioning method for the development of performance-based alkali-activated slag-based concrete, Cem. Concr. Compos., 93 (2018) 163-174.

[61] L. Xu, F. Matalkah, P. Soroushian, N. Darsanasiri, S. Hamadneh, W. Wu, Effects of citric acid on the rheology, hydration and strength development of alkali aluminosilicate cement, Adv. Cem. Res., 30 (2018) 75-82.

[62] N. Schneider, D. Stephan, The effect of d-gluconic acid as a retarder of ground granulated blast-furnace slag pastes, Constr. Build. Mater, 123 (2016) 99-105.

[63] C. Dupuy, J. Havette, A. Gharzouni, N. Texier-Mandoki, X. Bourbon, S. Rossignol, Metakaolin-based geopolymer: Formation of new phases influencing the setting time with the use of additives, Constr. Build. Mater, 200 (2019) 272-281.

[64] N. Li, C. Shi, Q. Wang, Z. Zhang, Z. Ou, Composition design and performance of alkali-activated cements, Mater. Struct., 50 (2017) #178.

[65] J. Rouyer, A. Poulesquen, Evidence of a fractal percolating network during geopolymerization, J. Am. Ceram. Soc, 98 (2015) 1580-1587.

[66] Z.Z. Li N, A study on the setting characteristics of alkali-activated slag cement., in: W. H (Ed.) The 3rd International Conference on Chemical Activated Materials, Australia 2017, pp. 65.

[67] N. Li, Z. Zhang, C. Shi, J. Zhang, Some progresses in the challenges for geopolymer, IOP Conf. Series: Mater. Sci. Eng., 2018, #022003.

[68] F. Winnefeld, M. Ben Haha, G. Le Saout, M. Costoya, S.-C. Ko, B. Lothenbach, Influence

of slag composition on the hydration of alkali-activated slags, J. Sust. Cem-Based Mater., 4 (2015) 85-100.

[69] M. Criado, B. Walkley, X. Ke, J.L. Provis, S.A. Bernal, Slag and activator chemistry control the reaction kinetics of sodium metasilicate-activated slag cements, Sustainability, 10 (2018) #4709.

[70] C. Shi, R.L. Day, A calorimetric study of early hydration of alkali-slag cements, Cem Concr. Res., 25 (1995) 1333-1346.

[71] S.A. Bernal, R. San Nicolas, J.S.J. van Deventer, J.L. Provis, Alkali-activated slag cements produced with a blended sodium carbonate/silicate activator, Adv. Cem. Res., 28 (2016) 262-273.

[72] A.M. Humad, J.L. Provis, A. Cwirzen, Alkali-activation of a high MgO GGBS – Fresh and hardened properties, Mag. Concr. Res, 70 (2018) 1256-1264.

[73] A. Fernández-Jiménez, F. Puertas, Setting of alkali-activated slag cement. Influence of activator nature, Advances in Cement Research, 13 (2001) 115-121.

[74] M. Kovtun, E.P. Kearsley, J. Shekhovtsova, Chemical acceleration of a neutral granulated blast-furnace slag activated by sodium carbonate, Cem. Concr. Res., 72 (2015) 1-9.

[75] C. Duran Atiş, C. Bilim, Ö. Çelik, O. Karahan, Influence of activator on the strength and drying shrinkage of alkali-activated slag mortar, Constr. Build. Mater., 23 (2009) 548-555.

[76] A. Fernández-Jiménez, F. Puertas, Effect of activator mix on the hydration and strength behaviour of alkali-activated slag cements, Adv. Cem. Res., 15 (2003) 129-136.

[77] N. Garg, C.E. White, Mechanism of zinc oxide retardation in alkali-activated materials: an in situ X-ray pair distribution function investigation, J. Mater. Chem. A, 5 (2017) 11794-11804.

[78] B. Lothenbach, A. Nonat, Calcium silicate hydrates: Solid and liquid phase composition, Cem Concr. Res., 78 (2015) 57-70.

[79] E. L'Hôpital, B. Lothenbach, D.A. Kulik, K. Scrivener, Influence of calcium to silica ratio on aluminium uptake in calcium silicate hydrate, Cem. Concr. Res., 85 (2016) 111-121.

[80] E. L'Hôpital, B. Lothenbach, K. Scrivener, D.A. Kulik, Alkali uptake in calcium alumina silicate hydrate (C-A-S-H), Cem. Concr. Res., 85 (2016) 122-136.

[81] E. Kapeluszna, Ł. Kotwica, A. Różycka, Ł. Gołek, Incorporation of Al in C-A-S-H gels with various Ca/Si and Al/Si ratio: Microstructural and structural characteristics with DTA/TG, XRD, FTIR and TEM analysis, Constr. Build. Mater., 155 (2017) 643-653.

[82] R.J. Myers, S.A. Bernal, J.L. Provis, J.D. Gehman, J.S.J. van Deventer, The role of Al in cross-linking of alkali-activated slag cements, J. Am. Ceram. Soc, 98 (2015) 996-1004.

[83] R.J. Myers, S.A. Bernal, R. San Nicolas, J.L. Provis, Generalized structural description of calcium-sodium aluminosilicate hydrate gels: The crosslinked substituted tobermorite model, Langmuir, 29 (2013) 5294-5306.

[84] J. Yang, D. Hou, Q. Ding, Structure, dynamics, and mechanical properties of cross-linked calcium aluminosilicate hydrate: A molecular dynamics study, ACS Sust. Chem. Eng., 6 (2018) 9403-9417.

[85] G. Sun, J.F. Young, R.J. Kirkpatrick, The role of Al in C–S–H: NMR, XRD, and compositional results for precipitated samples, Cem. Concr. Res., 36 (2006) 18-29.

[86] F. Puertas, M. Palacios, H. Manzano, J.S. Dolado, A. Rico, J. Rodríguez, A model for the C-A-S-H gel formed in alkali-activated slag cements, J. Eur. Ceram. Soc., 31 (2011) 2043-2056.

[87] X. Pardal, F. Brunet, T. Charpentier, I. Pochard, A. Nonat, ^{27}Al and ^{29}Si solid-state NMR

characterization of calcium-aluminosilicate-hydrate, Inorg. Chem., 51 (2012) 1827-1836.

[88] I.G. Richardson, Model structures for C-(A)-S-H (I), Acta Cryst B, 70 (2014) 903-923.

[89] T. Egami, S.J.L. Billinge, Underneath the Bragg peaks: structural analysis of complex materials, Elsevier 2003.

[90] K. Gong, C.E. White, Impact of chemical variability of ground granulated blast-furnace slag on the phase formation in alkali-activated slag pastes, Cem. Concr. Res., 89 (2016) 310-319.

[91] R. Si, S. Guo, Q. Dai, Influence of calcium content on the atomic structure and phase formation of alkali-activated cement binder, Journal of the American Ceramic Society, (2018).

[92] L. Valentini, Modeling dissolution–precipitation kinetics of alkali-activated metakaolin, ACS Omega, 3 (2018) 18100-18108.

[93] K. Yang, V.O. Özçelik, N. Garg, K. Gong, C.E. White, Drying-induced atomic structural rearrangements in sodium-based calcium-alumino-silicate-hydrate gel and the mitigating effects of ZrO_2 nanoparticles, Phys. Chem. Chem. Phys., 20 (2018) 8593-8606.

[94] B. Walkley, R. San Nicolas, M.-A. Sani, J.D. Gehman, J.S.J. van Deventer, J.L. Provis, Synthesis of stoichiometrically controlled reactive aluminosilicate and calcium-aluminosilicate powders, Powder Technol., 297 (2016) 17-33.

[95] B. Walkley, R. San Nicolas, M.-A. Sani, J.D. Gehman, J.S.J. van Deventer, J.L. Provis, Phase evolution of Na_2O–Al_2O_3–SiO_2–H_2O gels in synthetic aluminosilicate binders, Dalton Trans., 45 (2016) 5521-5535.

[96] B. Walkley, R. San Nicolas, M.-A. Sani, G.J. Rees, J.V. Hanna, J.S.J. van Deventer, J.L. Provis, Phase evolution of C-(N)-A-S-H/N-A-S-H gel blends investigated via alkali-activation of synthetic calcium aluminosilicate precursors, Cem. Concr. Res., 89 (2016) 120-135.

[97] B. Walkley, G.J. Rees, R. San Nicolas, J.S.J. van Deventer, J.V. Hanna, J.L. Provis, New structural model of hydrous sodium aluminosilicate gels and the role of charge-balancing extra-framework Al, J. Phys. Chem. C, 122 (2018) 5673-5685.

[98] S. Greiser, G.J.G. Gluth, P. Sturm, C. Jäger, ^{29}Si{^{27}Al}, ^{27}Al{^{29}Si} and ^{27}Al{^{1}H} double-resonance NMR spectroscopy study of cementitious sodium aluminosilicate gels (geopolymers) and gel–zeolite composites, RSC Adv., 8 (2018) 40164-40171.

[99] J. Brus, L. Kobera, M. Urbanová, D. Koloušek, J. Kotek, Insights into the structural transformations of aluminosilicate inorganic polymers: A comprehensive solid-state NMR study, J. Phys. Chem. C, 116 (2012) 14627-14637.

[100] Q. Wan, F. Rao, S. Song, R.E. García, R.M. Estrella, C.L. Patiño, Y. Zhang, Geopolymerization reaction, microstructure and simulation of metakaolin-based geopolymers at extended Si/Al ratios, Cem. Concr. Compos., 79 (2017) 45-52.

[101] Z. Pan, Z. Tao, Y.F. Cao, R. Wuhrer, T. Murphy, Compressive strength and microstructure of alkali-activated fly ash/slag binders at high temperature, Cem. Concr. Compos., 86 (2018) 9-18.

[102] P. Suraneni, M. Palacios, R.J. Flatt, New insights into the hydration of slag in alkaline media using a micro-reactor approach, Cem Concr. Res., 79 (2016) 209-216.

[103] I.G. Richardson, S. Li, Composition and structure of an 18-year-old 5M KOH-activated ground granulated blast-furnace slag paste, Constr. Build. Mater, 168 (2018) 404-411.

[104] X. Ke, S.A. Bernal, J.L. Provis, Layered double hydroxides modify the reaction of sodium silicate-activated slag cements, Green Mater., (2019) in press, DOI 10.1680/jgrma.1618.00024.

[105] S.D. Wang, K.L. Scrivener, Hydration products of alkali-activated slag cement, Cem Concr. Res., 25 (1995) 561-571.

[106] S.J. Mills, A.G. Christy, J.-M.R. Génin, T. Kameda, F. Colombo, Nomenclature of the hydrotalcite supergroup: natural layered double hydroxides, Miner. Mag., 76 (2012) 1289-1336.

[107] A.E. Morandeau, J.P. Fitts, H.D. Lee, S.M. Shubeita, L.C. Feldman, T. Gustafsson, C.E. White, Nanoscale heterogeneities in a fractured alkali-activated slag binder: A helium ion microscopy analysis, Cem. Concr. Res., 79 (2016) 45-48.

[108] D. Cohen-Tanugi, N. Yao, Superior imaging resolution in scanning helium-ion microscopy: A look at beam-sample interactions, J. Appl. Phys., 104 (2008) #063504.

[109] R. Williams, A. Van Riessen, The first 20 hours of geopolymerization: An in situ WAXS study of flyash-based geopolymers, Materials, 9 (2016) #552.

[110] C.E. White, J.L. Provis, B. Bloomer, N.J. Henson, K. Page, In situ X-ray pair distribution function analysis of geopolymer gel nanostructure formation kinetics, Phys. Chem. Chem. Phys, 15 (2013) 8573-8582.

[111] C.E. White, D.P. Olds, M. Hartl, R.P. Hjelm, K. Page, Evolution of the pore structure during the early stages of the alkali-activation reaction: an in situ small-angle neutron scattering investigation, J. Appl. Cryst., 50 (2017) 61-75.

[112] J.P. Gevaudan, K.M. Campbell, T.J. Kane, R.K. Shoemaker, W.V. Srubar, Mineralization dynamics of metakaolin-based alkali-activated cements, Cem Concr. Res., 94 (2017) 1-12.

[113] Z. Sun, A. Vollpracht, Isothermal calorimetry and in-situ XRD study of the NaOH activated fly ash, metakaolin and slag, Cem. Concr. Res., 103 (2018) 110-122.

[114] V. Benavent, F. Frizon, A. Poulesquen, Effect of composition and aging on the porous structure of metakaolin-based geopolymers, J. Appl. Cryst., 49 (2016) 2116-2128.

[115] J. Melar, G. Renaudin, F. Leroux, A. Hardy-Dessources, J.-M. Nedelec, C. Taviot-Gueho, E. Petit, P. Steins, A. Poulesquen, F. Frizon, The porous network and its interface inside geopolymers as a function of alkali cation and aging, J. Phys. Chem. C, 119 (2015) 17619-17632.

[116] X. Liu, C. Shi, X. Hu, Study of hydration and microstructure of alkali-activated slag cement and portland cement by impedance spectroscopy, Materials Review, 29 (2015) 130-135 (in Chinese).

[117] A.F. Sosa Gallardo, J. Provis, D.C. Sinclair, Electrochemical characterisation of cement hydration and properties by alternating current impedance spectroscopy, ECI International Conference on Alkali Activated Materials and Geopolymers: Versatile Materials Offering High Performance and Low Emissions, Tomar, Portugal (2018).

[118] M. Chaouche, X.X. Gao, M. Cyr, M. Cotte, L. Frouin, On the origin of the blue/green color of blast-furnace slag-based materials: Sulfur K-edge XANES investigation, J. Am. Ceram. Soc, 100 (2017) 1707-1716.

[119] D. Le Cornec, Q. Wang, L. Galoisy, G. Renaudin, L. Izoret, G. Calas, Greening effect in slag cement materials, Cem. Concr. Compos., 84 (2017) 93-98.

[120] F. Lolli, H. Manzano, J.L. Provis, M.C. Bignozzi, E. Masoero, Atomistic simulations of geopolymer models: the impact of disorder on structure and mechanics, ACS Appl. Mater. Interf., 10 (2018) 22809-22820.

[121] W. Loewenstein, The distribution of aluminum in the tetrahedra of silicates and aluminates, Am. Miner., 39 (1954) 92-96.

[122] K. Yang, C.E. White, Modeling the formation of alkali aluminosilicate gels at the mesoscale using coarse-grained Monte Carlo, Langmuir, 32 (2016) 11580-11590.

[123] R.J. Myers, S.A. Bernal, J.L. Provis, A thermodynamic model for C-(N-)A-S-H gel: CNASH_ss. Derivation and validation, Cem. Concr. Res., 66 (2014) 27-47.

[124] R.J. Myers, E. L'Hopital, J.L. Provis, B. Lothenbach, Composition-solubility-structure relationships in calcium (alkali) aluminosilicate hydrate (C-(N,K-)A-S-H), Dalton Trans., 44 (2015) 13530-13544.

[125] R.J. Myers, B. Lothenbach, S.A. Bernal, J.L. Provis, Thermodynamic modelling of alkali-activated slag cements, Appl. Geochem., 61 (2015) 233-247.

[126] Y. Zuo, M. Nedeljković, G. Ye, Coupled thermodynamic modelling and experimental study of sodium hydroxide activated slag, Constr. Build. Mater, 188 (2018) 262-279.

[127] H. Ye, A. Radlińska, Shrinkage mitigation strategies in alkali-activated slag, Cem Concr. Res., 101 (2017) 131-143.

[128] R.J. Myers, S.A. Bernal, J.L. Provis, Phase diagrams for alkali-activated slag binders, Cem Concr. Res., 95 (2017) 30-38.

[129] L. Gomez-Zamorano, M. Balonis, B. Erdemli, N. Neithalath, G. Sant, C–(N)–S–H and N–A–S–H gels: Compositions and solubility data at 25°C and 50°C, J. Am. Ceram. Soc, 100 (2017) 2700-2711.

[130] G.D. Miron, T. Wagner, D.A. Kulik, C.A. Heinrich, Internally consistent thermodynamic data for aqueous species in the system Na–K–Al–Si–O–H–Cl, Geochim. Cosmochim. Acta, 187 (2016) 41-78.

[131] M.U. Okoronkwo, M. Balonis, L. Katz, M. Juenger, G. Sant, A thermodynamics-based approach for examining the suitability of cementitious formulations for solidifying and stabilizing coal-combustion wastes, J. Environ. Manag., 217 (2018) 278-287.

[132] Y. Ding, J.-G. Dai, C.-J. Shi, Mechanical properties of alkali-activated concrete: A state-of-the-art review, Constr. Build. Mater, 127 (2016) 68-79.

[133] R.J. Thomas, S. Peethamparan, Alkali-activated concrete: Engineering properties and stress–strain behavior, Constr. Build. Mater, 93 (2015) 49-56.

[134] A. Noushini, F. Aslani, A. Castel, R.I. Gilbert, B. Uy, S. Foster, Compressive stress-strain model for low-calcium fly ash-based geopolymer and heat-cured Portland cement concrete, Cem. Concr. Compos., 73 (2016) 136-146.

[135] K.-M. Lee, S. Choi, J.F. Choo, S.-W. Yoo, Y.C. Choi, Flexural and shear behaviors of reinforced alkali-activated slag concrete beams, Adv. Mater. Sci. Eng., 2017 (2017) #5294290.

[136] R.J. Thomas, S. Peethamparan, Effect of specimen size and curing condition on the compressive strength of alkali-activated concrete, Transp. Res. Record, 2629 (2017) 9-14.

[137] C.H. Un, J.G. Sanjayan, R. San Nicolas, J.S.J. van Deventer, Predictions of long-term deflection of geopolymer concrete beams, Constr. Build. Mater, 94 (2015) 10-19.

[138] Y. Ding, J.-G. Dai, C.-J. Shi, Fracture properties of alkali-activated slag and ordinary Portland cement concrete and mortar, Constr. Build. Mater, 165 (2018) 310-320.

[139] P. Nath, P.K. Sarker, Fracture properties of GGBFS-blended fly ash geopolymer concrete cured in ambient temperature, Mater. Struct., 50 (2017) #32.

[140] R. San Nicolas, J.L. Provis, The interfacial transition zone in alkali-activated slag mortars, Front. Mater., 2 (2015) #70.

[141] A. Dakhane, S. Das, S. Kailas, N. Neithalath, Elucidating the crack resistance of alkali-activated slag mortars using coupled fracture tests and image correlation, J. Am. Ceram. Soc, 99 (2016) 273-280.

[142] V.S. Cândido, A.C.R. da Silva, N.T. Simonassi, E.S. Lima, F.S. da Luz, S.N. Monteiro, Mechanical and microstructural characterization of geopolymeric concrete subjected to fatigue, J. Mater. Res. Technol., 7 (2018) 566-570.

[143] J.-S. Mun, K.-H. Yang, S.-J. Kim, Tests on the compressive fatigue performance of various concretes, J. Mater. Civ. Eng., (2016) #04016099.

[144] N. Ranjbar, M. Mehrali, M.R. Maheri, M. Mehrali, Hot-pressed geopolymer, Cem Concr. Res., 100 (2017) 14-22.

[145] J. Rouyer, V. Benavent, F. Frizon, A. Poulesquen, Influence of geopolymer formulation parameters on the elastic and porous properties over a one-year monitoring, Mater. Lett., 207 (2017) 121-124.

[146] A. Blyth, C.A. Eiben, G.W. Scherer, C.E. White, Impact of activator chemistry on permeability of alkali-activated slags, J. Am. Ceram. Soc, 100 (2017) 4848-4859.

[147] S.A. Bernal, R. San Nicolas, J.S.J. van Deventer, J.L. Provis, Water content modifies the structural development of sodium metasilicate-activated slag binders (El contenido de agua modifica el desarrollo estructural de cementantes de escoria activada con metasilicato de sodio), ALCONPAT J., 5 (2015) 30-41.

[148] M. Babaee, A. Castel, Water vapor sorption isotherms, pore structure, and moisture transport characteristics of alkali-activated and Portland cement-based binders, Cem Concr. Res., 113 (2018) 99-120.

[149] X. Hu, C. Shi, Z. Shi, L. Zhang, Compressive strength, pore structure and chloride transport properties of alkali-activated slag/fly ash mortars, Cement and Concrete Composites, Accepted for publication (2019), Doi: https://doi.org/10.1016/j.cemconcomp.2019.01.010.

[150] T. Luukkonen, Z. Abdollahnejad, J. Yliniemi, P. Kinnunen, M. Illikainen, One-part alkali-activated materials: A review, Cem. Concr. Res., 103 (2018) 21-34.

[151] J.L. Provis, J.S.J. van Deventer, Alkali-Activated Materials: State-of-the-Art Report, RILEM TC 224-AAM, Springer/RILEM, Dordrecht, 2014.

[152] A. Hajimohammadi, J.S.J. van Deventer, Characterisation of one-part geopolymer binders made from fly ash, Waste Biomass Valoriz., 8 (2017) 225-233.

[153] B. Nematollahi, J. Sanjayan, J. Qiu, E.-H. Yang, Micromechanics-based investigation of a sustainable ambient temperature cured one-part strain hardening geopolymer composite, Constr. Build. Mater., 131 (2017) 552-563.

[154] K.-t. Wang, L.-q. Du, X.-s. Lv, Y. He, X.-m. Cui, Preparation of drying powder inorganic polymer cement based on alkali-activated slag technology, Powder Technol., 312 (2017) 204-209.

[155] I. Garcia-Lodeiro, S. Donatello, A. Fernández-Jiménez, Á. Palomo, Hydration of hybrid alkaline cement containing a very large proportion of fly ash: A descriptive model, Materials, 9 (2016) #605.

[156] A. Fernández-Jiménez, I. Garcia-Lodeiro, O. Maltseva, A. Palomo, Hydration mechanisms of hybrid cements as a function of the way of addition of chemicals, J. Am. Ceram. Soc., 102 (2018) 427-436.

[157] F. Matalkah, P. Soroushian, Synthesis and characterization of alkali aluminosilicate

hydraulic cement that meets standard requirements for general use, Constr. Build. Mater, 158 (2018) 42-49.

[158] T. Luukkonen, Z. Abdollahnejad, J. Yliniemi, P. Kinnunen, M. Illikainen, Comparison of alkali and silica sources in one-part alkali-activated blast furnace slag mortar, J. Cleaner Prod., 187 (2018) 171-179.

[159] K. Neupane, P. Kidd, D. Chalmers, D. Baweja, R. Shrestha, Investigation on compressive strength development and drying shrinkage of ambient cured powder-activated geopolymer concretes, Aust. J. Civil Eng., 14 (2016) 72-83.

[160] A. Hajimohammadi, T. Ngo, A. Kashani, Sustainable one-part geopolymer foams with glass fines versus sand as aggregates, Constr. Build. Mater, 171 (2018) 223-231.

[161] M.X. Peng, Z.H. Wang, Q.G. Xiao, F. Song, W. Xie, L.C. Yu, H.W. Huang, S.J. Yi, Effects of alkali on one-part alkali-activated cement synthesized by calcining bentonite with dolomite and Na_2CO_3, Appl. Clay Sci., 139 (2017) 64-71.

[162] P. Sturm, G.J.G. Gluth, S. Simon, H.J.H. Brouwers, H.C. Kühne, The effect of heat treatment on the mechanical and structural properties of one-part geopolymer-zeolite composites, Thermochim. Acta, 635 (2016) 41-58.

[163] P. Sturm, G.J.G. Gluth, H.J.H. Brouwers, H.C. Kühne, Synthesizing one-part geopolymers from rice husk ash, Constr. Build. Mater, 124 (2016) 961-966.

[164] X. Ke, S.A. Bernal, N. Ye, J.L. Provis, J. Yang, One-part geopolymers based on thermally treated red mud/NaOH blends, J. Am. Ceram. Soc, 98 (2015) 5-11.

[165] N. Ye, Y. Chen, J. Yang, S. Liang, Y. Hu, J. Hu, S. Zhu, W. Fan, B. Xiao, Transformations of Na, Al, Si and Fe species in red mud during synthesis of one-part geopolymers, Cem Concr. Res., 101 (2017) 123-130.

[166] Z. Zhang, J.L. Provis, X. Ma, A. Reid, H. Wang, Efflorescence and subflorescence induced microstructural and mechanical evolution in fly ash-based geopolymers, Cem. Concr. Compos., 92 (2018) 165-177.

[167] Z. Zhang, J.L. Provis, A. Reid, H. Wang, Fly ash-based geopolymers: The relationship between composition, pore structure and efflorescence, Cem. Concr. Res., 64 (2014) 30-41.

[168] X. Xue, Y.-L. Liu, J.-G. Dai, C.-S. Poon, W.-D. Zhang, P. Zhang, Inhibiting efflorescence formation on fly ash–based geopolymer via silane surface modification, Cem. Concr. Compos., 94 (2018) 43-52.

[169] B. Qu, A. Martin, J. Pastor, A. Palomo, A. Fernández-Jiménez, Characterisation of pre-industrial hybrid cement and effect of pre-curing temperature, Cem. Concr. Compos., 73 (2016) 281-288.

[170] B. Qu, A. Palomo, A. Fernández-Jiménez, A. Martin, J.Y. Pastor, High-temperature effect on the mechanical behaviour of hybrid cement, Materiales de Construcción, MC-133-18, (Under review) 2018.

[171] B. Qu, Temperature effect on performance of Portland cement versus advanced hybrid cements and alkali-fly ash cement, PhD thesis, Department of materials science, E.T.S.I. Caminos, Canales y Puerdos, Universidad Politécnica de Madrid, Madrid, Spain, 2018.

[172] D.F. Velandia, C.J. Lynsdale, J.L. Provis, F. Ramirez, Effect of mix design inputs, curing and compressive strength on the durability of Na_2SO_4-activated high volume fly ash concretes, Cem. Concr. Compos., 91 (2018) 11-20.

[173] M. Mastali, P. Kinnunen, A. Dalvand, R. Mohammadi Firouz, M. Illikainen, Drying shrinkage in alkali-activated binders – A critical review, Constr. Build. Mater, 190 (2018) 533-550.

[174] Y. Ma, G. Ye, The shrinkage of alkali activated fly ash, Cem Concr. Res., 68 (2015) 75-82.

[175] A. Rodrigue, J. Duchesne, B. Fournier, B. Bissonnette, Influence of added water and fly ash content on the characteristics, properties and early-age cracking sensitivity of alkali-activated slag/fly ash concrete cured at ambient temperature, Constr. Build. Mater, 171 (2018) 929-941.

[176] D. Ballekere Kumarappa, S. Peethamparan, M. Ngami, Autogenous shrinkage of alkali activated slag mortars: Basic mechanisms and mitigation methods, Cem Concr. Res., 109 (2018) 1-9.

[177] H. Ye, A. Radlińska, Shrinkage mechanisms of alkali-activated slag, Cem Concr. Res., 88 (2016) 126-135.

[178] G. Fang, H. Bahrami, M. Zhang, Mechanisms of autogenous shrinkage of alkali-activated fly ash-slag pastes cured at ambient temperature within 24 h, Constr. Build. Mater, 171 (2018) 377-387.

[179] R.J. Thomas, D. Lezama, S. Peethamparan, On drying shrinkage in alkali-activated concrete: Improving dimensional stability by aging or heat-curing, Cem Concr. Res., 91 (2016) 13-23.

[180] X. Gao, Q.L. Yu, H.J.H. Brouwers, Assessing the porosity and shrinkage of alkali activated slag-fly ash composites designed applying a packing model, Constr. Build. Mater, 119 (2016) 175-184.

[181] G. Wang, Y. Ma, Drying shrinkage of alkali-activated fly ash/slag blended system, J. Sust. Cement-Based Mater., 7 (2018) 203-213.

[182] A.M.A. Aboshia, R.A. Rahmat, M.F.M. Zain, A. Ismail, Early age shrinkage cracking of restrained metakaolin-slag-palm oil fuel ash binder geopolymer mortars, J. Sust. Cement-Based Mater., 7 (2018) 271-295.

[183] V. Bílek, L. Kalina, R. Novotný, J. Tkacz, L. Pařízek, Some issues of shrinkage-reducing admixtures application in alkali-activated slag systems, Materials, 9 (2016) 462.

[184] L. Kalina, V. Bilek Jr, R. Novotny, Influence of alkali ions on the efficiency of shrinkage reduction by polypropylene glycol in alkali activated systems, Adv. Cem. Res., 30 (2017) 240-244.

[185] C. Nguyen, P. Mangat, G. Jones, Effect of shrinkage reducing admixture on the strength and shrinkage of alkali activated cementitious mortar, IOP Conf. Series: Mater. Sci. Eng., 2018, #012022.

[186] X. Hu, C. Shi, Z. Zhang, Z. Hu, Autogenous and drying shrinkage of alkali-activated slag mortars, J. Am. Ceram. Soc., Accepted (2019).

[187] S. Oh, Y.C. Choi, Superabsorbent polymers as internal curing agents in alkali activated slag mortars, Constr. Build. Mater, 159 (2018) 1-8.

[188] W. Tu, Y. Zhu, G. Fang, X. Wang, M. Zhang, Internal curing of alkali-activated fly ash-slag pastes using superabsorbent polymer, Cem Concr. Res., 116 (2019) 179-190.

[189] C. Song, Y.C. Choi, S. Choi, Effect of internal curing by superabsorbent polymers – Internal relative humidity and autogenous shrinkage of alkali-activated slag mortars, Constr. Build. Mater, 123 (2016) 198-206.

[190] B. Yuan, Q.L. Yu, H.J.H. Brouwers, Phase modification induced drying shrinkage reduction

on Na_2CO_3 activated slag by incorporating Na_2SO_4, Mater. Struct., 50 (2017) 220.

[191] K. Arbi, M. Nedeljković, Y. Zuo, G. Ye, A review on the durability of alkali-activated fly ash/slag systems: Advances, issues, and perspectives, Ind. Eng. Chem. Res., 55 (2016) 5439-5453.

[192] J.S.J. van Deventer, R. San Nicolas, I. Ismail, S.A. Bernal, D.G. Brice, J.L. Provis, Microstructure and durability of alkali-activated materials as key parameters for standardisation, J. Sust. Cem-Based Mater., 4 (2015) 116-128.

[193] S.A. Bernal, J.L. Provis, Durability of alkali-activated materials: progress and perspectives, J. Am. Ceram. Soc, 97 (2014) 997-1008.

[194] J.L. Provis, Alkali-activated cements and concretes – durability testing to underpin standardisation, in: P.A.M. Basheer (Ed.) Proceedings of the Sixth International Conference on the Durability of Concrete Structures, Leeds, UK, 2018, pp. 16-26.

[195] J.L. Provis, F. Winnefeld, “Testing the test” –the outcomes of the round robin tests of RILEM TC 247-DTA on the durability of alkali-activated concrete, in: H. Beushausen (Ed.) Proceedings of the 5th International Conference on Concrete Repair, Rehabilitation and Retrofitting, Cape Town, South Africa, 2018.

[196] K. Yang, C. Yang, B. Magee, S. Nanukuttan, J. Ye, Establishment of a preconditioning regime for air permeability and sorptivity of alkali-activated slag concrete, Cem. Concr. Compos., 73 (2016) 19-28.

[197] I. Ismail, S.A. Bernal, J.L. Provis, S. Hamdan, J.S.J. van Deventer, Drying-induced changes in the structure of alkali-activated pastes, J. Mater. Sci, 48 (2013) 3566-3577.

[198] Z. Zhang, Y. Zhu, H. Zhu, Y. Zhang, J.L. Provis, H. Wang, Effect of drying procedures on pore structure and phase evolution of alkali-activated cements, Cem. Concr. Compos., 96 (2019) 194-203.

[199] British Standards Institute, BSI PAS 8820:2016, Construction materials – Alkali-activated cementitious material and concrete – Specification, London, UK, 2016.

[200] S.A. Bernal, J.L. Provis, D.G. Brice, A. Kilcullen, P. Duxson, J.S.J. van Deventer, Accelerated carbonation testing of alkali-activated binders significantly underestimates service life: The role of pore solution chemistry, Cem Concr. Res., 42 (2012) 1317-1326.

[201] R. Pouhet, M. Cyr, Carbonation in the pore solution of metakaolin-based geopolymer, Cem Concr. Res., 88 (2016) 227-235.

[202] M.S.H. Khan, A. Castel, A. Noushini, Carbonation of a low-calcium fly ash geopolymer concrete, Mag. Concr. Res, 69 (2017) 24-34.

[203] S.A. Bernal, J.L. Provis, R. Mejía de Gutiérrez, J.S.J. van Deventer, Accelerated carbonation testing of alkali-activated slag/metakaolin blended concretes: effect of exposure conditions, Mater. Struct., 48 (2015) 653-669.

[204] S.A. Bernal, Effect of the activator dose on the compressive strength and accelerated carbonation resistance of alkali silicate-activated slag/metakaolin blended materials, Constr. Build. Mater, 98 (2015) 217-226.

[205] M. Nedeljković, B. Šavija, Y. Zuo, M. Luković, G. Ye, Effect of natural carbonation on the pore structure and elastic modulus of the alkali-activated fly ash and slag pastes, Construction and Building Materials, 161 (2018) 687-704.

[206] M. Nedeljković, B. Ghiassi, S. van der Laan, Z. Li, G. Ye, Effect of curing conditions on the pore solution and carbonation resistance of alkali-activated fly ash and slag pastes, Cem Concr.

Res., 116 (2019) 146-158.

[207] Z. Shi, C. Shi, S. Wan, N. Li, Z. Zhang, Effect of alkali dosage and silicate modulus on carbonation of alkali-activated slag mortars, Cem Concr. Res., 113 (2018) 55-64.

[208] M.S.H. Khan, A. Castel, Effect of MgO and Na_2SiO_3 on the carbonation resistance of alkali activated slag concrete, Mag. Concr. Res, 70 (2018) 685-692.

[209] S.A. Bernal, R. San Nicolas, R.J. Myers, R. Mejía de Gutiérrez, F. Puertas, J.S.J. van Deventer, J.L. Provis, MgO content of slag controls phase evolution and structural changes induced by accelerated carbonation in alkali-activated binders, Cem Concr. Res., 57 (2014) 33-43.

[210] S.M. Park, J.G. Jang, H.K. Lee, Unlocking the role of MgO in the carbonation of alkali-activated slag cement, Inorg. Chem. Front., 5 (2018) 1661-1670.

[211] H. Ye, A. Radlińska, Carbonation-induced volume change in alkali-activated slag, Constr. Build. Mater, 144 (2017) 635-644.

[212] M. Babaee, M.S.H. Khan, A. Castel, Passivity of embedded reinforcement in carbonated low-calcium fly ash-based geopolymer concrete, Cem. Concr. Compos., 85 (2018) 32-43.

[213] M.S. Badar, K. Kupwade-Patil, S.A. Bernal, J.L. Provis, E.N. Allouche, Corrosion of steel bars induced by accelerated carbonation in low and high calcium fly ash geopolymer concretes, Constr. Build. Mater, 61 (2014) 79-89.

[214] J. Osio-Norgaard, J.P. Gevaudan, W.V. Srubar, A review of chloride transport in alkali-activated cement paste, mortar, and concrete, Constr. Build. Mater, 186 (2018) 191-206.

[215] C. Shi, L. Zhang, J. Zhang, N. Li, Z. Ou, Advances in testing methods and influencing factors of chloride ion transport properties of alkali-activated materials, Materials Review, 31 (2017) 95-100 (in Chinese).

[216] R.J. Thomas, E. Ariyachandra, D. Lezama, S. Peethamparan, Comparison of chloride permeability methods for alkali-activated concrete, Constr. Build. Mater, 165 (2018) 104-111.

[217] A. Noushini, A. Castel, Performance-based criteria to assess the suitability of geopolymer concrete in marine environments using modified ASTM C1202 and ASTM C1556 methods, Mater. Struct., 51 (2018) #146.

[218] M. Babaee, A. Castel, Chloride-induced corrosion of reinforcement in low-calcium fly ash-based geopolymer concrete, Cem Concr. Res., 88 (2016) 96-107.

[219] X. Ke, S.A. Bernal, J.L. Provis, Uptake of chloride and carbonate by Mg-Al and Ca-Al layered double hydroxides in simulated pore solutions of alkali-activated slag cement, Cem Concr. Res., 100 (2017) 1-13.

[220] X. Ke, S.A. Bernal, O.H. Hussein, J.L. Provis, Chloride binding and mobility in sodium carbonate-activated slag pastes and mortars, Mater. Struct., 50 (2017) #252.

[221] M. Babaee, A. Castel, Chloride diffusivity, chloride threshold, and corrosion initiation in reinforced alkali-activated mortars: Role of calcium, alkali, and silicate content, Cem Concr. Res., 111 (2018) 56-71.

[222] Q. Ma, S.V. Nanukuttan, P.A.M. Basheer, Y. Bai, C. Yang, Chloride transport and the resulting corrosion of steel bars in alkali activated slag concretes, Mater. Struct., 49 (2016) 3663-3677.

[223] X. Yu, L. Jiang, J. Xu, Electrochemical and semiconducting properties of passive films on steel surfaces in alkali-activated slag extraction solution, J. Mater. Civ. Eng., 30 (2018) 04018146.

[224] J. Shi, J. Ming, W. Sun, Electrochemical performance of reinforcing steel in alkali-activated slag extract in the presence of chlorides, Corros. Sci., 133 (2018) 288-299.

[225] W. Wang, H. Chen, X. Li, Z. Zhu, Corrosion behavior of steel bars immersed in simulated pore solutions of alkali-activated slag mortar, Constr. Build. Mater, 143 (2017) 289-297.

[226] S. Mundra, S.A. Bernal, M. Criado, P. Hlaváček, G. Ebell, S. Reinemann, G.J.G. Gluth, J.L. Provis, Steel corrosion in reinforced alkali-activated materials, RILEM Tech. Lett., 2 (2017) 33-39.

[227] M. Holloway, J.M. Sykes, Studies of the corrosion of mild steel in alkali-activated slag cement mortars with sodium chloride admixtures by a galvanostatic pulse method, Corros. Sci., 47 (2005) 3097-3110.

[228] M. Criado, J.L. Provis, Alkali activated slag mortars provide high resistance to chloride-induced corrosion of steel, Front. Mater., 5 (2018) #34.

[229] M. Criado, S.A. Bernal, P. Garcia-Triñanes, J.L. Provis, Influence of slag composition on the stability of steel in alkali-activated cementitious materials, J. Mater. Sci, 53 (2018) 5016-5035.

[230] S. Mundra, M. Criado, S.A. Bernal, J.L. Provis, Chloride-induced corrosion of steel rebars in simulated pore solutions of alkali-activated concretes, Cem Concr. Res., 100 (2017) 385-397.

[231] C. Tennakoon, A. Shayan, J.G. Sanjayan, A. Xu, Chloride ingress and steel corrosion in geopolymer concrete based on long term tests, Mater. Des., 116 (2017) 287-299.

[232] C. Monticelli, M.E. Natali, A. Balbo, C. Chiavari, F. Zanotto, S. Manzi, M.C. Bignozzi, Corrosion behavior of steel in alkali-activated fly ash mortars in the light of their microstructural, mechanical and chemical characterization, Cem Concr. Res., 80 (2016) 60-68.

[233] C. Shi, Z.G. Shi, X. Hu, R. Zhao, L. Chong, A review on alkali-aggregate reactions in alkali-activated mortars/ concretes made with alkali-reactive aggregates, Mater. Struct., 48 (2015) 621-628.

[234] R. Pouhet, M. Cyr, Alkali–silica reaction in metakaolin-based geopolymer mortar, Mater. Struct., 48 (2015) 571-583.

[235] R. Tänzer, Y. Jin, D. Stephan, Effect of the inherent alkalis of alkali activated slag on the risk of alkali silica reaction, Cem Concr. Res., 98 (2017) 82-90.

[236] Z. Shi, C. Shi., R. Zhao, S. Wan, Comparison of alkali-silica reactions in alkali-activated slag and Portland cement mortars, Mater. Struct., 48 (2015) 743-751.

[237] T. Williamson, M.C.G. Juenger, The role of activating solution concentration on alkali–silica reaction in alkali-activated fly ash concrete, Cem Concr. Res., 83 (2016) 124-130.

[238] Z. Shi, C. Shi, J. Zhang, S. Wan, Z. Zhang, Z. Ou, Alkali-silica reaction in waterglass-activated slag mortars incorporating fly ash and metakaolin, Cem Concr Res, 108 (2018) 10-19.

[239] Z. Shi, C. Shi, S. Wan, Z. Ou, Effect of alkali dosage on alkali-silica reaction in sodium hydroxide activated slag mortars, Constr. Build. Mater, 143 (2017) 16-23.

[240] L. Gu, P. Visintin, T. Bennett, Evaluation of accelerated degradation test methods for cementitious composites subject to sulfuric acid attack; application to conventional and alkali-activated concretes, Cem. Concr. Compos., 87 (2018) 187-204.

[241] Y. Xie, X. Lin, W. Pan, T. Ji, Y. Liang, H. Zhang, Study on corrosion mechanism of alkali-activated concrete with biogenic sulfuric acid, Constr. Build. Mater, 188 (2018) 9-16.

[242] T.A. Aiken, J. Kwasny, W. Sha, M.N. Soutsos, Effect of slag content and activator dosage on the resistance of fly ash geopolymer binders to sulfuric acid attack, Cem Concr. Res., 111 (2018)

23-40.

[243] P. Sturm, G.J.G. Gluth, C. Jäger, H.J.H. Brouwers, H.C. Kühne, Sulfuric acid resistance of one-part alkali-activated mortars, Cem Concr. Res., 109 (2018) 54-63.

[244] J. Kwasny, T.A. Aiken, M.N. Soutsos, J.A. McIntosh, D.J. Cleland, Sulfate and acid resistance of lithomarge-based geopolymer mortars, Constr. Build. Mater, 166 (2018) 537-553.

[245] A. Koenig, A. Herrmann, S. Overmann, F. Dehn, Resistance of alkali-activated binders to organic acid attack: Assessment of evaluation criteria and damage mechanisms, Constr. Build. Mater, 151 (2017) 405-413.

[246] T.A. Aiken, W. Sha, J. Kwasny, M.N. Soutsos, Resistance of geopolymer and Portland cement based systems to silage effluent attack, Cem Concr. Res., 92 (2017) 56-65.

[247] A. Buchwald, M. Vanooteghem, E. Gruyaert, H. Hilbig, N. Belie, Purdocement: application of alkali-activated slag cement in Belgium in the 1950s, Mater. Struct., 48 (2015) 501-511.

[248] H. Xu, J.L. Provis, J.S.J. van Deventer, P.V. Krivenko, Characterization of aged slag concretes, ACI Mater. J., 105 (2008) 131-139.

[249] K. Pasupathy, M. Berndt, J. Sanjayan, P. Rajeev, D.S. Cheema, Durability of low-calcium fly ash based geopolymer concrete culvert in a saline environment, Cem Concr. Res., 100 (2017) 297-310.

[250] H.A. Khan, M.S.H. Khan, A. Castel, J. Sunarho, Deterioration of alkali-activated mortars exposed to natural aggressive sewer environment, Constr. Build. Mater, 186 (2018) 577-597.

[251] K. Pasupathy, M. Berndt, J. Sanjayan, P. Rajeev, D.S. Cheema, Durability performance of precast fly ash-based geopolymer concrete under atmospheric exposure conditions, J. Mater. Civ. Eng., 30 (2018) 04018007.

[252] K. Pasupathy, M. Berndt, A. Castel, J. Sanjayan, R. Pathmanathan, Carbonation of a blended slag-fly ash geopolymer concrete in field conditions after 8 years, Constr. Build. Mater, 125 (2016) 661-669.

[253] J. Aldred, J. Day, T. Glasby, Geopolymer concrete - No longer labcrete!, 40th Conference on Our World in Concrete & Structures, Singapore, 2015.

[254] R.D. Hooton, Current developments and future needs in standards for cementitious materials, Cem Concr. Res., 78 (2015) 165-177.

[255] D. Bondar, Q. Ma, M. Soutsos, M. Basheer, J.L. Provis, S. Nanukuttan, Alkali activated slag concretes designed for a desired slump, strength and chloride diffusivity, Constr. Build. Mater, 190 (2018) 191-199.

[256] K. Yang, C. Yang, J. Zhang, Q. Pan, L. Yu, Y. Bai, First structural use of site-cast, alkali-activated slag concrete in China, Proc. ICE Struct. Build., 171 (2018) 800-809.

[257] V. Bilek, J. Hurta, P. Done, L. Zidek, Development of alkali-activated concrete for structures–mechanical properties and durability, Persp. Sci., 7 (2016) 190-194.

[258] L.N. Assi, E. Deaver, M.K. ElBatanouny, P. Ziehl, Investigation of early compressive strength of fly ash-based geopolymer concrete, Constr. Build. Mater, 112 (2016) 807-815.

[259] A. Rafeet, R. Vinai, M. Soutsos, W. Sha, Guidelines for mix proportioning of fly ash/GGBS based alkali activated concretes, Constr. Build. Mater, 147 (2017) 130-142.

[260] B. Tempest, C. Snell, T. Gentry, M. Trejo, K. Isherwood, Manufacture of full-scale geopolymer cement concrete components: A case study to highlight opportunities and challenges, PCI J., 60 (2015) 39-50.

[261] R. Pouhet, M. Cyr, Formulation and performance of flash metakaolin geopolymer concretes, Constr. Build. Mater, 120 (2016) 150-160.

[262] N. Vandevenne, R.I. Iacobescu, Y. Pontikes, R. Carleer, E. Thijssen, K. Gijbels, S. Schreurs, W. Schroeyers, Incorporating Cs and Sr into blast furnace slag inorganic polymers and their effect on matrix properties, J. Nucl. Mater., 503 (2018) 1-12.

[263] M. Arbel Haddad, E. Ofer-Rozovsky, G. Bar-Nes, E.J.C. Borojovich, A. Nikolski, D. Mogiliansky, A. Katz, Formation of zeolites in metakaolin-based geopolymers and their potential application for Cs immobilization, J. Nucl. Mater., 493 (2017) 168-179.

[264] E. Ofer-Rozovsky, M.A. Haddad, G. Bar-Nes, E.J.C. Borojovich, A. Binyamini, A. Nikolski, A. Katz, Cesium immobilization in nitrate-bearing metakaolin-based geopolymers, J. Nucl. Mater., 514 (2019) 247-254.

[265] J. Wang, J. Wang, Y. Huang, K. Zhang, Y. Li, X. Wu, Preparation of alkali-activated slag-fly ash-metakaolin hydroceramics for immobilizing simulated sodium-bearing waste, J. Am. Ceram. Soc, 98 (2015) 1393-1399.

[266] B.D. Williams, J.J. Neeway, M.M.V. Snyder, M.E. Bowden, J.E. Amonette, B.W. Arey, E.M. Pierce, C.F. Brown, N.P. Qafoku, Mineral assemblage transformation of a metakaolin-based waste form after geopolymer encapsulation, J. Nucl. Mater., 473 (2016) 320-332.

[267] V. Cantarel, D. Lambertin, A. Poulesquen, F. Leroux, G. Renaudin, F. Frizon, Geopolymer assembly by emulsion templating: Emulsion stability and hardening mechanisms, Ceram. Int., 44 (2018) 10558-10568.

[268] C.A. Davy, G. Hauss, B. Planel, D. Lambertin, 3D structure of oil droplets in hardened geopolymer emulsions, J. Am. Ceram. Soc, 102 (2019) 949-954.

[269] P. Kryvenko, C. Hailin, O. Petropavlovskyi, L. Weng, O. Kovalchuk, Applicability of alkali-activated cement for immobilization of low-level radioactive waste in ion-exchange resins, East. Eur. J. Enterpr. Technol., 1 (2016) 40-45.

[270] C. Kuenzel, J.F. Cisneros, T.P. Neville, L.J. Vandeperre, S.J.R. Simons, J. Bensted, C.R. Cheeseman, Encapsulation of Cs/Sr contaminated clinoptilolite in geopolymers produced from metakaolin, J. Nucl. Mater., 466 (2015) 94-99.

[271] D. Chartier, B. Muzeau, L. Stefan, J. Sanchez-Canet, C. Monguillon, Magnesium alloys and graphite wastes encapsulated in cementitious materials: reduction of galvanic corrosion using alkali hydroxide activated blast furnace slag, J. Hazard Mater., 326 (2017) 197-210.

[272] D. Rodrigues, C. Cannes, N. Barré, D. Lambertin, S. Delpech, Role of fluoride ions on the uranium oxidation mechanism in highly alkaline solutions, Electrochim. Acta, 266 (2018) 384-394.

[273] A. Rooses, D. Lambertin, D. Chartier, F. Frizon, Galvanic corrosion of Mg-Zr fuel cladding and steel immobilized in Portland cement and geopolymer at early ages, J. Nucl. Mater., 435 (2013) 137-140.

[274] F. Chupin, A. Dannoux-Papin, Y. Ngono Ravache, J.-B. d'Espinose de Lacaillerie, Water content and porosity effect on hydrogen radiolytic yields of geopolymers, J. Nucl. Mater., 494 (2017) 138-146.

[275] N. Mobasher, S.A. Bernal, H. Kinoshita, J.L. Provis, Gamma irradiation resistance of early age $Ba(OH)_2$-Na_2SO_4-slag cementitious grouts, J. Nucl. Mater., 482 (2016) 266-277.

[276] N. Deng, H. An, H. Cui, Y. Pan, B. Wang, L. Mao, J. Zhai, Effects of gamma-ray irradiation

on leaching of simulated $^{133}\mathrm{Cs}^{+}$ radionuclides from geopolymer wasteforms, J. Nucl. Mater., 459 (2015) 270-275.

[277] C. Bai, P. Colombo, Processing, properties and applications of highly porous geopolymers: a review, Ceram. Int., 44 (2018) 16103-16118.

[278] Z. Zhang, J.L. Provis, A. Reid, H. Wang, Geopolymer foam concrete: an emerging material for sustainable construction, Constr. Build. Mater, 56 (2014) 113-127.

[279] C. Bai, T. Ni, Q. Wang, H. Li, P. Colombo, Porosity, mechanical and insulating properties of geopolymer foams using vegetable oil as the stabilizing agent, J. Eur. Ceram. Soc., 38 (2018) 799-805.

[280] C. Bai, G. Franchin, H. Elsayed, A. Zaggia, L. Conte, H. Li, P. Colombo, High-porosity geopolymer foams with tailored porosity for thermal insulation and wastewater treatment, J. Mater. Res., 32 (2017) 3251-3259.

[281] Z. Zhang, J.L. Provis, A. Reid, H. Wang, Mechanical, thermal insulation, thermal resistance and acoustic absorption properties of geopolymer foam concrete, Cem. Concr. Compos., 62 (2015) 97-105.

[282] A. De Rossi, J. Carvalheiras, R.M. Novais, M.J. Ribeiro, J.A. Labrincha, D. Hotza, R.F.P.M. Moreira, Waste-based geopolymeric mortars with very high moisture buffering capacity, Constr. Build. Mater, 191 (2018) 39-46.

[283] A. Hajimohammadi, T. Ngo, P. Mendis, J. Sanjayan, Regulating the chemical foaming reaction to control the porosity of geopolymer foams, Mater. Design, 120 (2017) 255-265.

[284] J.R. Mackechnie, L.A. Bellamy, Thermal performance of variable density wall panels made using Portland cement or inorganic polymer concrete, Mater. Struct., 48 (2015) 643-651.

[285] M.D.M. Paiva, E.C.C.M. Silva, D.M.A. Melo, A.E. Martinelli, J.F. Schneider, A geopolymer cementing system for oil wells subject to steam injection, J. Petrol. Sci. Eng., 169 (2018) 748-759.

[286] J. Du, Y. Bu, X. Cao, Z. Shen, B. Sun, Utilization of alkali-activated slag based composite in deepwater oil well cementing, Constr. Build. Mater, 186 (2018) 114-122.

[287] T. Sugama, T. Pyatina, Effect of sodium carboxymethyl celluloses on water-catalyzed self-degradation of 200°C-heated alkali-activated cement, Cem. Concr. Compos., 55 (2015) 281-289.

[288] R.M. Wimalasinghe, C.A. Weatherly, M.F. Wahab, N. Thakur, D.W. Armstrong, Geopolymers as a new class of high pH stable supports with different chromatographic selectivity, Anal. Chem., 90 (2018) 8139-8146.

[289] R.A. Sá Ribeiro, M.G. Sá Ribeiro, W.M. Kriven, A review of particle- and fiber-reinforced metakaolin-based geopolymer composites, J. Ceram. Sci. Technol., 8 (2017) 307-322.

[290] G.C.H. Doudart de la Grée, V. Caprai, J.E.G. van Dam, H. van As, H.J.H. Brouwers, Q.L. Yu, Ionic interaction and liquid absorption by wood in lignocellulose inorganic mineral binder composites, J. Cleaner Prod., 206 (2019) 808-818.

[291] M. Ohno, V.C. Li, An integrated design method of engineered geopolymer composite, Cem. Concr. Compos., 88 (2018) 73-85.

[292] J.-I. Choi, B.Y. Lee, R. Ranade, V.C. Li, Y. Lee, Ultra-high-ductile behavior of a polyethylene fiber-reinforced alkali-activated slag-based composite, Cem. Concr. Compos., 70 (2016) 153-158.

[293] M.H. Al-Majidi, A. Lampropoulos, A.B. Cundy, Tensile properties of a novel fibre reinforced geopolymer composite with enhanced strain hardening characteristics, Compos. Struct.,

168 (2017) 402-427.

[294] S. Kramar, A. Šajna, V. Ducman, Assessment of alkali activated mortars based on different precursors with regard to their suitability for concrete repair, Constr. Build. Mater, 124 (2016) 937-944.

[295] G. Franchin, P. Scanferla, L. Zeffiro, H. Elsayed, A. Baliello, G. Giacomello, M. Pasetto, P. Colombo, Direct ink writing of geopolymeric inks, J. Eur. Ceram. Soc., 37 (2017) 2481-2489.

[296] B. Panda, S. C. Paul, M. J. Tan, Anisotropic mechanical performance of 3D printed fiber reinforced sustainable construction material, Mater. Lett, 209 (2017) 146-149.

[297] B. Nematollahi, M. Xia, J. Sanjayan, P. Vijay, Effect of type of fiber on inter-layer bond and flexural strengths of extrusion-based 3D printed geopolymer, Mater. Sci. Forum, 939 (2018) 155-162.

[298] M. Xia, B. Nematollahi, J. Sanjayan, Influence of binder saturation level on compressive strength and dimensional accuracy of powder-based 3D printed geopolymer, Mater Sci. Forum, 939 (2018) 177-183.

[299] O.G. Rivera, W.R. Long, C.A. Weiss Jr, R.D. Moser, B.A. Williams, K. Torres-Cancel, E.R. Gore, P.G. Allison, Effect of elevated temperature on alkali-activated geopolymeric binders compared to portland cement-based binders, Cem Concr. Res., 90 (2016) 43-51.

[300] W.D.A. Rickard, G.J.G. Gluth, K. Pistol, In-situ thermo-mechanical testing of fly ash geopolymer concretes made with quartz and expanded clay aggregates, Cem Concr. Res., 80 (2016) 33-43.

[301] G.J.G. Gluth, W.D.A. Rickard, S. Werner, S. Pirskawetz, Acoustic emission and microstructural changes in fly ash geopolymer concretes exposed to simulated fire, Mater. Struct., 49 (2016) 5243-5254.

[302] S.M. Park, J.G. Jang, N.K. Lee, H.K. Lee, Physicochemical properties of binder gel in alkali-activated fly ash/slag exposed to high temperatures, Cem Concr. Res., 89 (2016) 72-79.

[303] G. Habert, C. Ouellet-Plamondon, Recent update on the environmental impact of geopolymers, RILEM Tech. Lett., 1 (2016) 17-23.

[304] Beyond Zero Emissions, Zero Carbon Industry Plan - Rethinking Cement, Melbourne, 2017.

[305] A. Passuello, E.D. Rodríguez, E. Hirt, M. Longhi, S.A. Bernal, J.L. Provis, A.P. Kirchheim, Evaluation of the potential improvement in the environmental footprint of geopolymers using waste-derived activators, J. Cleaner Prod., 166 (2017) 680-689.

[306] D.A. Salas, A.D. Ramirez, N. Ulloa, H. Baykara, A.J. Boero, Life cycle assessment of geopolymer concrete, Constr. Build. Mater, 190 (2018) 170-177.

[307] J. Dahmen, J. Kim, C.M. Ouellet-Plamondon, Life cycle assessment of emergent masonry blocks, J. Cleaner Prod., 171 (2018) 1622-1637.

[308] A. Heath, K. Paine, M. McManus, Minimising the global warming potential of clay based geopolymers, J. Cleaner Prod., 78 (2014) 75-83.

[309] A. Peys, L. Arnout, B. Blanpain, H. Rahier, K. Van Acker, Y. Pontikes, Mix-design parameters and real-life considerations in the pursuit of lower environmental impact inorganic polymers, Waste Biomass Valor., 9 (2018) 879-889.

[310] A. Petrillo, R. Cioffi, F. De Felice, F. Colangelo, C. Borrelli, An environmental evaluation: A comparison between geopolymer and OPC concrete paving blocks manufacturing process in Italy, Environ. Progr. Sust. Energy, 35 (2016) 1699-1708.

[311] S.H. Teh, T. Wiedmann, A. Castel, J. de Burgh, Hybrid life cycle assessment of greenhouse gas emissions from cement, concrete and geopolymer concrete in Australia, J. Cleaner Prod., 152 (2017) 312-320.

[312] M. Sandanayake, C. Gunasekara, D. Law, G. Zhang, S. Setunge, Greenhouse gas emissions of different fly ash based geopolymer concretes in building construction, J. Cleaner Prod., 204 (2018) 399-408.

[313] A. Di Maria, M. Salman, M. Dubois, K. Van Acker, Life cycle assessment to evaluate the environmental performance of new construction material from stainless steel slag, Int. J. Life Cycle Assess., 23 (2018) 2091-2109.

[314] A. Akbarnezhad, M. Huan, S. Mesgari, A. Castel, Recycling of geopolymer concrete, Constr. Build. Mater, 101 (2015) 152-158.

[315] N.A. Chaliasou, A. Heath, K. Paine, J. Calabria Holley, Chemical aspects related to using recycled geopolymers as aggregates, Adv. Cem. Res., 30 (2018) 361-370.

[316] A. Keulen, A. van Zomeren, J.J. Dijkstra, Leaching of monolithic and granular alkali activated slag-fly ash materials, as a function of the mixture design, Waste Manag., 78 (2018) 497-508.

[317] H.A. van der Sloot, D.S. Kosson, N. Impens, N. Vanhoudt, T. Almahayni, H. Vandenhove, L. Sweeck, R. Wiegers, J.L. Provis, C. Gascó, W. Schroeyers, 8 - Leaching assessment as a component of environmental safety and durability analyses for NORM containing building materials, in: W. Schroeyers (Ed.) Naturally Occurring Radioactive Materials in Construction, Woodhead Publishing, Duxford, UK, 2017, pp. 253-288.

[318] J. Labrincha, F. Puertas, W. Schroeyers, K. Kovler, Y. Pontikes, C. Nuccetelli, P. Krivenko, O. Kovalchuk, O. Petropavlovsky, M. Komljenovic, E. Fidanchevski, R. Wiegers, E. Volceanov, E. Gunay, M.A. Sanjuán, V. Ducman, B. Angjusheva, D. Bajare, T. Kovacs, G. Bator, S. Schreurs, J. Aguiar, J.L. Provis, 7 - From NORM by-products to building materials, in: W. Schroeyers (Ed.) Naturally Occurring Radioactive Materials in Construction, Woodhead Publishing, Duxford, UK, 2017, pp. 183-252.

[319] C. Shi, F. He, A. Fernández-Jiménez, P.V. Krivenko, A. Palomo, Classification and characteristics of alkali-activated cements, J. Chinese Ceram. Soc., 40 (2012) 69-75.

[320] X. Pan, C. Shi, X. Hu, Z. Ou, Effects of CO_2 surface treatment on strength and permeability of one-day-aged cement mortar, Construction and Building Materials, 154 (2017) 1087-1095.

[321] W. Ashraf, J. Olek, Carbonation behavior of hydraulic and non-hydraulic calcium silicates: potential of utilizing low-lime calcium silicates in cement-based materials, J Mater Sci, 51 (2016) 6173-6191.

[322] B. Qian, X. Li, X. Shen, Preparation and accelerated carbonation of low temperature sintered clinker with low Ca/Si ratio, J. Cleaner Prod., 120 (2016) 249-259.

[323] B. Lu, C. Shi, G. Hou, Strength and microstructure of CO_2 cured low-calcium clinker, Constr Build Mater, 188 (2018) 417-423.

[324] W. Ashraf, J. Olek, Carbonation activated binders from pure calcium silicates: Reaction kinetics and performance controlling factors, Cem Concr Compos, 93 (2018) 85-98.

[325] W. Ashraf, J. Olek, J. Jain, Microscopic features of non-hydraulic calcium silicate cement paste and mortar, Cem Concr Res, 100 (2017) 361-372.

[326] W. Ashraf, J. Olek, Elucidating the accelerated carbonation products of calcium silicates

using multi-technique approach, J. CO_2 Utilization, 23 (2018) 61-74.

[327] Y. Mu, Z. Liu, F. Wang, X. Huang, Carbonation characteristics of γ-dicalcium silicate for low-carbon building material, Constr. Build. Mater., 177 (2018) 322-331.

[328] J. Chang, Y. Fang, X. Shang, The role of β-C_2S and γ-C_2S in carbon capture and strength development, Mater Struct, 49 (2016) 4417-4424.

[329] X. Guan, S. Liu, C. Feng, M. Qiu, The hardening behavior of γ-C_2S binder using accelerated carbonation, Constr. Build. Mater., 114 (2016) 204-207.

[330] S. Liu, Z. Dou, S. Zhang, H. Zhang, X. Guan, C. Feng, J. Zhang, Effect of sodium hydroxide on the carbonation behavior of β-dicalcium silicate, Constr. Build. Mater., 150 (2017) 591-594.

[331] V. Shah, K. Scrivener, B. Bhattacharjee, S. Bishnoi, Changes in microstructure characteristics of cement paste on carbonation, Cem. Concr. Res., 109 (2018) 184-197.

[332] C. Shi, F. He, Y. Wu, Effect of pre-conditioning on CO_2 curing of lightweight concrete blocks mixtures, Constr. Build. Mater., 26 (2012) 257-267.

[333] M. Castellote, L. Fernandez, C. Andrade, C. Alonso, Chemical changes and phase analysis of OPC pastes carbonated at different CO_2 concentrations, Mater Struct, 42 (2009) 515-525.

[334] C. Shi, Y. Wu, Studies on some factors affecting CO_2 curing of lightweight concrete products, Resourc Conserv Recyc, 52 (2008) 1087-1092.

[335] C. Shi, D. Wang, F. He, M. Liu, Weathering properties of CO_2-cured concrete blocks, Resourc Conserv Recyc, 65 (2012) 11-17.

[336] S. Monkman, P.A. Kenward, G. Dipple, M. MacDonald, M. Raudsepp, Activation of cement hydration with carbon dioxide, J Sust Cement-Based Mater, 7 (2018) 160-181.

[337] P. He, C. Shi, Z. Tu, C.S. Poon, J. Zhang, Effect of further water curing on compressive strength and microstructure of CO_2-cured concrete, Cem Concr Compos, 72 (2016) 80-88.

[338] M. Auroy, S. Poyet, P. Le Bescop, J.-M. Torrenti, T. Charpentier, M. Moskura, X. Bourbon, Comparison between natural and accelerated carbonation (3% CO_2): Impact on mineralogy, microstructure, water retention and cracking, Cem Concr Res, 109 (2018) 64-80.

[339] J.H. Seo, S.M. Park, H.K. Lee, Evolution of the binder gel in carbonation-cured Portland cement in an acidic medium, Cem Concr Res, 109 (2018) 81-89.

[340] L. Mo, D.K. Panesar, Accelerated carbonation – A potential approach to sequester CO_2 in cement paste containing slag and reactive MgO, Cem Concr Compos, 43 (2013) 69-77.

[341] P. He, C.S. Poon, D.C.W. Tsang, Effect of pulverized fuel ash and CO_2 curing on the water resistance of magnesium oxychloride cement (MOC), Cem Concr Res, 97 (2017) 115-122.

[342] L. Mo, D.K. Panesar, Effects of accelerated carbonation on the microstructure of Portland cement pastes containing reactive MgO, Cem Concr Res, 42 (2012) 769-777.

[343] F.P. Glasser, G. Jauffret, J. Morrison, J.-L. Galvez-Martos, N. Patterson, M.S.-E. Imbabi, Sequestering CO_2 by mineralization into useful nesquehonite-based products, Front. Energy Res., 4 (2016) #3.

[344] N.T. Dung, C. Unluer, Development of MgO concrete with enhanced hydration and carbonation mechanisms, Cem Concr Res, 103 (2018) 160-169.

[345] S.A. Walling, J.L. Provis, Magnesia based cements – a journey of 150 years, and cements for the future?, Chem. Rev., 116 (2016) 4170-4204.

[346] C. Shi, J. Qian, High performance cementing materials from industrial slags — a review, Resourc Conserv Recyc, 29 (2000) 195-207.

[347] C. Shi, Steel slag—its production, processing, characteristics, and cementitious properties, J Mater Civil Eng, 16 (2004) 230-236.

[348] P.S. Humbert, J. Castro-Gomes, CO_2 activated steel slag-based materials: A review, J. Cleaner Prod., 208 (2019) 448-457.

[349] L. Mo, F. Zhang, M. Deng, Mechanical performance and microstructure of the calcium carbonate binders produced by carbonating steel slag paste under CO_2 curing, Cem Concr Res, 88 (2016) 217-226.

[350] Z. Ghouleh, R.I.L. Guthrie, Y. Shao, High-strength KOBM steel slag binder activated by carbonation, Constr Build Mater, 99 (2015) 175-183.

[351] L. Mo, F. Zhang, M. Deng, F. Jin, A. Al-Tabbaa, A. Wang, Accelerated carbonation and performance of concrete made with steel slag as binding materials and aggregates, Cem Concr Compos, 83 (2017) 138-145.

[352] S. Monkman, Y. Shao, C. Shi, Carbonated ladle slag fines for carbon uptake and sand substitute, J. Mater. Civil Eng., 21 (2009) 657-665.

[353] N.L. Ukwattage, P.G. Ranjith, M. Yellishetty, H.H. Bui, T. Xu, A laboratory-scale study of the aqueous mineral carbonation of coal fly ash for CO_2 sequestration, J. Cleaner Prod., 103 (2015) 665-674.

[354] A. Dindi, D.V. Quang, L.F. Vega, E. Nashef, M.R.M. Abu-Zahra, Applications of fly ash for CO_2 capture, utilization, and storage, J. CO_2 Utilization, 29 (2019) 82-102.

[355] Z. Wei, B. Wang, G. Falzone, E.C. La Plante, M.U. Okoronkwo, Z. She, T. Oey, M. Balonis, N. Neithalath, L. Pilon, G. Sant, Clinkering-free cementation by fly ash carbonation, J. CO_2 Utilization, 23 (2018) 117-127.

[356] Y. Shao, M. Mahoutian, Low temperature synthesis of cement from ladle slag and fly ash, J.Sust Cement-Based Mater, 5 (2016) 247-258.

[357] C.W. Hargis, J. Moon, B. Lothenbach, F. Winnefeld, H.-R. Wenk, P.J.M. Monteiro, Calcium sulfoaluminate sodalite ($Ca_4Al_6O_{12}SO_4$) crystal structure evaluation and bulk modulus determination, J. Am. Ceram. Soc., 97 (2014) 892-898.

[358] L. Zhang, M. Su, Y. Wang, Development of the use of sulfo- and ferroaluminate cements in China, Adv. Cem. Res., 11 (1999) 15-21.

[359] E. Gartner, H. Hirao, A review of alternative approaches to the reduction of CO_2 emissions associated with the manufacture of the binder phase in concrete, Cem Concr Res, 78 (2015) 126-142.

[360] E. Gartner, T. Sui, Alternative cement clinkers, Cem Concr Res, 114 (2018) 27-39.

[361] T. Hanein, I. Galan, A. Elhoweris, S. Khare, S. Skalamprinos, G. Jen, M. Whittaker, M.S. Imbabi, F.P. Glasser, M.N. Bannerman, Production of belite calcium sulfoaluminate cement using sulfur as a fuel and as a source of clinker sulfur trioxide: pilot kiln trial, Adv. Cem. Res., 28 (2016) 643-653.

[362] L. Zhang, F.P. Glasser, Investigation of the microstructure and carbonation of $C\bar{S}A$-based concretes removed from service, Cem Concr Res, 35 (2005) 2252-2260.

[363] F. Winnefeld, B. Lothenbach, Hydration of calcium sulfoaluminate cements — Experimental findings and thermodynamic modelling, Cem Concr Res, 40 (2010) 1239-1247.

[364] C.W. Hargis, A.P. Kirchheim, P.J.M. Monteiro, E.M. Gartner, Early age hydration of calcium sulfoaluminate (synthetic ye'elimite, $C_4A_3\bar{S}$) in the presence of gypsum and varying

amounts of calcium hydroxide, Cem Concr Res, 48 (2013) 105-115.

[365] H. Beltagui, G. Jen, M. Whittaker, M.S. Imbabi, The influence of variable gypsum and water content on the strength and hydration of a belite-calcium sulphoaluminate cement, Adv. Appl. Ceram., 116 (2017) 199-206.

[366] A. Cuesta, G. Álvarez-Pinazo, S.G. Sanfélix, I. Peral, M.A.G. Aranda, A.G. De la Torre, Hydration mechanisms of two polymorphs of synthetic ye'elimite, Cem Concr Res, 63 (2014) 127-136.

[367] G. Álvarez-Pinazo, I. Santacruz, M.A.G. Aranda, Á.G. De la Torre, Hydration of belite–ye'elimite–ferrite cements with different calcium sulfate sources, Adv. Cem. Res, 28 (2016) 529-543.

[368] M. García-Maté, I. Santacruz, Á.G. De la Torre, L. León-Reina, M.A.G. Aranda, Rheological and hydration characterization of calcium sulfoaluminate cement pastes, Cem Concr Compos, 34 (2012) 684-691.

[369] M. García-Maté, A.G. De la Torre, L. León-Reina, E.R. Losilla, M.A.G. Aranda, I. Santacruz, Effect of calcium sulfate source on the hydration of calcium sulfoaluminate eco-cement, Cem Concr Compos, 55 (2015) 53-61.

[370] V. Morin, P. Termkhajornkit, B. Huet, G. Pham, Impact of quantity of anhydrite, water to binder ratio, fineness on kinetics and phase assemblage of belite-ye'elimite-ferrite cement, Cem Concr Res, 99 (2017) 8-17.

[371] M.T. Blanco-Varela, A. Palomo, F. Puertas, T. Vázquez, CaF_2 and $CaSO_4$ in white cement clinker production, Adv Cem Res, 9 (1997) 105-113.

[372] J.D. Zea-Garcia, I. Santacruz, M.A.G. Aranda, A.G. De la Torre, Alite-belite-ye'elimite cements: Effect of dopants on the clinker phase composition and properties, Cem Concr Res, 115 (2019) 192-202.

[373] N. Chitvoranund, F. Winnefeld, C.W. Hargis, S. Sinthupinyo, B. Lothenbach, Synthesis and hydration of alite-calcium sulfoaluminate cement, Adv Cem Res, 29 (2017) 101-111.

[374] D. Londono-Zuluaga, J.I. Tobón, M.A.G. Aranda, I. Santacruz, A.G. De la Torre, Clinkering and hydration of belite-alite-ye´elimite cement, Cem Concr Compos, 80 (2017) 333-341.

[375] D. Londono-Zuluaga, J.I. Tobón, M.A.G. Aranda, I. Santacruz, A.G. De la Torre, Influence of fly ash blending on hydration and physical behavior of belite–alite–ye’elimite cements, Mater Struct, 51 (2018) #128.

[376] T. Duvallet, Y. Zhou, K.R. Henke, T.L. Robl, R. Andrews, Effects of ferrite concentration on synthesis, hydration and mechanical properties of alite-calcium sulfoaluminate-ferrite cements, J Sust Cement-Based Mater, 6 (2017) 85-110.

[377] M. Ben Haha, F. Bullerjahn, M. Zajac, On the reactivity of ternesite, 14th International Congress on the Chemistry of Cement, Beijing, 2015.

[378] M. Montes, E. Pato, P.M. Carmona-Quiroga, M.T. Blanco-Varela, Can calcium aluminates activate ternesite hydration?, Cem Concr Res, 103 (2018) 204-215.

[379] M.T. Blanco-Varela, P.M. Carmona-Quiroga, Ternesite as a component of sulfobelitic cements, MATEC Web Conf., 149 (2018) #01011.

[380] T. Hanein, I. Galan, F.P. Glasser, S. Skalamprinos, A. Elhoweris, M.S. Imbabi, M.N. Bannerman, Stability of ternesite and the production at scale of ternesite-based clinkers, Cem. Concr. Res., 98 (2017) 91-100.

[381] I. Galan, T. Hanein, A. Elhoweris, M.N. Bannerman, F.P. Glasser, Phase compatibility in the system CaO–SiO_2–Al_2O_3–SO_3–Fe_2O_3 and the effect of partial pressure on the phase stability, Ind. Eng. Chem. Res., 56 (2017) 2341-2349.